# DESIGN AND SYNTHESIS OF NEAR INFRA-RED (NIR) DYES TOWARDS THEIR APPLICATION AS PROBES FOR FLUORESCENCE BIO-SENSING.

## GRADUATE SCHOOL OF LIFE SCIENCE AND SYSTEM ENGINEERING
## KYUSHU INSTITUTE OF TECHNOLOGY

## DISSERTATION

## FOR THE DEGREE OF

## DOCTOR OF PHILOSOPHY


## M SAI KIRAN

## PH.D. SUPERVISOR

## PROFESSOR. TAMAKI KATO

DEPARTMENT OF BIOLOGICAL FUNCTIONS ENGINEERING

GRADUATE SCHOOL OF LIFE SCIENCE AND SYSTEMS ENGINEERING

KYUSHU INSTITUTE OF TECHNOLOGY

# Abstract

Easy and fast detection of diseases is now demand of time for monitoring the health conditions and sustaining the ever-improving lifestyle in both of the developed as well as developing countries. Biosensors are analytical devices that transform a biological response into an electrical signal. Biosensors are extremely specific and are independent of physical parameters such as pH and temperature and should be ecofriendly. Development of biosensors such as enzyme sensors, immune-sensors, microbial sensors, ion channel sensors etc. is one of fast growing sectors and is being actively promoted world-wide. Some of the most commonly used biosensors include Enzyme sensors for the measurement of blood glucose level using glucose oxidase activity measurement, immune-sensors and ELISA. Since detector is one of the important part of biosensors, fluorescence detection has a great potential for the detection of trace amount of analytes due to high sensitivity measurement as compared with the optical absorption especially for very dilute samples.

Fluorescent biosensors plays a key role in discovery of drugs and in cancer. Single chain FRET biosensor is potential example which consists of a pair of auto fluorescent protein (AFP`s) where fluorescence resonance energy transfer occurs between them when brought close together. Conventionally, FRET based biosensor using visible fluorescent molecules is influenced by auto-fluorescence from the clinical samples like blood, serum or other body fluids leading to low signal to noise (SN) ratio and attainment of high sensitivity is hampered significantly. A FRET biosensor utilizing NIR fluorescent and quenchers can easily detect resulting fluorescence signals from the body of several 10 cm from a detector outside the body with high SN ratio (high sensitivity). This means that it is very suitable for pathological imaging in vivo. In order to increase the sensitivity of the biosensor using near infrared FRET, it is desirable that the wavelengths of the dye absorption and fluorescence emission should perfectly match. It is also necessary to adjust the peptide sequence of the enzyme active site so that the position of the quenching group and the fluorescent group are within the Forster radius. Protein and peptide biosensors are manufactured easily through synthetic chemistry followed by enzymatic labelling using synthetic fluorophores.

A biosensor based on NIR-FRET system is advantageous for high sensitivity in terms of not being easily influenced by auto-fluorescence of water or biomolecules and high penetrability of near infrared rays. At the same time, by changing the peptide sequence between

the dyes having fluorescent groups and quenching groups in different wavelength ranges, it is possible to control the absorption wavelength specifically for the enzyme. This means that simultaneous measurement of multiple specimens is possible, and the detected image leads to the construction of a disease database enabling multifaceted examination as a disease pattern and diagnosis with higher accuracy. By immobilizing to the substrate, it can be applied to on-chip biosensor in-vitro too. Fluorescent biosensors are potentially employed for early detection of biomarkers in clinical and molecular diagnostics for disease progress monitoring and response to treatment.

In the development of near infrared FRET biosensor, development of NIR dyes (fluorescent group and quenching group) and design of enzyme recognition site are necessary. Current thesis gives the insights about the synthesis and characterization of far-red sensitive squaraine dyes with varying wavelengths and NIR cyanine dyes. Apart from this, an effort has been made to evaluate amino acid sequences that are selective for specific enzymes and incorporating them to develop model NIR-FRET system.

## Table of Contents

# Chapter 1: Point-of-Care Biosensor Systems their applications as diagnostic tools for health care

## 1. Introduction

Easy and accurate detection of diseases is currently the demand of time for monitoring the health conditions and sustaining the ever-improving lifestyle in both of the developed as well as developing countries. This has become possible due to increase in the knowledge, awareness along with tremendous growth in medical science to control the epidemic and dreadful diseases. Statistical data on the world population as shown in figure 1 clearly reveals that overall world population is increasing but the major contribution to this population growth is mainly contributed by people from Asia, Africa and Latin America although there is projected negative population growth in developed countries like North America, Europe including Japan. To sustain this increasing standard of life with the increasing overall world population, it is necessary to monitor health, with fast and accurate detection of disease with easy to handle testing devices before going to hospitals for in-depth consultation and treatment. This is where Point of Care Testing (POCT) devices have come into the picture.

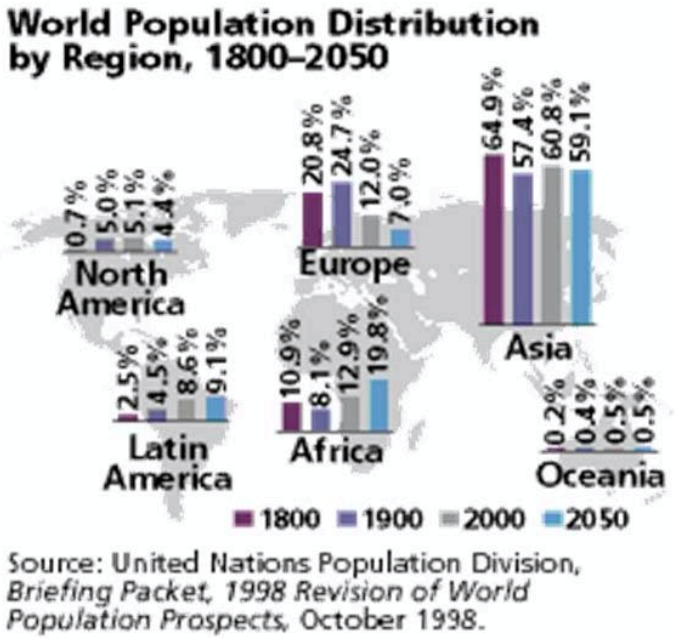


Figure 1. Estimated population growth of Asia

POCT refers to the test conducted outside a lab, hospital or clinic by the patients themselves. Biosensors have emerged as one of the potential POCT devices and played a vital role towards

the patient care through real-time and remote health monitoring. Over the past few decades, tremendous researches have been conducted in the field of biosensors to detect biomarkers and provide information on their concentration in biological samples for robust diagnosis.

The main objectives of POCT devices are to improve quality and efficiency of the patient care, increase the satisfaction of both physician and patient, improve patient education as the device can be operated by a patient himself and to decrease the risk liability (1). Some of the recent advancements of POCT systems are as follows: The study of Genomics and proteomics research has revealed many new biomarkers that have the potential to advance healthcare (2–3). The availability of multiple biomarkers is believed to be precarious in the diagnosis of complex diseases (4). Detection of biomarkers related to different stages of disease could further enable early detection of diseases and their infection rate (5). Extensive use of these biomarkers will rest on the development of point-of-care (POC) biosensor devices that will permit rapid, real-time, label-free, and multiplexed detection with high sensitivity and selectivity. Despite the rapid development of genomics and proteomics research, a few of these biomarkers have transitioned into clinical settings. This is due to the lack of rapid diagnostic techniques that can successfully detect them. For example, tuberculosis (TB), a prevalent public health issue (6), has confirmed to be curable (7). However, WHO estimation for 2009 suggest that a global detection rate of around 63%, with only 50% of TB cases in Africa being detected (8). The delayed diagnosis has serious consequences since one untreated pulmonary case can raise the chances to be epidemic (9-10). To prevent such problems, a diagnostic tool is desirable that is less dependent on the laboratory facilities or demand for specialized training. It has been assessed that a single diagnostic test offering 100% accuracy could save around 625,000 lives per year if widely employed, and a test with only 85% sensitivity and 97% specificity might save 392,000 lives or 22.4% of the current annual worldwide deaths (11). These numbers signify that there is a pressing need to develop new POC diagnostic tools to reduce the number of fatalities and the costs incurred due to growing health concerns.

As health care costs are growing and with an aging world population (12), there is a cumulative need to remotely monitor the health disorder of patients. This takes the account of situations where patients are not confined to hospitals. To report this issue, a variety of POC system prototypes have been developed. Such systems provide a real-time response to the health condition of patients, either to a medical database accessible to health care providers to the patients themselves. Thus, POC systems establish a new approach to address the issue of

monitoring and managing the health of patients suffering from chronic diseases, postoperative patients and elderly people by executing tasks that are conventionally performed using laboratory testing (13-14).

The keystones for biosensors to emerge as the immense potentiality in medical diagnostics in improving patient care through real-time and remote health monitoring are their simplicity in operation, higher sensitivity, utilization of small amount of biological samples, ability to perform multiple analysis and capability to be integrated with different function on the same chip (15). Witnessing, the market trends, it is clearly indicated that there is increasing the growth rate of POCT and home health care diagnostics where biosensors play a key role. Looking at biosensor market, the biggest fraction and sale is achieved for point of care testing and home diagnosis when compared to other biosensor industry. The statistics of biosensor are 7.3 billion dollars in 2003, which has increased up to 10.2 by 2007 (16). POC systems for health monitoring consists of different types of biosensors that are implantable or wearable and effective in measuring physiological parameters such as heart rate, changes in plasma protein profile, patterns of multiple biomarkers and oxygen saturation. The sensed information is then transferred through a wired or wireless link to a central data acquisition node, for example, a Personal Digital Assistant (PDA), which can, in turn, transmit the sensed signals to a medical center (17). These systems would not only reduce response time but would also make testing available in environments where laboratory testing is least feasible (18). These systems not only have applications in medical diagnostics and biological warfare agent detection (19), but the sensor configuration can be modified to suit other applications, such as food quality assurance (20), environmental monitoring (21), and industrial process control (22-23). Other probable applications are also emerging, which includes the identification of animal and plant pathogens, water purity analysis, diagnostic testing in case of malarial strains and field tissue and gene analysis (18). Additionally, early diagnosis of critical health changes could empower the prevention of fatal events (24). Such early diagnosis requires uninterrupted monitoring, yet current physiological sensing systems are unsuitable for long-term, recurrent, unobtrusive and low-cost health monitoring. The next generation of POC biosensor systems could enable better early detection of critical changes in a patient's health condition. Hence, POC biosensor systems are expected to act not only as data collection systems, but they must also learn the health baselines of individual patients and discover problems autonomously by detecting alarming health trends using advanced information processing algorithms. Also, next-

generation POC systems should satisfy certain medical criteria while operating under several ergonomic constraints and significant hardware resource limitations. Designing such systems is a very challenging task since a lot of highly constraining and often conflicting requirements have to be considered. Specifically, the design needs to take into account size and weight factors; also, its presence should not hinder a patient's actions. Furthermore, radiation concerns and other issues need to be accounted for. Also, the security and privacy of the collected clinical data must be guaranteed, while system power consumption must be minimal in order to increase the operational life of the system (25-26).

Biosensors are analytical devices that transform a biological response into a detectable physical signal (27). The biosensor can detect, record and transmit information regarding a physiological change or the presence of various chemical or biological materials in the environment. The term biosensor was coined by cammann (28) and is defined as chemical sensor where the recognition method utilizes a biochemical mechanism (29-30). Biosensors are extremely specific and are independent of physical parameters such as pH and temperature and should be eco-friendly (31-32). The role of biosensors in the field of medical science towards the application of early stage detection of human diseases has become the important aspect. The basic characteristics of the biosensor comprise of linearity which should be high for the detection of high substrate concentration, sensitivity, selectivity: the chemical interference must be minimized for obtaining reliable results and response time. The potential advantages of biosensors in medical applications include high specificity, linear response, biocompatible, ease of use, durability, require small sample volume, stable, rapid and accurate response. In spite of huge and fast growing research in the area of the biosensor, still intriguing problems like processing single analyte at a time, difficulty in handling with interfering agents, prior analyte processing for high sensitivity and low throughput detection need their amicable solutions. In order to overcome we need highly sensitive and high throughput detection and is good if it is biocompatible with imaging technologies. To achieve this, optical detection system has caught much attention for its high sensitivity and if this is incorporated with microarray technology can achieve high throughput detection also.

## 1.1. Optical Biosensors

Optical biosensors are potential devices which are alternative to conventional analytical methods due to their small size, high sensitivity, high specificity and cost effectiveness (33). Optical biosensors comprise of the light source along with optical components to produce desired light source and direct this light to a modulating agent which is a modified sensing head along with photodetector (34). Though promising developments in the field of optical biosensors have been reported, there are fewer reports about their use in the practical field (35). The research and technological development of optical biosensors have exhibited the exponential growth and has a unique potential for real-time, direct and label-free detection of various biological and chemical analytes (36). A multidisciplinary approach along with MEMS, nano-bio technology, molecular biology, microelectronics and chemistry is required for the design and implementation of new devices (37). Optical biosensors are the potential candidates which can accommodate all the above-mentioned requirements. The applications of optical biosensors range from the field of medicine, biotechnology and environment having their own requirements in terms of analyte concentration to be measured, sample concentration, required precision output, the time taken to complete the probe, cleaning requirements and to enable reuse of biosensors (38). Optical detection is based on exploiting the interactions between biological recognition element and optical field. Optical bio sensing can be divided into two categories: label -free and label based sensing. In the label-free mode, the signal detected is due to the interaction of analyzed material with the transducer. On the other hand, label based sensing involves the use of a suitable label and the signal is then generated in the form of a fluorescence emission or color change. An optical biosensor is a compact device comprised of a bio recognition element integrated with an optical transducer which converts the result of binding interactions between the biomolecule and bio-recognition element into measurable optical signals such as fluorescence, color change or chemiluminescence responses. The basic principle involved is to produce the signal which is appropriate to the concentration of the analyte. This biosensor can use numerous biological materials like enzymes, receptors, antigens, antibodies, whole cells and tissues and nucleic acids as bio recognition elements (39). Since the detector is the most important tool of biosensors, various detection methods such as surface plasmon resonance, wave fluorescence, optical waveguides and fluorescence detection are used to detect the interactions between the bio-recognition elements with the analyte. Amongst all of the detection methods, fluorescence detection has been most widely utilized in

biomolecular imaging for the detection of trace amounts of analytes due to their high sensitivity (40).

Fluorescence detection is the most widely used analytical tool used in biological studies utilized for quenching and re-appearance of fluorescence in presence of biomarker. The instrumentation in this field has greatly enhanced and possible to detect fluorescent molecules or single photons. Fluorescent biosensors are potentially used as imaging agents in cancer and drug discovery. Various types of fluorescent biosensors were constructed by many researchers in past decade based on fluorescence ON and OFF biosensors which include biological macromolecular receptors such as proteins (41) and aptamers (42). One example with fluorescence OFF mode where fluorophore (OG-Oligreen) displacement is taking place upon aptamer binding. This sensor specifically detects the $K^+$ ion over many other cations such as $Na^+$, $Li^+$, $Mg^{2+}$, $Ca^{2+}$ etc. with a detection limit in nM range (43). A schematic model for fluorescence ON biosensing has been shown in figure 2.

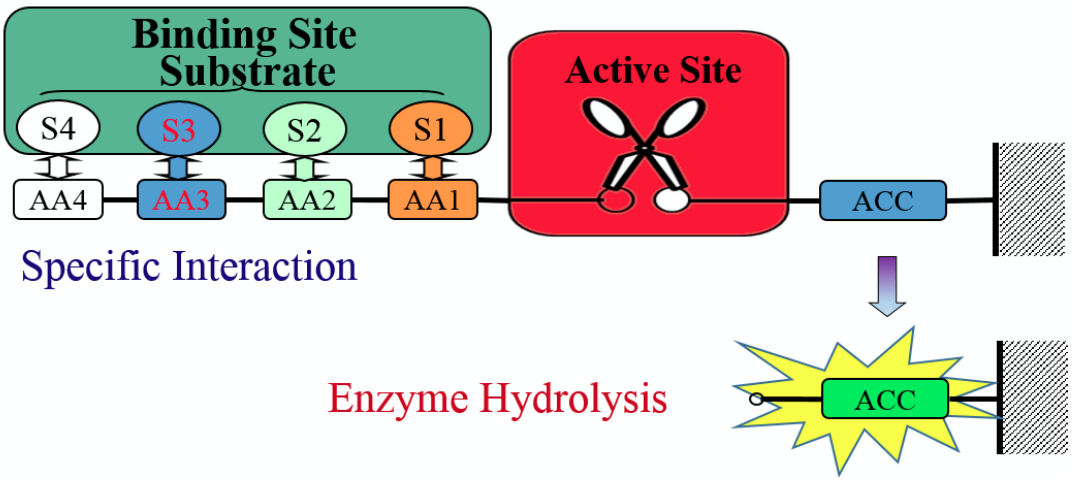


Figure 2. Schematic representation for the fluorescence ON biosensor

The construction of fluorescent biosensors relies on the following method. In the first step, there is a need for suitable macromolecule receptor with appropriate specificity and affinity to the target. The second step involves the integration of signal transduction function persuaded by molecular recognition event (44). Fluorescent biosensors are small frameworks on to which one or several fluorescent probes are mounted chemically, genetically or enzymatically through a receptor. The receptor involves in identifying a specific analyte thereby generating a

fluorescence signal which is readily detected and measured (45). Fluorescence Resonance Energy Transfer (FRET) between the two chromophores leads to quenching of the fluorescence emanating from a fluorophore and has been widely used in the biosensor development. Quenching this fluorescence by FRET demands not only the presence of two fluorophores within the Forster radius but also there should be sufficient spectral overlapping between their electronic absorption and fluorescence emission spectra. Different types of FRET systems have been widely utilized for the development of fluorescence biosensor. For example utilization of self-quenching, where the probe is labeled with the same fluorophore which possesses weak fluorescence. Moderate fluorescence is exhibited by the interaction of the fluorophore with protein molecules and hetero FRET where the probe is labeled with two different fluorophore moieties. Hetero FRET system is best and most efficient. Once these are de-quenched they exhibit enhanced fluorescence representing fluorescence ON bio sensing (46).

Fluorescent biosensors are commonly used in drug discovery in order to identify drugs by high content screening, high-throughput. These biosensors and detection methods are considered as potential tools for preclinical evaluation, pharmacokinetics and bio-distribution candidate drugs (47-48). Fluorescent biosensors are efficiently employed in the early detection of biomarkers in clinical and molecular diagnostics, for monitoring disease progression and response to treatment or therapeutics (49). An illustration of genetically-encoded FRET-based biosensor has been reported for the detection of Bcr-Abl kinase activity employed on cells of a cancer patient to assess Bcr-Abl kinase activity and to establish an interrelation with the disease status in chronic blood cancer (leukemia). This probe was further engaged to regulate the onset of drug-resistance cells and response to therapy in order to obtain the prediction for alternative therapeutics (50-51). In an interesting review by Ren and Ai, there is an in-depth discussion about the utilization the redox probes based on fluorescent proteins (52). In this review, genetically encoded probes susceptible to the redox processes in biological systems has been discussed in detail along with their merits, demerits, molecular mechanisms providing ironic information to biologists for the use of redox fluorescent probes in their studies. Benčina offers a thorough summary of genetically encoded pH probes, which are based on fluorescent proteins (53). Both ratiometric and intensity based probes are summarized in this study. Their instrumentation steps, spectral properties and pH of intracellular organelles are also discussed. This review will support researchers in selecting pH-sensitive fluorescent protein for their

specific experiments. In this issue, Benčina and coworkers contributed a research article (54), which reports a high-throughput technique built on ratiometric flow cytometry to detect the single-cell analysis of HIV protease activity. In order to meet the requirements, at first, the development of HIV protease sensor from a pair of fluorescent proteins, mCerulean and mCitrine was conducted and developed sensor was utilized for HIV protease inhibitor screening assays and intracellular quantitative detection of HIV protease activity.

Bodart *et al.*, in their study, reported that the sensor developed exhibits the enhanced dynamics ranges to image Epidermal Growth Factor (EGF) stimulation of living cells by utilization and optimization of fluorescent protein-based Extracellular signal-regulated Kinase (ERK kinase) probe model (55). The lifetime imaging and ratiometric mode were executed with this new probe which was the highlighted of this article. Campbell *et al.*, described regarding mutagenesis studies on CH-GECO2.1, which is red fluorescent protein-based $Ca^{2+}$ ion sensor constructed by their group (56). A large variety of mutants were designed and characterized, leading to the identification of a key residue, Gln163, which is known to involve in the conformational change that transduces $Ca^{2+}$ binding leading to change in fluorescence emission. They also emphasized that the interfaces and inter-domain linkers play an important role for binding affinities of these chimeric $Ca^{2+}$ sensors. Aliaga *et al.* reported two synthetic coumarin-based "turn-off" fluorescent probes towards the detection of $Cu^{2+}$ and $Fe^{3+}$ ions (57). Both metal ions exhibited quenched fluorescence of the two dye molecules. The $Cu^{2+}$ and $Fe^{3+}$ ions in human neuroblastoma SH-SY5Y cells were imaged by utilizing epifluorescence microscopy.

Conventionally, FRET-based biosensor using visible fluorescent molecules is influenced by auto-fluorescence from the clinical samples like blood, serum or other body fluids leading to low signal to noise (SN) ratio and attainment of high sensitivity is hampered significantly. A FRET biosensor utilizing near infraed (NIR) fluorescent and quencher molecules can easily detect the resulting fluorescence signals from the body of several 10 cms from a detector outside the body with high SN ratio (high sensitivity). This means that it is very suitable for pathological imaging in vivo. In order to increase the sensitivity of the biosensor using NIR-FRET, it is desirable that the wavelengths of the dye absorption and fluorescence emission should perfectly match. It is also necessary to adjust the peptide sequence of the

enzyme active site so that the position of the quenching group and the fluorescent group are within the Forster radius. A biosensor based on NIR probe is advantageous for high sensitivity in terms of not being easily influenced by auto-fluorescence of water or biomolecules and high tissue penetrability of near-infrared rays. At the same time, by changing the peptide sequence between the dyes having fluorescent groups and quenching groups in different wavelength ranges, it is possible to control the absorption wavelength specifically for the enzyme. In the development of NIR-FRET biosensor, development of NIR dyes (fluorescent group and quenching group) and design of enzyme recognition site are necessary. Current thesis gives the insights about the synthesis and characterization of NIR dyes with varying wavelengths. Apart from this, efforts have also been made to evaluate amino acid sequences that are selective for specific enzymes and incorporating them to develop model NIR probe to demonstrate their application towards fluorescence biosensing.

## 1.2. Types of fluorescent molecules used in biosensors

Dyes that are active in NIR region have caught much attention due to their diverse applications in biological and biomedical-related fields. The potential advantages of these dyes include minimal interfering absorption and fluorescence from biological analytes, low-cost laser diode excitation, reduced scattering and enhanced tissue penetration depth. However, there are relatively few class of molecules that are readily available as NIR dyes towards their application in fluorescence biosensors. These include squaraine dyes, cyanine dyes and phthalocyanine dyes. Figure 3, clearly indicates that biological tissues and fluids have several orders of magnitude lower light absorption in the NIR wavelength (700-900 nm) region as compared that of their visible region counterparts. The absorption spectra of human hand demonstrate that hand is transparent to light of wavelength between 700 t0 900 nm. Therefore, this region is known as the diagnostic window (58). The report given by Frangioni John V et al gives the complete image about the need of the development of NIR fluorophores for FRET systems (59). The significant advancements have been achieved on the recent development of NIR dyes with enhanced chemical and photostability, high fluorescence intensity and long fluorescent lifetime. A variety of dyes has also been designed and synthesized with improved water soluble property in order to avoid aggregation in biological systems and tissues. These class of dyes holds promise as suitable candidates for biomedical imaging and biosensing applications.

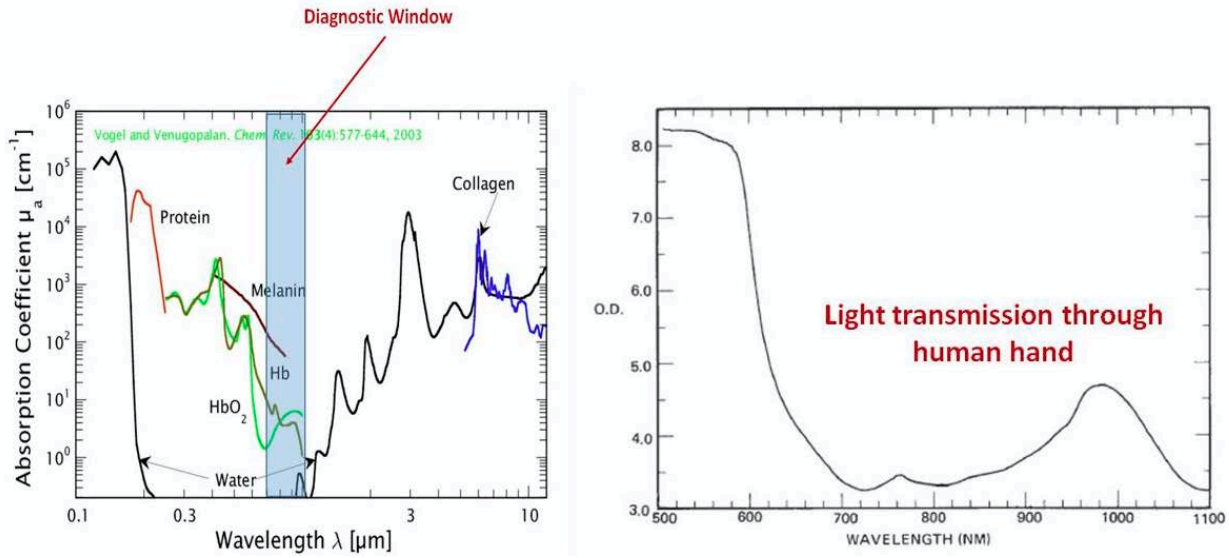


Figure 3. An example of NIR spectral window on measuring biological tissues. Within the therapeutical window, wavelength specific sensitivity to oxy and deoxyhemoglobin are measured and optical properties of absorption and scattering are quantified (left) and Absorption spectra of Human hand (right).

### 1.2.1. Squaraine Dyes

Squaraines consist of an oxocyclobutenolate core with heterocyclic and aromatic components at either end of the molecule. Squaraine dyes are considered as far-red sensitizers due to their superior physio-chemical properties such as good photoconductivity, intense absorption near 600 to 700 nm and high molar absorption coefficient (60). An important property of water solubility of conventional squaraines still remains an important challenge due to their large and planar hydrophobic π-conjugated molecular structure. To overcome the above-mentioned limitation Suzuki et al (61) designed a dye KSQ-4-H by introducing four sulfonate moieties to enhance the solubility of dyes in phosphate buffer solution (PBS) with sharp absorption. This dye is believed to be very favorable for in vivo imaging and protein detection. Later in the work reported by Nakazumi et al (62) who demonstrated a conjugate with two squaraine dyes linked through thiophene or pyrene unit to synthesize bis-squaraine dyes. These bis-squaraine dyes exhibited enhanced fluorescence in NIR region once they bind to Bovine serum albumin (BSA). In the recent work reported by Gassensmith et al (63) wherein a squaraine dye with two rotaxanes has been demonstrated. A rotaxane with four tri(ethyleneoxy) chains on squaraine is to improve water solubility and another rotaxane that possess an encapsulating macrocycle is

to improve stability. In his article, it has been also reported that these type of squaraines exhibit high stability in different solvents indicating a potential fluorescent scaffold for constructing various types of NIR imaging probes. In the present investigation, a series of squaraine dyes have been designed by logical molecular design and synthesized with different alkyl chains and substituents at 'N' position of indole producing absorption and emission in the range of 650 to 672 nm. In order to explore their potential application as fluorescent probes to sense protein in phosphate buffer solution (PBS), these dyes were employed to investigate their interaction using (BSA) and thereafter to utilize these dyes as good fluorophores in the FRET-based probes to detect the fluorescence enhancement upon hydrolysis of an enzyme.

### 1.2.2. Cyanine Dyes

Cyanine dyes are the class of molecules with aromatic heterocyclic rings linked through a polymethine bridge. The monomethine and trimethine cyanines fall their absorption in the visible region, but by each extension of one vinyl group a bathochromic shift of about 100 nm can be achieved. Therefore, pentamethine (Cy5) and heptamethine (Cy7) derivatives display their absorption in the NIR wavelength region. The Cy5 and Cy7 dyes have been utilized widely as active ingredients in bio-probes for nucleic acids and proteins (64). Indocyanine green (ICG) has been approved by FDA for evaluating blood flow and clearance. However, many cyanine dyes suffer due to low quantum yield, photostability, undesired aggregation and mild fluorescence in aqueous solutions (65). With the continuous research on cyanine dyes, significant progress has been achieved to overcome these limitations. The studies led to the discovery that the introduction of rigid cyclohexenyl substitution in the middle of the Polymethine Bridge can increase the photostability and quantum yield (66).

Peng et al (67) have demonstrated the photostability of newly synthesized 3H-indocyanine dyes with different N-substituents and found that the presence of electron withdrawing group at N-position strongly affects the photostability of dyes and whereas the presence of electron donating substituent is much favorable to obtain dyes with refining photochemical stability. Other studies of cyanine dyes revealed that the efficiency of fluorescence is greatly increased upon binding with nucleic acids and proteins (68). In recent studies, some cyanine dyes by an introduction of carboxyl or sulfonic acid groups have been discovered with strong fluorescence, enhanced improvement in water solubility and large stoke shift (69). Strekowski and co-workers (70) have developed dyes containing two cyanine subunits which exhibit negligible fluorescence but fluorescence signal was highly pronounced upon their binding with proteins.

Grag et al (71) reported a zwitterionic heptamethine cyanine dye which showed its advantages towards in vivo applications such as ultra-low non-specific tissues, no serum protein binding and high signal to noise ratio after conjugation with tumor targeting ligands.

Therefore, the above-discussed literature and review helps researchers to design versatile group of cyanine dyes by incorporating electron donating and withdrawing groups, alkylation at N-positon of indole ring, alkylation with different substituents at the terminal and by varying vinyl chain length to obtain remarkable photophysical behavior of dyes. In this current investigation, we had designed heptamethine cyanine dyes with –COOH group at one end of the indole ring and substituents like –OH, -Br and –I to study the electron withdrawing, donating and heavy ion effect on interacting with Bovine Serum Albumin (BSA) as a model protein to utilize these dyes as good quenchers in FRET-based bio-probes.

### 1.2.3. Phthalocyanines

Phthalocyanines are a class of molecules with two-dimensional 18π-electron aromatic porphyrin derivatives, composed of four bridged pyrrole subunits linked through nitrogen atoms. The fundamental chromophore of phthalocyanine is (4n+2) π electron cloud in its ring moiety providing strong delocalization to the π-electrons around their perimeter. Phthalocyanines are stable chemically and thermally and also support intense electromagnetic radiation due to their electronic delocalization. In order to allow the fine-tuning of physical properties of phthalocyanines, the two central H atoms can be replaced by several metal ions and varying substituents can be incorporated both at the peripherals of the macrocycle and axial positions (72) to control their optical behavior.

These unique tuning of physical properties led phthalocyanines and its derivatives to utilize them as not only dyes but also molecular materials used in electronics (73) biomedicine (74) and optoelectronics (75). Phthalocyanines though possess long π-π electronic conjugation which provides good photostability and strong absorption band, which falls often below 700 nm. Studies revealed that incorporation of benzene ring enables Phthalocyanines to tune their absorption from visible to NIR spectral regions. In spite of their wavelength tuning and unique physical properties, phthalocyanines were less explored for their application in bioimaging due to their ease of aggregation in biological systems. Tremendous enhancement in advancing and tuning the physical properties of phthalocyanines towards their application in bioimaging and

potential utilization in cancer therapy (76-82), in this current dissertation, we focused on two classes of NIR molecules namely squaraine and cyanine dyes mainly.

## 1.3. Bovine Serum Albumin (BSA) as Protein model

The most recognized type of albumin is serum albumin. It is utmost common in the blood or serum but it may also appear in other fluid compartments. Serum albumin is the most abundant protein in blood plasma and is produced in the liver. It forms a large proportion of all plasma protein and acts as the transporter and disposition of many drugs. The specific type of albumin proteins includes Human Serum Albumin (HSA) and Bovine Serum Albumin (BSA). The human version is human serum albumin, and it normally constitutes about 60% of human plasma protein. In general, albumin play the significant role in the human and animal body. BSA has been frequently used as a model protein for investigating protein folding and ligand binding mechanism (83). In this regard, Bovine Serum Albumin (BSA) has been studied extensively, partly because of its structural homology with Human Serum Albumin (HSA) (84-85).

BSA is a globular protein composed of 3 structurally similar domains, each, in turn, possess two sub-domains which are stabilized by 17 disulfide bridges. It is acknowledged that heterocyclic and aromatic ligands were observed to bind hydrophobic sites in subdomains IIA and IIIA which are known as the site I and II respectively. The intrinsic fluorescence property of BSA protein is considered to be originating from the tryptophan (Trp), tyrosine (Tyr), and phenylalanine (Phe) residues (86). When it interacts with new compounds, its intrinsic fluorescence property regularly changes with that of ligand's concentration. The specific interactions of dye with BSA originates from the presence of two structurally selective binding sites, a namely the site I and site II. The binding affinity offered by site I is purely hydrophobic interactions whereas the site II involves a combination of hydrophobic, hydrogen bonding and electrostatic interactions (87). Thus the mechanism of interactions between ligands and proteins can be studied by employing fluorescence spectroscopy technique (88).

## 1.4. Aim and Motivation of Thesis

Biosensors have become a major scientific interest with a huge potential application towards POCT devices for the monitoring of healthcare and medical diagnostics owing to their ease of handling, eco-friendliness and use of small amount of analytes. The major applications of biosensors include monitoring glucose level in diabetes patients, food analysis, environmental application, drug discovery, protein engineering, the study of biomolecules and their interactions, industrial process control medical diagnosis and waste management treatment.

Though different types of biosensors were developed in past and are commercially available as well, the most successful story for a biosensor is with the detection of glucose level by Glucose Biosensor. In spite of the fact that enzyme based biosensors are extensively used, the limitations such as loss of activity during immobilization and interference from other analytes should be considered for developing the robust biosensor. A variety of microbial sensors were also developed towards the application in the environmental, food and biomedical arena, but the design and development of highly satisfactory sensor are still hampered due to their long response time, low sensitivity and poor selectivity. With the enhanced knowledge of improved recombinant DNA techniques and genetic information of microbes, an efficient fast responsive and the extremely selective sensor can be designed.

In the aspect of immune-sensor, the studies are yet to be explored in two different outlines. Firstly the construction of immunosensor arrays to monitor antigen-antibody reactions and secondly the expansion and acceleration of antibody production through recombinant techniques. The important prerequisite for the development of highly sensitive and satisfactory ion channel sensor is still hampered in the aspect of improving the stability of bilayer membrane which governs as ligand-gated ion channels. DNA based biosensors were motivated by their application to clinical diagnosis, forensic investigations, and genome mutation detection. Though different types of DNA sensors were designed based on electrochemical and piezoelectric sensors to detect and bind complementary strands of DNA to an analyte, scope and ability to recognize a change in single nucleotide signifies a remarkable development and promising challenges for geno-sensor technology. Limitations of different types of electrochemical-based biosensors include short shelf life of sensor, cross-sensitivity due to interference with other components present in the system, sensors tolerate limited temperature range and low humidity and high temperature leads sensor electrolyte to dry out, therefore,

greater exposure of the sensor to specific targets shortens the life span.

Considering the above-mentioned limitations with different types of biosensors, optical biosensors have emerged as potential candidates for the POCT devices due to their small size, flexibility to use in various applications and fast response, no electrical device interactions and good biocompatibility. The technological development of optical based biosensors met exponential growth due to their unique potential for real time monitoring, direct and label-free detection of different analytes. Although optical sensors are strong contenders for POCT devices due to the existing challenges such as utilization of single analyte at a time, sensitivity towards interfering agents, prior analyte processing for high sensitivity and low throughput are to be considered. To overcome these limitations, we need sensitive high-throughput detection and is best if it is compatible with the imaging process.

The aim of the current thesis is to focus on fluorescence-based sensing by design and development of novel sensitive fluorescent probes for the detection of the target enzyme. Detection of fluorescence is rather more sensitive as compared to its optical detection counterparts and if it is compatible with the microarray technology, high-throughput detection can also be ascertained. Of course, NIR dyes have been a material of choice, because of their features like high potential for in-vitro/in-vivo Bio-imaging, good tissue penetration depth, lower noise due to auto-fluorescence of biological components, the possibility of direct use of biological fluids and last but not least is the possibility of simultaneous multi-color and multi-target detection. Taking these advantageous features of NIR dyes into consideration, efforts have been directed to design and develop NIR fluorescent dye molecules with wavelength tunability to develop bio-probe. Prior to FRET application, these dyes were subjected to the investigation of their interactions of BSA which is most versatile protein model to understand their biocompatibility. Finally, a one-pot dye-peptide conjugate (SQ 1 PC) was synthesized and its efficient fluorescence quenching was demonstrated which led to the fluorescence ON biosensing in the presence of the enzyme.

## 1.5. Organization of Present Thesis

This thesis explores and displays the synthesis of far-red and near infra-red sensitive squaraine and cyanine dyes respectively. The effort had been made to utilize these dyes for interactions with biomolecules to understand the effect of substituents and their aggregation behavior on complexed with serum albumin.

The first chapter describes the role of biosensors in the field of medicinal science towards the application of early stage detection of human diseases. The current status and necessity of biosensors in various fields are also discussed from clinical on-site treatment using Point of Care testing (POCT) devices along with merits and demerits of different types of biosensors which are developed towards the application. This chapter highlights the significant research and technological development of optical biosensors which met exponential growth for real-time detection of various biological and chemical analytes. This chapter also highlights current status and development of fluorescent biosensors in order to overcome the limitations such as autofluorescence from biological samples, high sensitivity and throughput detection.

The second chapter deals with the details of instruments, techniques and characterization methods used in this current thesis.

The third chapter summarizes the successful synthesis of direct carboxy ring functionalized symmetrical NIR squaraine dyes (**SQ-1, SQ-2, SQ-3 and SQ-4**) from their respective quaternary heterocyclic ammonium salt containing N-alkylated group and effort had been made in order to explore their potential application as fluorescent probes to sense protein in phosphate buffer solution (PBS), these dyes were subjected to investigate their interaction using Bovine serum albumin (BSA) as a model protein to observe the influence of alkyl chain with varying functional groups of the dyes.

The fourth chapter summarizes the detailed synthesis and photophysical characterization of representative unsymmetrical NIR cyanine dyes bearing direct carboxyl functionalized indole ring at one end and whereas the other terminal indole ring was substituted with electron donating -OH and electronic withdrawing -I groups. The study had been made to investigate the behavior of these dyes on interaction with Bovine Serum Albumin as a protein model. These newly designed dyes bearing -COOH functionalized indole ring provide the capability of covalent coupling with biomolecules such as peptides, oligonucleotides and proteins to enhance their application potential as fluorescence probes.

The fifth chapter deals with the synthesis of unsymmetrical squaraine dye (SQ-1) bearing –COOH functionalized indole ring which facilitates its easy coupling with biomolecules. Near infra-red (NIR) sensitive and self-quenching fluorescent probe based on the dye-peptide conjugate (SQ 1 PC) was designed and synthesized by facile and efficient one-pot synthetic route for the detection of Elastase activity. The fluorescence of the peptide conjugate was self-quenched owing to the assembled fluorophores on the substrate-assisted by strong dye aggregation in phosphate buffer solution. Very fast and efficient fluorescence recovery was observed on hydrolysis of the peptide conjugate by elastase enzyme. This facile one pot synthetic strategy and possibility of wavelength tuning of squaraine dyes offers the potential application for the design and development of novel NIR probes for the efficient profiling of proteases.

## 1.6. References


1) J.L. Shaw, Practical challenges related to point of care testing, Practical Laboratory Medicine, 4 (2016) 22-29.
2) C. Sander, Genomic medicine and the future of health care, Science, 287 (2000) 1977-1978.
3) H.F. Willard, M. Angrist, G.S. Ginsburg, Genomic medicine: genetic variation and its impact on the future of health care, Philosophical Transactions of the Royal Society of London B: Biological Sciences, 360 (2005) 1543-1550.
4) S.A. Soper, K. Brown, A. Ellington, B. Frazier, G. Garcia-Manero, V. Gau, S.I. Gutman, D.F. Hayes, B. Korte, J.L. Landers, Point-of-care biosensor systems for cancer diagnostics/prognostics, Biosensors and Bioelectronics, 21 (2006) 1932-1942.
5) R. Etzioni, N. Urban, S. Ramsey, M. McIntosh, S. Schwartz, B. Reid, J. Radich, G. Anderson, L. Hartwell, The case for early detection, Nature reviews. Cancer, 3 (2003) 243.
6) R. McNerney, P. Daley, Towards a point-of-care test for active tuberculosis: obstacles and opportunities, Nature reviews. Microbiology, 9 (2011) 204.
7) W. Fox, G.A. Ellard, D.A. Mitchison, Studies on the treatment of tuberculosis undertaken by the British Medical Research Council tuberculosis units, 1946–1986, with relevant subsequent publications, The International Journal of Tuberculosis and Lung Disease, 3 (1999) S231-S279.

8) K. Lönnroth, K.G. Castro, J.M. Chakaya, L.S. Chauhan, K. Floyd, P. Glaziou, M.C. Raviglione, Tuberculosis control and elimination 2010–50: cure, care, and social development, The Lancet, 375 (2010) 1814-1829.
9) C. Lienhardt, J. Rowley, K. Manneh, G. Lahai, D. Needham, P. Milligan, K. McAdam, Factors affecting time delay to treatment in a tuberculosis control programme in a sub-Saharan African country: the experience of The Gambia, The international journal of tuberculosis and lung disease, 5 (2001) 233-239.
10) J. Golub, S. Bur, W. Cronin, S. Gange, N. Baruch, G. Comstock, R. Chaisson, Delayed tuberculosis diagnosis and tuberculosis transmission, The international journal of tuberculosis and lung disease, 10 (2006) 24-30.
11) E. Keeler, M.D. Perkins, P. Small, C. Hanson, S. Reed, J. Cunningham, J.E. Aledort, L. Hillborne, M.E. Rafael, F. Girosi, Reducing the global burden of tuberculosis: the contribution of improved diagnostics, Nature, 444 (2006) 49-57.
12) Y. Hao, R. Foster, Wireless body sensor networks for health-monitoring applications, Physiological measurement, 29 (2008) R27.
13) P. Bonato, Advances in wearable technology and applications in physical medicine and rehabilitation, Journal of neuroengineering and rehabilitation, 2 (2005) 2.
14) P. Bonato, Wearable sensors/systems and their impact on biomedical engineering, IEEE Engineering in Medicine and Biology Magazine, 22 (2003) 18-20.
15) S. Patel, R. Nanda, S. Sahoo, E. Mohapatra, Biosensors in Health Care: The Milestones Achieved in Their Development towards Lab-on-Chip-Analysis, Biochemistry research international, 2016 (2016).
16) http://www.grandviewresearch.com/industry-analysis/biosensors-market, http://www.sensorsmag.com/specialty-markets/medical/strong-growth-predicted-biosensors-market-7640
17) A. Pantelopoulos, N.G. Bourbakis, A survey on wearable sensor-based systems for health monitoring and prognosis, IEEE Transactions on Systems, Man, and Cybernetics, Part C (Applications and Reviews), 40 (2010) 1-12.
18) B. Feltis, B. Sexton, F. Glenn, M. Best, M. Wilkins, T. Davis, A hand-held surface plasmon resonance biosensor for the detection of ricin and other biological agents, Biosensors and Bioelectronics, 23 (2008) 1131-1136.
19) J.J. Gooding, Biosensor technology for detecting biological warfare agents: Recent progress and future trends, Analytica Chimica Acta, 559 (2006) 137-151.

20) L.A. Terry, S.F. White, L.J. Tigwell, The application of biosensors to fresh produce and the wider food industry, Journal of agricultural and food chemistry, 53 (2005) 1309-1316.
21) S. Rodriguez-Mozaz, M.J.L. de Alda, D. Barceló, Biosensors as useful tools for environmental analysis and monitoring, Analytical and bioanalytical chemistry, 386 (2006) 1025-1041.
22) A.J. Baeumner, Biosensors for environmental pollutants and food contaminants, Analytical and bioanalytical chemistry, 377 (2003) 434-445.
23) Y. Huang, M. Pecht, Arvind Sai Sarathi Vasan1, Ravi Doraiswami1, Dinesh Michael Mahadeo1.
24) N. Bourbakis, J. Gallagher, A synergistic co-operative framework of health diagnostic systems for people with disabilities and the elderly: a case study, in: Proceedings of the 12th WSEAS international conference on Computers, World Scientific and Engineering Academy and Society (WSEAS), 2008, pp. 730-735.
25) D. Raskovic, T. Martin, E. Jovanov, Medical monitoring applications for wearable computing, The computer journal, 47 (2004) 495-504.
26) U. Anliker, J. Beutel, M. Dyer, R. Enzler, P. Lukowicz, L. Thiele, G. Troster, A systematic approach to the design of distributed wearable systems, IEEE Transactions on Computers, 53 (2004) 1017-1033.
27) P. Mehrotra, Biosensors and their applications–A review, Journal of oral biology and craniofacial research, 6 (2016) 153-159.
28) K. Cammann, Bio-sensors based on ion-selective electrodes, Fresenius' Zeitschrift für Analytische Chemie, 287 (1977) 1-9.
29) D.R. Thevenot, K. Toth, R.A. Durst, G.S. Wilson, Electrochemical biosensors: recommended definitions and classification, Pure and Applied Chemistry, 71 (1999) 2333-2348.
30) D.R. Thévenot, K. Toth, R.A. Durst, G.S. Wilson, Electrochemical biosensors: recommended definitions and classification, Biosensors and Bioelectronics, 16 (2001) 121-131.
31) M. Bruchez, M. Moronne, P. Gin, S. Weiss, A.P. Alivisatos, Semiconductor nanocrystals as fluorescent biological labels, science, 281 (1998) 2013-2016.
32) I.L. Medintz, H.T. Uyeda, E.R. Goldman, H. Mattoussi, Quantum dot bioconjugates for imaging, labelling and sensing, Nature materials, 4 (2005) 435-446.

33) X.-L. Luo, J.-J. Xu, W. Zhao, H.-Y. Chen, Glucose biosensor based on ENFET doped with SiO 2 nanoparticles, Sensors and Actuators B: Chemical, 97 (2004) 249-255.
34) R.J. Leatherbarrow, P.R. Edwards, Analysis of molecular recognition using optical biosensors, Current opinion in chemical biology, 3 (1999) 544-547.
35) J.-C. Chen, J.-C. Chou, T.-P. Sun, S.-K. Hsiung, Portable urea biosensor based on the extended-gate field effect transistor, Sensors and actuators B: Chemical, 91 (2003) 180-186.
36) A. Soldatkin, J. Montoriol, W. Sant, C. Martelet, N. Jaffrezic-Renault, A novel urea sensitive biosensor with extended dynamic range based on recombinant urease and ISFETs, Biosensors and Bioelectronics, 19 (2003) 131-135.
37) L.M. Lechuga, F. Prieto, B. Sepúlveda, Interferometric Biosensors for environmental pollution detection, in: Optical Sensors, Springer, 2004, pp. 227-250.
38) D. Dey, T. Goswami, Optical biosensors: a revolution towards quantum nanoscale electronics device fabrication, BioMed Research International, 2011 (2011).
39) P. Damborský, J. Švitel, J. Katrlík, Optical biosensors, Essays in biochemistry, 60 (2016) 91-100
40) K. Johnsson, Visualizing biochemical activities in living cells, Nature chemical biology, 5 (2009) 63-65.
41) H.W. Hellinga, J.S. Marvin, Protein engineering and the development of generic biosensors, Trends in biotechnology, 16 (1998) 183-189.
42) J. Liu, Z. Cao, Y. Lu, Functional nucleic acid sensors, Chemical reviews, 109 (2009) 1948-1998.
43) R. E Wang, Y. Zhang, J. Cai, W. Cai, T. Gao, Aptamer-based fluorescent biosensors, Current medicinal chemistry, 18 (2011) 4175-4184.
44) K. Tainaka, R. Sakaguchi, H. Hayashi, S. Nakano, F.F. Liew, T. Morii, Design strategies of fluorescent biosensors based on biological macromolecular receptors, Sensors, 10 (2010) 1355-1376.
45) H. Wang, E. Nakata, I. Hamachi, Recent Progress in Strategies for the Creation of Protein-Based Fluorescent Biosensors, ChemBioChem, 10 (2009) 2560-2577.
46) H. Kobayashi, M. Ogawa, R. Alford, P.L. Choyke, Y. Urano, New strategies for fluorescent probe design in medical diagnostic imaging, Chemical reviews, 110 (2009) 2620-2640.

47) K.A. Giuliano, D.L. Taylor, Fluorescent-protein biosensors: new tools for drug discovery, Trends in biotechnology, 16 (1998) 135-140.
48) J.K. Willmann, N. Van Bruggen, L.M. Dinkelborg, S.S. Gambhir, Molecular imaging in drug development, Nature reviews Drug discovery, 7 (2008) 591-607.
49) M.C. Morris, Fluorescent biosensors—probing protein kinase function in cancer and drug discovery, Biochimica et Biophysica Acta (BBA)-Proteins and Proteomics, 1834 (2013) 1387-1395.
50) T. Mizutani, T. Kondo, S. Darmanin, M. Tsuda, S. Tanaka, M. Tobiume, M. Asaka, Y. Ohba, A novel FRET-based biosensor for the measurement of BCR-ABL activity and its response to drugs in living cells, Clinical cancer research, 16 (2010) 3964-3975.
51) A. Tunceroglu, M. Matsuda, R.B. Birge, Real-time fluorescent resonance energy transfer analysis to monitor drug resistance in chronic myelogenous leukemia, Molecular cancer therapeutics, 9 (2010) 3065-3073.
52) W. Ren, H.-W. Ai, Genetically encoded fluorescent redox probes, Sensors, 13 (2013) 15422-15433.
53) M. Benčina, Illumination of the spatial order of intracellular pH by genetically encoded pH-sensitive sensors, Sensors, 13 (2013) 16736-16758.
54) R. Gaber, A. Majerle, R. Jerala, M. Benčina, Noninvasive high-throughput single-cell analysis of HIV protease activity using ratiometric flow cytometry, Sensors, 13 (2013) 16330-16346.
55) P. Vandame, C. Spriet, F. Riquet, D. Trinel, K. Cailliau-Maggio, J.-F. Bodart, Optimization of ERK activity biosensors for both ratiometric and lifetime FRET measurements, Sensors, 14 (2014) 1140-1154.
56) H.J. Carlson, R.E. Campbell, Mutational analysis of a red fluorescent protein-based calcium ion indicator, Sensors, 13 (2013) 11507-11521.
57) O. García-Beltrán, B.K. Cassels, C. Pérez, N. Mena, M.T. Núñez, N.P. Martínez, P. Pavez, M.E. Aliaga, Coumarin-based fluorescent probes for dual recognition of copper (II) and iron (III) ions and their application in bio-imaging, Sensors, 14 (2014) 1358-1371.
58) S.B. Wigal, C.M. Polzonetti, A. Stehli, E. Gratton, Phase synchronization of oxygenation waves in the frontal areas of children with attention-deficit hyperactivity disorder detected by optical diffusion spectroscopy correlates with medication, Journal of biomedical optics, 17 (2012) 127002-127002.

59) J.V. Frangioni, In vivo near-infrared fluorescence imaging, Current opinion in chemical biology, 7 (2003) 626-634.
60) D.G. Devi, T. Cibin, D. Ramaiah, A. Abraham, Bis (3, 5-diiodo-2, 4, 6-trihydroxyphenyl) squaraine: A novel candidate in photodynamic therapy for skin cancer models in vivo, Journal of Photochemistry and Photobiology B: Biology, 92 (2008) 153-159.
61) K. Umezawa, D. Citterio, K. Suzuki, Water-soluble NIR fluorescent probes based on squaraine and their application for protein labeling, Analytical Sciences, 24 (2008) 213-217.
62) H. Nakazumi, T. Ohta, H. Etoh, T. Uno, C.L. Colyer, Y. Hyodo, S. Yagi, Near-infrared luminescent bis-squaraine dyes linked by a thiophene or pyrene spacer for noncovalent protein labeling, Synthetic metals, 153 (2005) 33-36.
63) J.J. Gassensmith, J.M. Baumes, B.D. Smith, Discovery and early development of squaraine rotaxanes, Chemical Communications, (2009) 6329-6338.
64) T. Ishizawa, Y. Bandai, N. Harada, A. Muraoka, M. Ijichi, K. Kusaka, M. Shibasaki, N. Kokudo, Indocyanine green-fluorescent imaging of hepatocellular carcinoma during laparoscopic hepatectomy: An initial experience, Asian Journal of Endoscopic Surgery, 3 (2010) 42-45.
65) R.P. Haugland, The handbook: a guide to fluorescent probes and labeling technologies, Molecular probes, 2005.
66) T. Górecki, G. Patonay, L. Strekowski, R. Chin, N. Salazar, Synthesis of novel near-infrared cyanine dyes for metal ion determination, Journal of heterocyclic chemistry, 33 (1996) 1871-1876.
67) X. Chen, X. Peng, A. Cui, B. Wang, L. Wang, R. Zhang, Photostabilities of novel heptamethine 3H-indolenine cyanine dyes with different N-substituents, Journal of Photochemistry and Photobiology A: Chemistry, 181 (2006) 79-85.
68) V.B. Kovalska, K.D. Volkova, M.Y. Losytskyy, O.I. Tolmachev, A.O. Balanda, S.M. Yarmoluk, 6, 6′-Disubstituted benzothiazole trimethine cyanines–new fluorescent dyes for DNA detection, Spectrochimica Acta Part A: Molecular and Biomolecular Spectroscopy, 65 (2006) 271-277.
69) L.-C. Zhou, G.-J. Zhao, J.-F. Liu, K.-L. Han, Y.-K. Wu, X.-J. Peng, M.-T. Sun, The charge transfer mechanism and spectral properties of a near-infrared heptamethine

cyanine dye in alcoholic and aprotic solvents, Journal of Photochemistry and Photobiology A: Chemistry, 187 (2007) 305-310.

70) L. Strekowski, Heterocyclic polymethine dyes: synthesis, properties and applications, Springer, 2008.

71) J.L. Gragg, Synthesis of near-infrared heptamethine cyanine dyes, (2010).

72) G. de la Torre, C.G. Claessens, T. Torres, Phthalocyanines: old dyes, new materials. Putting color in nanotechnology, Chemical Communications, (2007) 2000-2015.

73) M. Kimura, H. Ueki, K. Ohta, H. Shirai, N. Kobayashi, Self-organization of low-symmetry adjacent-type metallophthalocyanines having branched alkyl chains, Langmuir, 22 (2006) 5051-5056.

74) K. Záruba, J. Králová, P. Řezanka, P. Poučková, L. Veverková, V. Král, Modified porphyrin–brucine conjugated to gold nanoparticles and their application in photodynamic therapy, Organic & biomolecular chemistry, 8 (2010) 3202-3206.

75) G. De La Torre, P. Vázquez, F. Agullo-Lopez, T. Torres, Role of structural factors in the nonlinear optical properties of phthalocyanines and related compounds, Chemical Reviews, 104 (2004) 3723-3750.

76) Y. Tanaka, J.Y. Shin, A. Osuka, Facile Synthesis of Large meso-Pentafluorophenyl-Substituted Expanded Porphyrins, European Journal of Organic Chemistry, 2008 (2008) 1341-1349.

77) Y.S. Xie, K. Yamaguchi, M. Toganoh, H. Uno, M. Suzuki, S. Mori, S. Saito, A. Osuka, H. Furuta, Triply N-Confused Hexaphyrins: Near-Infrared Luminescent Dyes with a Triangular Shape, Angewandte Chemie International Edition, 48 (2009) 5496-5499.

78) M.K. Kuimova, H.A. Collins, M. Balaz, E. Dahlstedt, J.A. Levitt, N. Sergent, K. Suhling, M. Drobizhev, N.S. Makarov, A. Rebane, Photophysical properties and intracellular imaging of water-soluble porphyrin dimers for two-photon excited photodynamic therapy, Organic & biomolecular chemistry, 7 (2009) 889-896.

79) R.P. Briñas, T. Troxler, R.M. Hochstrasser, S.A. Vinogradov, Phosphorescent oxygen sensor with dendritic protection and two-photon absorbing antenna, Journal of the American Chemical Society, 127 (2005) 11851-11862.

80) V. Martos, P. Castreño, J. Valero, J. de Mendoza, Binding to protein surfaces by supramolecular multivalent scaffolds, Current opinion in chemical biology, 12 (2008) 698-706.

81) W.-D. Jang, N. Nishiyama, K. Kataoka, Supramolecular assembly of photofunctional dendrimers for biomedical nano-devices, Supramolecular Chemistry, 19 (2007) 309-314.
82) N. Nishiyama, W.-D. Jang, K. Kataoka, Supramolecular nanocarriers integrated with dendrimers encapsulating photosensitizers for effective photodynamic therapy and photochemical gene delivery, New Journal of Chemistry, 31 (2007) 1074-1082.
83) V.D. Suryawanshi, L.S. Walekar, A.H. Gore, P.V. Anbhule, G.B. Kolekar, Spectroscopic analysis on the binding interaction of biologically active pyrimidine derivative with bovine serum albumin, Journal of Pharmaceutical Analysis, 6 (2016) 56-63.
84) U. Mote, S. Bhattar, S. Patil, G. Kolekar, Interaction between felodipine and bovine serum albumin: fluorescence quenching study, Luminescence, 25 (2010) 1-8.
85) Y.-Q. Wang, H.-M. Zhang, G.-C. Zhang, W.-H. Tao, Z.-H. Fei, Z.-T. Liu, Spectroscopic studies on the interaction between silicotungstic acid and bovine serum albumin, Journal of pharmaceutical and biomedical analysis, 43 (2007) 1869-1875.
86) A. Papadopoulou, R.J. Green, R.A. Frazier, Interaction of flavonoids with bovine serum albumin: a fluorescence quenching study, Journal of Agricultural and Food Chemistry, 53 (2005) 158-163.
87) Jiménez MC, Miranda MA, Vayá I. Triplet excited states as chiral reporters for the binding of drugs to transport proteins. *Journal of the American Chemical Society.* 2005;127(29): 10134-10135.
88) Z. Chi, R. Liu, Y. Teng, X. Fang, C. Gao, Binding of oxytetracycline to bovine serum albumin: spectroscopic and molecular modeling investigations, Journal of agricultural and food chemistry, 58 (2010) 10262-10269.

# Chapter 2: Instrumentation and Characterization

## 2.1. Electronic Absorption Spectra

It refers to the use of ultraviolet (UV) and visible region of the electromagnetic radiations for getting the absorption and reflection properties of different materials such as transition metal ions, highly conjugated organic compounds, *etc*. The UV radiation ranges from 10 nm to 400 nm and visible radiation ranges from 400 nm to 760 nm. In electronic absorption spectroscopy, the electron is made to excite from an initial low energy state to a higher state by the photon energy provided by the spectrophotometer and is detected in the absorbance spectrum. The working principle of UV Spectrophotometer is shown in figure 1.

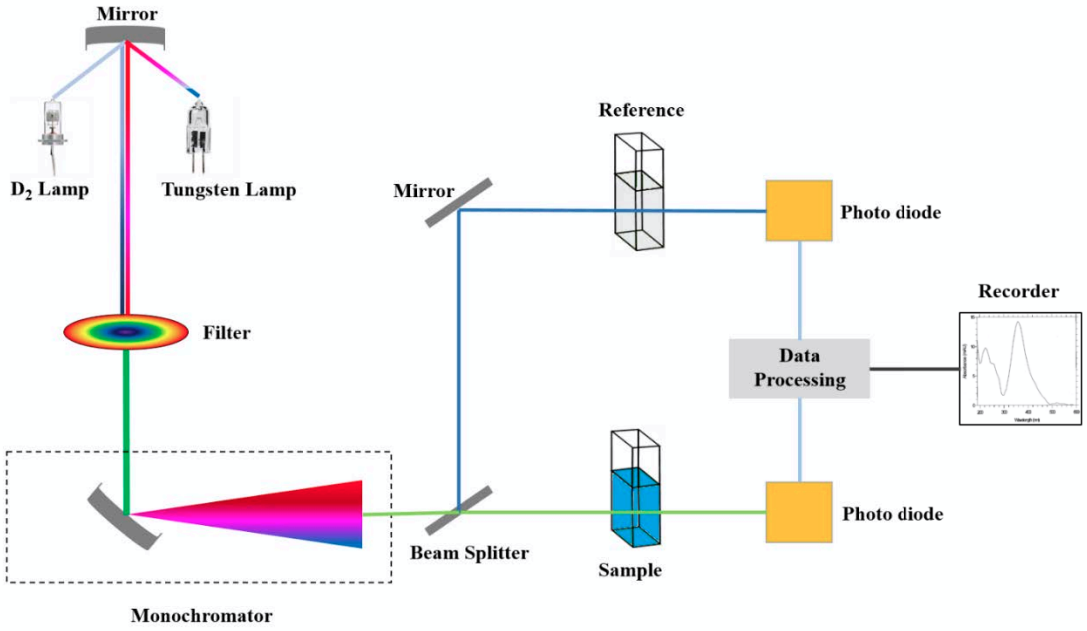


Figure 1. The working principle of UV-Vis Spectrophotometer

Absorbance is defined as a capacity of the substance to absorb light at the specified wavelength. Using absorbance of the substance one can calculate molar absorption coefficient of the substance. The molar absorption coefficient is a measurement to define how strongly a chemical species absorbs light at the particular wavelength. The units for molar extinction coefficient is expressed as $L.mol^{-1}.cm^{-1}$.

According to Beer lambert law

$$A = \varepsilon cl \ldots\ldots\ldots\ldots\ldots\ldots\ldots\ldots \text{[1]}$$

Where $\boldsymbol{\varepsilon}$ is molar extinction coefficient, $\boldsymbol{c}$ is the concentration of the substance, $\boldsymbol{l}$ is the path length of the cell.

**Equation 1 can be modified as**

$$\varepsilon = \frac{\boldsymbol{A}}{\boldsymbol{cl}}$$

Upon incidence of light on the material either gets reflected back or pass through or get absorbed. Absorbance is the difference the incident light ($I_0$) and transmitted light intensity (I). The absorbed light is either defined in terms of transmittance or absorbance. Light is guided through the sample and by detecting output light intensity absorbance is plotted as a function of wavelength is measured.


Figure 2. UV-Visible Spectrometer used in the present work

The presence of an absorbance band at a particular wavelength is used for identifying the material as the absorption peak is characteristic to a particular compound and therefore utilized to identify the material composition. The utilization of absorbance studies for characterization of material is very well reported (1-2). The model spectrophotometer used for the current study is JASCO V-670 as shown in figure 2.

## 2.2. Fluorescence Spectroscopy

Fluorescence spectroscopy is a kind of electromagnetic spectroscopy which analyzes fluorescence from a sample. Usually, an ultraviolet beam of light is used to excite electrons and cause them to emit light.

Molecules have different states referred as energy levels. Fluorescence is primarily concerned with vibrational and electronic states (3-4). The species is excited by absorbing a photon from its ground state to one of the different vibrational states in excited energy levels. The excited molecule loses it energy till it reaches the lowest state of excited energy level due to collision with other molecules. This process can be imagined with a Jablonski diagram as shown in figure 3a.

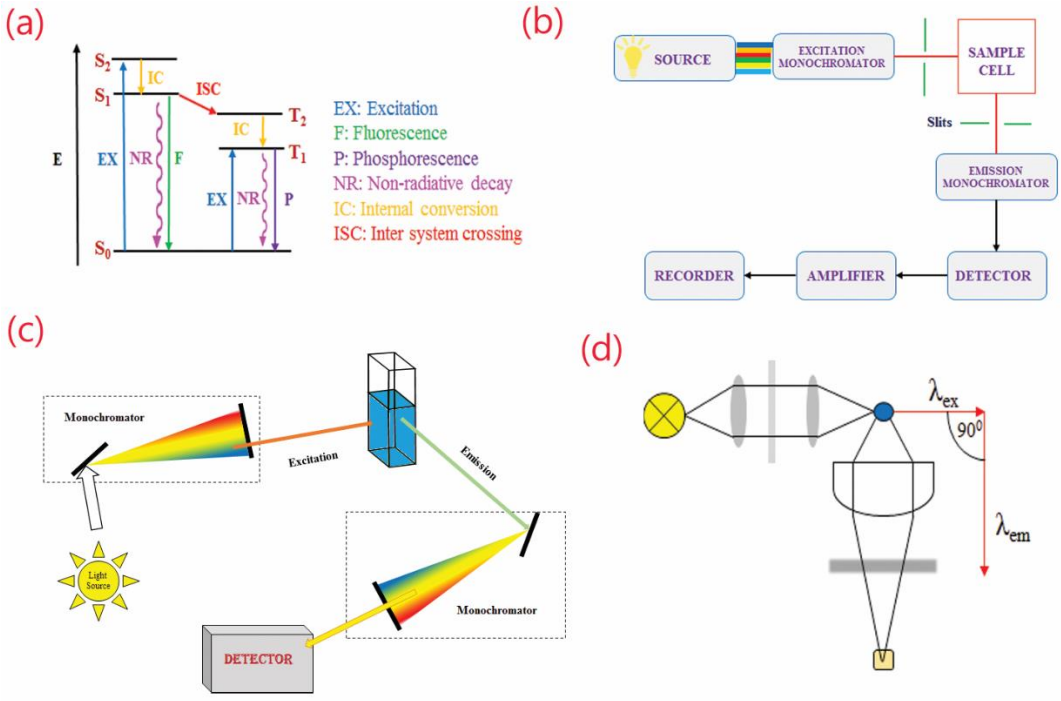


Figure 3 a) Jablonski diagram; b) Schematic representation of fluorescence spectroscopy; c) working principle of fluorescence and d) simple design of components of fluorimeter.

The molecule then drops to one of the different vibrational levels of ground electronic states by emitting a photon. The emitted photon will have different energies and frequencies. Therefore by analyzing the different frequencies of emitted light and their intensities, the

different vibrational levels of the structure can be determined. In emission measurement, the excitation wavelength is fixed and the detection wavelength is varied.

The light from the excitation source passes through a Monochromator or filter which strikes the sample. The incident light is absorbed by the sample and molecules get fluoresce. A proportion of this fluorescent light passes through the second monochromator of a filter and reaches detector which is placed in the right angle to the incident beam light. There are different types of light sources which can be used as excitation light sources which include, xenon arc lamp, mercury-vapor lamp, lasers and Led lights. The use of monochromator is to transmit light of an adjustable wavelength with regulating tolerance. The detectors used in fluorescence spectroscopy are of single-channeled or multi-channeled. The single –channeled detector can detect the intensity of one wavelength whereas multi-channeled detects the intensities of different wavelengths. The schematic representation, working principle and design of components of fluorimeter are shown in figure 3 b, c and d respectively.


Figure 4. Fluorescence spectrophotometer used in current thesis.

In this current thesis, the fluorescence spectroscopy is used to determine the quantum yield and fluorescence lifetime of synthesized NIR unsymmetrical cyanine and Far-red sensitive symmetrical and unsymmetrical squaraine dyes. Fluorescence spectroscopy is also used to determine the binding interactions of the dyes with BSA as a protein model and hence binding constant was calculated. The model fluorescence spectrophotometer used in this current thesis is Jasco FP-6600 shown in figure 4.

## 2.3. Fourier Transform Infrared (FTIR) Spectroscopy

Infrared spectroscopy involves the interaction of infrared radiation with matter. It is employed to study and identify chemicals, for a given sample which is of solid, liquid or gaseous. IR spectrum is basically a graph light absorbance with frequency or wavelength. The $cm^{-1}$ is the units in which the frequency is expressed. IR study involves triggering molecular vibrations through irradiation with infrared light. IR spectroscopy aides in providing the information about the presence of certain functional groups.

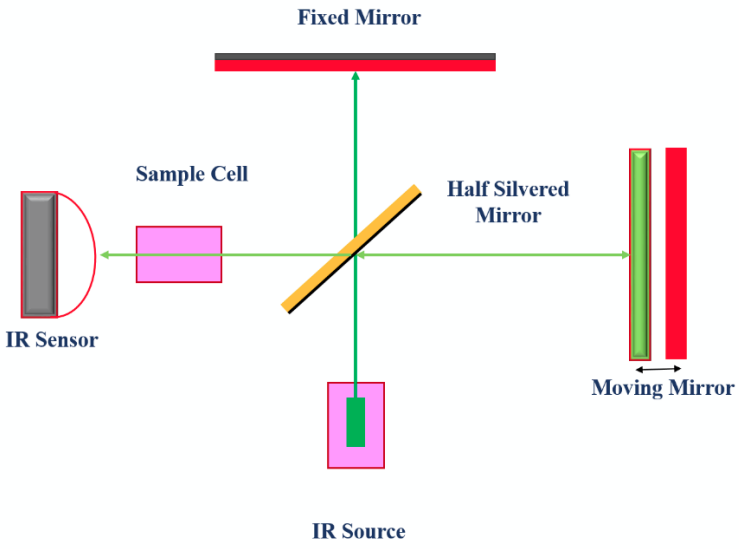


Figure 5. Schematic working principle of IR Spectroscopy

Infrared spectroscopy is based on the fact that when an infrared light is incident on the sample, the material absorbs specific frequencies characteristic of the bonds present. Upon incidence of infrared light the bonds or the functional groups present in the molecule vibrate and resonance occurs when the vibration frequency of incident light matches leading to absorption. These vibration frequencies are characteristic of a particular functional group or bond. Thus based on the absorbed vibration frequency the nature of the bond or functional group can be identified.

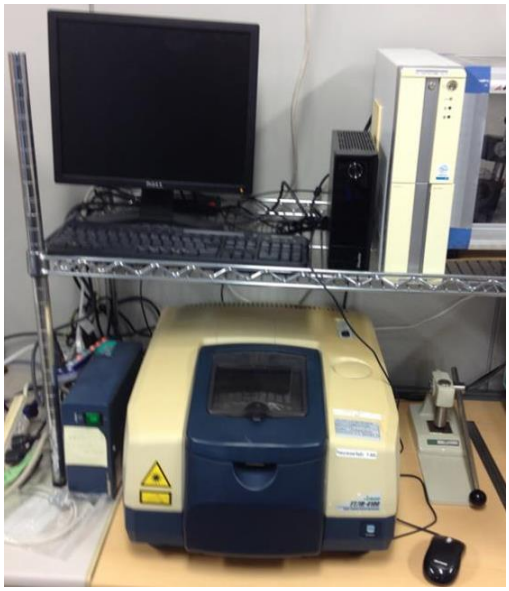

Figure 6. Fourier transform Infrared spectrometer used in this present work

In Fourier transform infrared (FTIR) spectroscopy infrared light is incident on the sample. The output light signal is detected and the instrument gives absorbance as a function of infrared wavelength (or equivalently, wavenumber). IR is used to identify the functional groups or bonds in a molecule (5-7). The IR spectrum was recorded on a JASCO FT/IR 4100 (figure 6). Samples for IR spectroscopy can be prepared in different ways. Since the current research deals with solid samples, the sample preparation for solid compounds is of two types. One method is to grind the sample with nujol mull which is a mineral oil. The second is to grind the samples with KBr salt. This powder mixture is then pressed between mechanical presses to make a translucent pellet through which the beam of the spectrometer can be passed (8). Potassium bromide pellet sample method was used for the compounds under investigation to measure IR.

## 2.4. Nuclear Magnetic Resonance Spectroscopy

The nuclear magnetic resonance (NMR) spectrum is applied in structure elucidation since the properties given by it can be associated with the molecular structure of the sample compound. NMR spectroscopy is dominantly employed in a characterization of organic materials (9). It is based on magnetic interactions of the nuclei with the external applied magnetic field (10). Upon application of external magnetic field, the spin of nuclei which is disoriented otherwise gets aligned. The working principle of NMR is as shown in figure 7. In NMR spectroscopy

electromagnetic radiation is employed to excite this oriented spin in presence of external magnetic field to a higher energy state resulting in induction of output radio signal which is detected and processed.

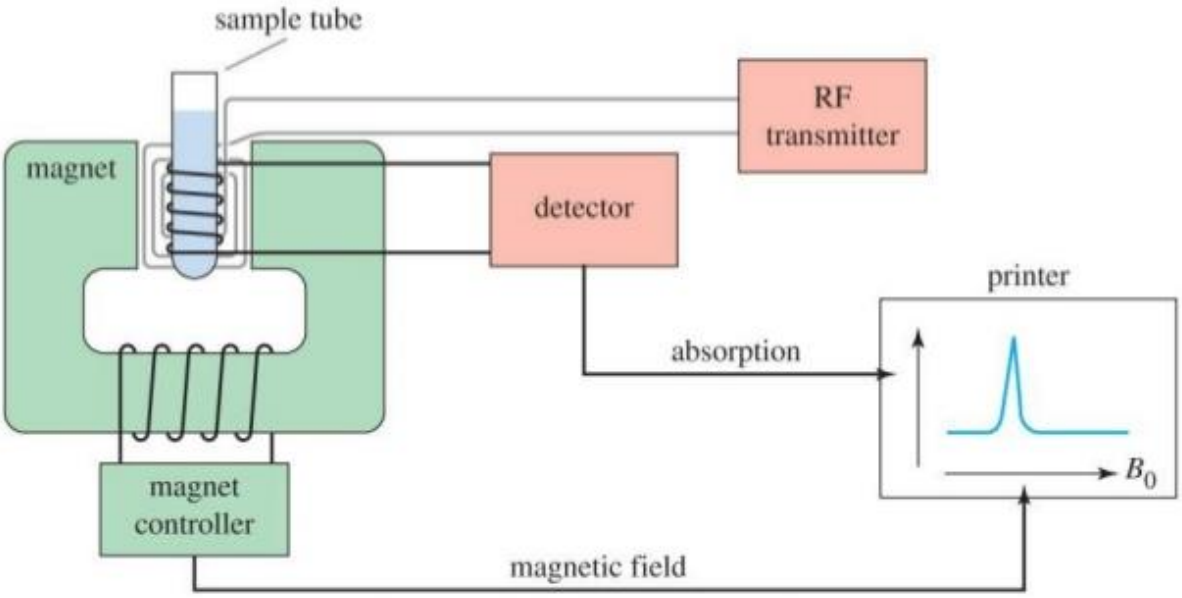


Figure 7. Principle involve in Nuclear Magnetic Resonance Spectrometer

The scalar coupling (or J-coupling) signifies an indirect interaction between individual nuclei in a chemical bond, mediated by electrons, and inappropriate conditions. The chemical shift is specific to particular nuclei and correlates its chemical environment. NMR is employed to detect various isotopes of nuclei, such as $^{1}H$ NMR for hydrogen, $^{13}C$ NMR for carbon, $^{31}P$ NMR for phosphorus and so on. The $^{13}C$ NMR is less sensitive than proton NMR since the $^{13}C$ is only 1% of the total carbon content on earth (11). $^{1}H$ NMR spectrum was recorded at $26^{0}C$ on JEOL JNM-A500 Nuclear Magnetic Resonance Spectrometer operated at 500 MHz. $^{13}C$ NMR spectrum was recorded at $24^{0}C$ on JEOL Nuclear Magnetic Resonance Spectrometer at 125 MHz. NMR spectra were measured in solution with TMS as an internal reference. All 1H shift values are given in parts per million (s = singlet; d = doublet; t = triplet; m = multiplet). The compounds were dissolved in appropriate deuterated solvents and NMR was performed.

## 2.5. Mass Spectrometer

### 2.5.1. Fast Atom Bombardment Ionization Mass Spectrometer

FAB is a soft ionization method producing deprotonated or protonated species and was developed by Michael Barber, University of Manchester (12-13). Mass spectroscopy is used to identify materials by determining the mass of the free ions in high vacuum (14). The mass spectrum provides a plot of ion signal versus mass to charge ratio and enables to conclude the mass to charge ratio and gas phase ions abundance (15). In mass spectrometer analysis, the target sample is ionized and these ions are segregated according to their mass to charge ratio by a mass analyzer and the mass spectrum is delivered by the detector. The working principle of Fab mass is as shown in figure 8.

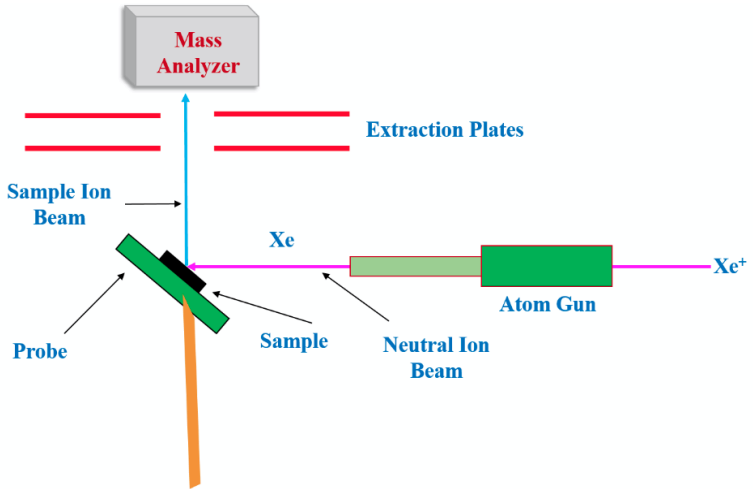


Figure 8. The schematic of a fast atom bombardment ion source for a mass spectrometer.

Different types of mass spectrometers are existing in the market. One of the critical variants among the mass spectrometers is the method of ionization. Samples are ionized by bombarding with high-energy source beam of atoms or ions (FAB) (16), by electron impact, or by photons (Laser desorption/Ionization). The material is mixed with a matrix and exposed to bombardment with the high-energy beam of atoms generally from an inert gas such as xenon or argon. Two most commonly used matrices are glycerol and m-nitro benzyl alcohol. In the current study, various compounds synthesized were characterized by the FAB mass spectrometer by mixing the samples with matrix 2, 2-dithiodiethanol.

### 2.5.2. Electrospray Ionization (ESI-Mass)

Electrospray is used in this technique, where high voltage is applied to the sample to create an aerosol to produce ions. The technique is different from other atmospheric pressure ionization processes since it produces multiple charged ions effectively. ESI is also known as soft ionization technique since there is very little fragmentation. This is advantageous as molecular ion peak is always observed. The ESI method was first reported by Masamichi Yamashita and John Fenn in 1984 (17). The schematic working principle of ESI-mass is shown in figure 9.

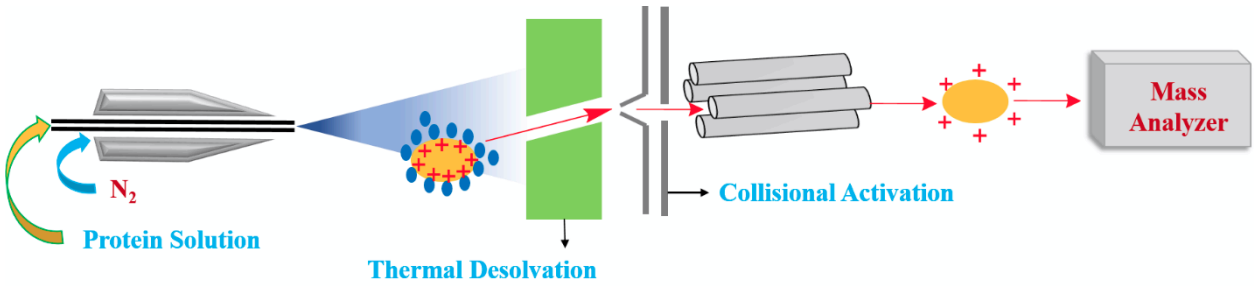


Figure 9. Working principle of ESI-Mass

The ionization mechanism includes a liquid containing the analyte of interest which is dispersed by electrospray (18) into fine aerosol. The formation of ion involves solvent evaporation, the typical solvents used for organic compounds are methanol and acetonitrile. The aerosol is sampled into first vacuum stage of spectrophotometer through a capillary which has the potential difference of about 3000V which is heated to aid further solvent evaporation. The solvent methanol is used in the current thesis to analyze the mass of dyes.

### 2.5.3. Matrix Assisted Laser Desorption Ionization Time of Flight (MALDI-TOF Mass)

It's one another soft ionization technique which is different from ESI-mass in producing far fewer multiply charged ions. TOF-Mass is used to analyze biomolecules such as peptides, proteins sugars, DNA and large organic molecules like polymers and macromolecules, which are likely to be fragile and fragment when ionized by conventional ionization methods. The schematic working principle of TOF mass is as shown in figure 10.

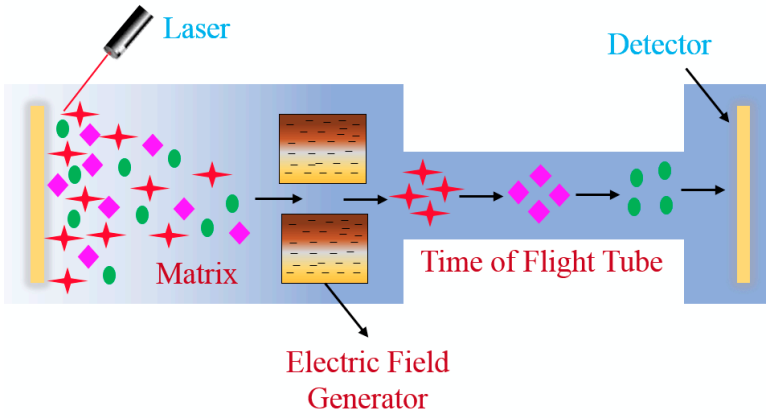


Figure 10. Principle involved in TOF mass

The samples were mixed with the matrix in analyzing molecules with TOF-Mass. The matrix consists of crystallized molecules which are different types of which 3 are most commonly used namely 3,5-dimethoxy-4-hydroxycinnamic acid, α-cyano-4-hydroxycinnamic acid (α-CHCA) and 2,5-dihydroxybenzoic acid (DHB) (19). A solution of the matrix is made in a mixture of purified water and organic solvents such as acetonitrile or ethanol. The matrix solution is mixed with analyte sample. This solution is spotted onto a MALDI plate. The solvent vaporizes leaving the recrystallized matrix. The matrix and analyte are supposed to be co-crystallized. Co-crystallization is a unique factor in choosing the matrix to obtain a better quality mass spectrum of the analyte of interest. However, molecules with the π-conjugated system like naphthalene can also serve as an electron acceptor and is used as the matrix (20). This is particularly used in studying molecules with π-conjugated systems (21). The dyes synthesized in this current thesis are of the π-conjugated system. Hence MALDI-TOF mass is used to analyze some of the dye molecules.

Figure 11. Time of Flight Mass Spectrophotometer

The TOF mass model used in this current thesis is Bruker Microflex-KI shown in figure 11. The instrumentation includes the use of UV lasers such as nitrogen lasers and ND: YAG lasers. The laser strikes the matrix crystals in the dried-droplet spot (22). The matrix absorbs the energy and is desorbed and ionized during the process. The hot cloud which is formed consist of neutral and ionized matrix molecules, nano-droplets, protonated and deprotonated molecules (23). The ion observed after this process contains molecules with ions added or removed such as $[M+H]^+$ in the case of an added proton, $[M+Na]^+$ in the situation of added sodium and $[M-H]^+$ in the case of removed proton, depending on the nature of matrix, the laser intensity and voltage used. TOF measurement is typically suited to ionization method since pulsed laser takes individual shots. TOF instrument is equipped with ion mirror which reflects ions using an electric field, thus doubling the ion flight path and increasing the resolution.

## 2.6. High Performance Liquid Chromatography (HPLC)

HPLC is an analytical instrument utilized to separate compounds which are dissolved in solution (24). It comprises of a pressurized sample inlet, column (stationary phase), pump for diffusing solvents (mobile phase) and a detector (25). The sample is injected and passed through the column. The working principle of HPLC includes injection of analytes into the mobile phase stream and are swept on to the column containing stationary phase. The analytes

which do not interact with stationary phase pass through the column, they elute first from the column. The analytes which strongly interacts with stationary phase remain on the column and never to be seen. The analytes which fall in between these two extremes are the ones which spend some time in the column. Each analyte spends a slightly different length of time. Hence by the end of the column, the individual components of the analyte sample can be separated and detected. The schematic working principle of HPLC is as shown in figure 12.

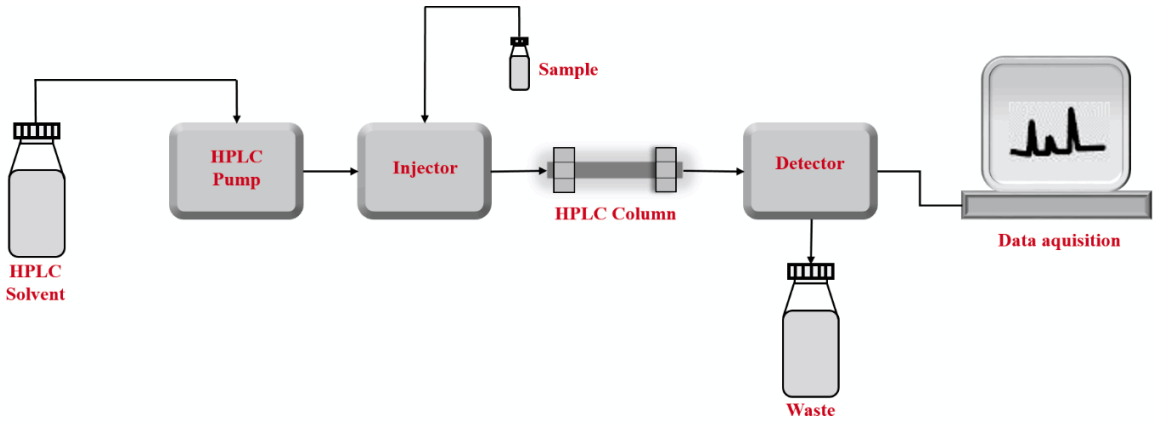


Figure 12. Outline working principle of HPLC

The components of a liquid mixture are separated based on their difference in interaction with the stationary phase which results in different flow rates for individual components (26). The transportation of different components of the mixture is assisted by the mobile phase. The interactions between the sample and column are defined by the adsorbent material of the column. Based on differences in adsorption the components in a mixture are separated if the column is alumina or silica (27), ion exchange if the column is a solid functionalized with sulfonic acid (28), size-exclusion if the column is a porous silica or polymeric particles.

Figure 13. HPLC used in this current work.

The purity of products was also checked by the HPLC (29). The HPLC used in this current thesis is shown in figure 13. Synthesized squaraine dyes and dye intermediates in this thesis were analyzed by high-performance liquid chromatography (HITACHI) equipped with chromolith analytical column (RP – 18e, φ 4.6 mm × 100 mm), Integrator D – 5700, UV-Vis detector L – 7420 and pump L - 7100.

## 2.7. References


1) M. Saikiran, D. Sato, S. Pandey, T. Kato, Photophysical investigations of squaraine and cyanine dyes and their interaction with bovine serum albumin, in: Journal of Physics: Conference Series, IOP Publishing, 2016, pp. 012012.
2) M. Saikiran, D. Sato, S.S. Pandey, T. Ohta, S. Hayase, T. Kato, Photophysical characterization and BSA interaction of the direct ring carboxy functionalized unsymmetrical NIR cyanine dyes, Dyes and Pigments, (2017)
3) https://en.wikipedia.org/wiki/Fluorescence_spectroscopy
4) K. Kawaoka, A. Khan, D.R. Kearns, Role of singlet excited states of molecular oxygen in the quenching of organic triplet states, The Journal of Chemical Physics, 46 (1967) 1842-1853.
5) D. Dutta, G. Sharma, A. Tyagi, S. Kulshreshtha, Gallium sulfide and indium sulfide nanoparticles from complex precursors: Synthesis and characterization, Materials Science and Engineering: B, 138 (2007) 60-64.
6) M.J. Yoo, S.H. Kim, S.D. Park, W.S. Lee, J.-W. Sun, J.-H. Choi, S. Nahm, Investigation of curing kinetics of various cycloaliphatic epoxy resins using dynamic thermal analysis, European Polymer Journal, 46 (2010) 1158-1162.
7) W.M. McDanel, M.G. Cowan, J.A. Barton, D.L. Gin, R.D. Noble, Effect of monomer structure on curing behavior, CO2 solubility, and gas permeability of ionic liquid-based epoxy–amine resins and ion-gels, Industrial & Engineering Chemistry Research, 54 (2014) 4396-4406.
8) A.K. Sarker, M.G. Kang, J.-D. Hong, A near-infrared dye for dye-sensitized solar cell: catecholate-functionalized zinc phthalocyanine, Dyes and Pigments, 92 (2012) 1160-1165.
9) R.S. Macomber, A complete introduction to modern NMR spectroscopy, Wiley New York, 1998.
10) T. Atta-Ur-Rahman, Nuclear magnetic resonance: basic principles, Springer Science & Business Media, 2012.
11) J. Keeler, Understanding NMR spectroscopy, John Wiley & Sons, 2011.
12) M. Barber, R. Bordoli, R. Sedgwick, A. Tyler, Fast atom bombardment of solids as an ion source in mass spectrometry, Nature, 293 (1981) 270-275.

13) K.B. Tomer, The development of fast atom bombardment combined with tandem mass spectrometry for the determination of biomolecules, Mass Spectrometry Reviews, 8 (1989) 445-482.
14) http://en.wikipedia.org/wiki/Mass_spectrometry
15) S.O. David, Mass spectrometry desk reference, Global View Pub, Pittsburgh, (2000).
16) M. Barber, R.S. Bordoli, R.D. Sedgwick, A.N. Tyler, Fast atom bombardment of solids (FAB): A new ion source for mass spectrometry, Journal of the Chemical Society, Chemical Communications, (1981) 325-327.
17) M. Yamashita, J.B. Fenn, Electrospray ion source: another variation on the free-jet theme, J. Phys. Chem.;(United States), 88 (1984).
18) B.P. Pozniak, R.B. Cole, Current measurements within the electrospray emitter, Journal of the American Society for Mass Spectrometry, 18 (2007) 737-748.
19) W.A. Korfmacher, Using mass spectrometry for drug metabolism studies, CRC Press, 2009.
20) M. Nazim Boutaghou, R.B. Cole, 9, 10-Diphenylanthracene as a matrix for MALDI-MS electron transfer secondary reactions, Journal of Mass Spectrometry, 47 (2012) 995-1003.
21) T. Suzuki, H. Midonoya, Y. Shioi, Analysis of chlorophylls and their derivatives by matrix-assisted laser desorption/ionization–time-of-flight mass spectrometry, Analytical biochemistry, 390 (2009) 57-62.
22) S. Hosseini, S.O. Martinez-Chapa, Principles and Mechanism of MALDI-ToF-MS Analysis, in: Fundamentals of MALDI-ToF-MS Analysis, Springer, 2017, pp. 1-19.
23) R. Knochenmuss, Ion formation mechanisms in UV-MALDI, Analyst, 131 (2006) 966-986.
24) F. Erni, R. Frei, Two-dimensional column liquid chromatographic technique for resolution of complex mixtures, Journal of Chromatography A, 149 (1978) 561-569.
25) M. Zapata, F. Rodríguez, J.L. Garrido, Separation of chlorophylls and carotenoids from marine phytoplankton: a new HPLC method using a reversed phase C8 column and pyridine-containing mobile phases, Marine Ecology Progress Series, 195 (2000) 29-45.
26) A. Rodrigues, L. Zuping, J. Loureiro, Residence time distribution of inert and linearly adsorbed species in a fixed bed containing “large-pore” supports: applications in separation engineering, Chemical engineering science, 46 (1991) 2765-2773.

27) G. Heinemann, J. Köhler, G. Schomburg, New polymer coated anion-exchange HPLC-phases: Immobilization of poly (2-hydroxy, 3N-ethylenediamino) butadiene on silica and alumina, Chromatographia, 23 (1987) 435-441.
28) C. Viklund, F. Svec, J.M. Frechet, K. Irgum, Fast Ion-Exchange HPLC of Proteins Using Porous Poly (glycidyl methacrylate-co-ethylene dimethacrylate) Monoliths Grafted with Poly (2-acrylamido-2-methyl-1-propanesulfonic acid), Biotechnology progress, 13 (1997) 597-600.
29) B.B. Lohray, V.B. Lohray, A.C. Bajji, S. Kalchar, R.R. Poondra, S. Padakanti, R. Chakrabarti, R.K. Vikramadithyan, P. Misra, S. Juluri, (−) 3-[4-[2-(Phenoxazin-10-yl) ethoxy] phenyl]-2-ethoxypropanoic acid [(−) DRF 2725]: a dual PPAR agonist with potent antihyperglycemic and lipid modulating activity, Journal of medicinal chemistry, 44 (2001) 2675-2678.

# Chapter 3: Synthesis, Photophysical Characterization and Binding Interactions of Far Red Sensitive Symmetrical Squaraine Dyes with BSA

**Abstract:** A series of symmetrical squaraine dyes with –COOH substituted at the 5$^{th}$ position and varying in the substituents at the N position of the indole were synthesized which readily absorbed in the far-red region of the solar spectrum. These dyes were then employed to interact with Bovine serum albumin (BSA) in phosphate buffer solution. These dyes presented a sharp absorption in the range of 550-700 nm with an appreciable high extinction coefficient ranging from 1.3 X $10^5$ $dm^3.mol^{-1}.cm^{-1}$. The rigid conformational structure of the dyes is vividly proved by the small stokes shift of 10-17 nm. Thus the dye-BSA conjugate formation was proved by the enhanced emission intensity as well as the bathochromic shift of the absorbance maxima. These newly synthesized dyes bind with about one order higher binding constant than the squaraine dyes reported till date. Amongst the squaraine dyes under study in this work, the one with trifluorobutyl substituent at the N position (**SQ-2**) proved to be outstanding with a binding constant of 8.01 x $10^6$ $M^{-1}$ with BSA.

## 3. Introduction

### 3.1. Squaraine Dyes Structure

The squaraine dyes belong to the interesting organic chromophoric system, where an oxocyclobutenolate core is linked by aromatic or heterocyclic components at both ends leading to donor–acceptor–donor molecular motif. Due to the planar structures and zwitterionic properties, squaraine dyes exhibit intense absorption and emission in NIR region. Sensitizing dyes belonging to squaraine family are of considerable interest as fluorescent labels/probes for biological and pharmaceutical research owing to their tunable absorption/emission from visible to NIR wavelength region, high molar absorptivity and reasonably good quantum yields (1-2). By logical molecular design, the absorption and emission behavior of these dyes can be tuned from visible to IR wavelength making them suitable for fluorescence imaging since they are exterior to the self-absorption and auto-fluorescence regions of biological matrices (3). The strong absorption and emission signal of Squarylium chromophores are due to charge transfer transitions, in consequence, these chromophores are sensitive to the neighboring environment (4-5). By estimating the change in optical properties of dyes, the change in environment can be monitored, which is a key factor and potential for squaraines to become good candidates as chemo-sensors (6).

A series of squaraine dyes have been synthesized with different alkyl chains and substituents at 'N' position of indole producing absorption and emission in the range of 650 to 672 nm. The unique chemical and physical properties of squaraine dyes find their versatile applications in the area as NIR fluorescent probes, environmental sensors (7), molecular sensors (8-9), bioimaging and biochemical labeling (10-13), nonlinear optical devices (14-15) which have gathered huge attentions from the scientific community. For an illustration, the main concern in sensing design is sensitivity, squaraine dyes can carry out this duty with a change in color or absorption intensities even at low concentrations.

## 3.2. Squaraine Dyes Aggregation

Organic dyes are capable of forming supramolecular aggregates comprised of numerous ordered subunits linked through noncovalent bonds, such as $\pi - \pi$ stacking, van der Waals forces, hydrophilic and/or hydrophilic interactions, electrostatic forces and H–bonds (16-17). This phenomenon is also common when biomolecules are taken into consideration, in which H–bond and $\pi$–$\pi$ stacking are very important interactions from DNA to proteins. Squaraine dyes are very likely to form J- or H-aggregates due to strong $\pi$–$\pi$ stacking interactions and their rigid and planar zwitterions structures. Though, it is still challenging to control and utilize ideal self-assembled functional materials established on squaraine chromophores (4). In order to exploit the properties of H- and J-aggregates in application towards advanced material devices, one must need to identify and categorize them.

An easy method used was absorption spectroscopy, H-aggregates are characterized by shorter absorption wavelength which is absorption compared to the monomer band (18). While aggregates that display a narrow red-shifted band in compare with the monomer band are generally designated as J-aggregates (19-20). Dye molecules that aggregate in parallel with a plane-to-plane stacking are termed as H-aggregates while a head-to-tail stacking can generate J-aggregates, figure 1 displays the formation of aggregates. During excitation, a transition from ground state to upper state in H-aggregates and to a lower state in J-aggregates leads to the shifts in absorption wavelength to blue and red, respectively.

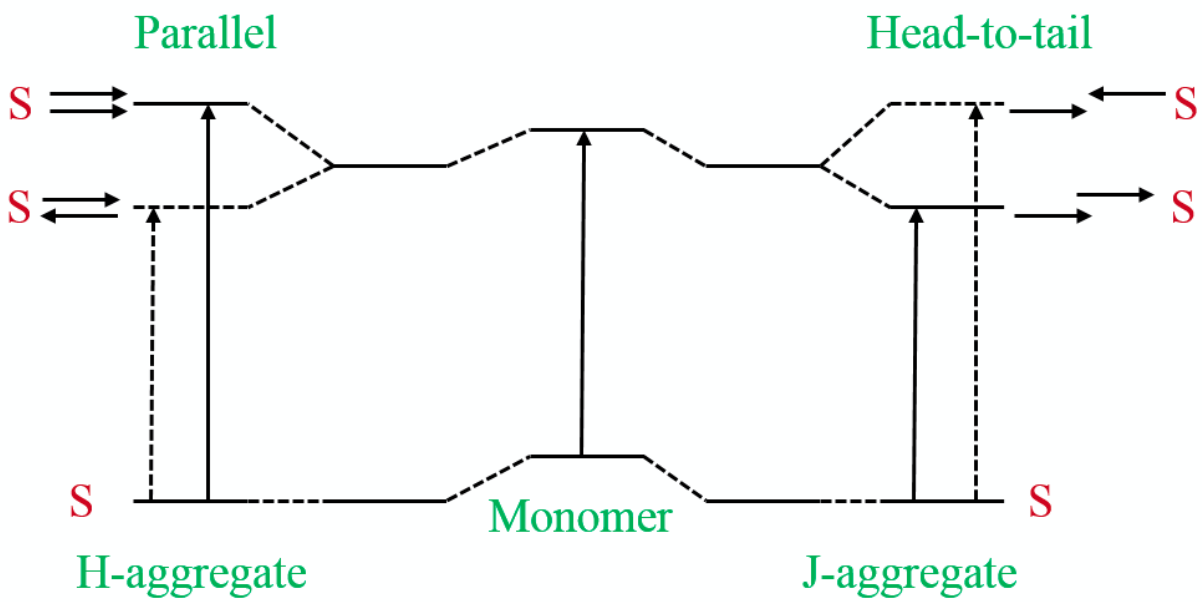


Figure. 1 Illustration of H and J-aggregates based on molecular exciton theory

## 3.3. Experimental

### 3.3.1. Materials and Methods

1-Iodobutane, 1,1,1-trifluoro-4-iodobutane, 1,3-propanesultone, Ethyl-4-bromobutanoate used in the present synthesis were purchased from Tokyo Kasei Co. Ltd. Solvents (reagent grade, Wako chemical company) and Squaric acid were purchased from Alfa Aesar and used as received. The purity of the synthesized squaraine dyes and dye intermediates were analyzed by high-performance liquid chromatography (HITACHI) equipped with chromolith analytical column (RP – 18e, φ 4.6 mm × 100 mm) using methanol-water solvent gradient. Figure 2 indicates the purity of final symmetrical squaraine dyes used for present investigation which was verified by HPLC. Mass of the intermediates, as well as final SQ dyes, were confirmed by MALDI-TOF-mass or fast ion bombardment (FAB) mass in positive ion monitoring mode. For final symmetrical squaraine dyes, high-resolution FAB-mass (HR-MS) in positive ion monitoring mode was also measured. Nuclear Magnetic Resonance (NMR) spectra were recorded on a JEOL JNM A500 MHz spectrometer in CDCl3 or d6-DMSO with reference to TMS for structural elucidation.

### 3.3.2. *Synthesis of SQ dyes and dye intermediates*

Aromatic ring carboxy functionalized indole 2,3,3-trimethyl-3H-indole-5-carboxylic acid was synthesized following the method reported (21). Symmetrical squaraine dyes and dye intermediates of 5-carboxy-2,3,3-trimethyl-indole have been synthesized following the method as shown in Scheme 1.

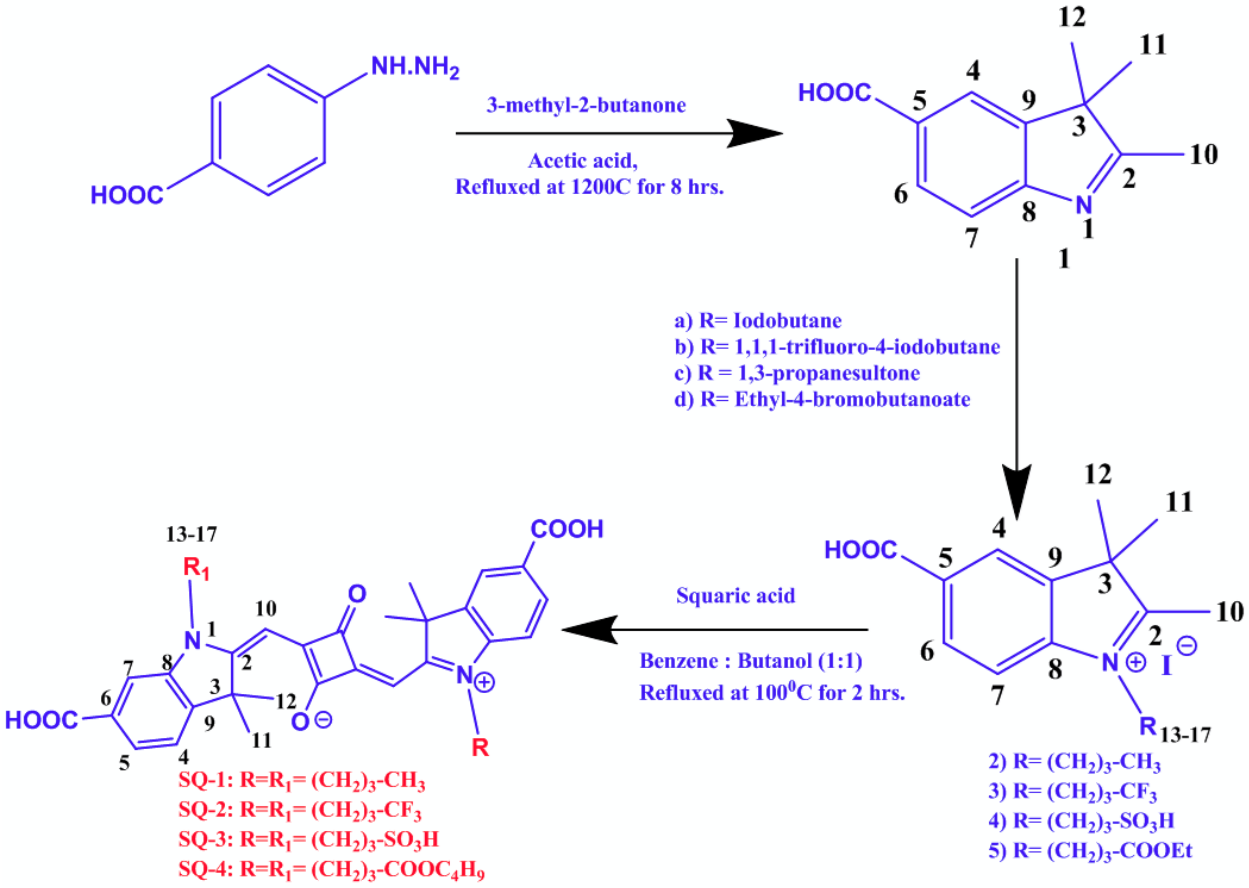


Scheme 1: Synthesis of Symmetrical squaraine dyes

***Synthesis of 5-carboxy-2,3,3-trimethyl-1-alkyl-3H-indolium iodide (2-5)***

2,3,3-trimethyl-3H-indole-5-carboxylic acid (1, 1 equiv.) and (a, 3 equiv, in Acetonitrile, 950C), (b, 3 equiv, in propionitrile, 1000C), (c, 3 equiv, in DCB, 1350C), (d, 3 equiv, in propionitrile, 1000C), were added and reaction mixture was refluxed for (a: 48 h, b: 24 h, c: 72 h, d: 24 h) under nitrogen atmosphere to give corresponding 5-carboxy-N-alkyl-indoium

iodides (2-5). After completion of the reaction as monitored by HPLC, the solvent was evaporated and the crude product was washed with ample diethyl ether giving the titled compound. The physical and spectral data of N-alkyl-indolium iodides (2-5) are as follows.

***Synthesis of 1-butyl-5-carboxy-2,3,3-trimethyl-3H-indolium (2):*** Yield 77% with 97% purity as confirmed by HPLC. FAB-mass (measured 260.0; calculated 260.16) confirms successful synthesis of the compound (22).

***Synthesis of 5-Carboxy-2,3,3-trimethyl-1-Trifluorobutyl-3H-indolium iodide (3):*** Yield 46% with 99% purity as confirmed by HPLC. FAB-mass (measured 441.0; calculated 441.04) confirms the successful synthesis of the compound (23).

***Synthesis of 5-carboxy-2,3,3-trimethyl-1-(3-sulfopropyl)-3H-indol-1-ium (4):*** Yield 59% with 99% purity as confirmed by HPLC. FAB-mass (measured 326.1066; calculated 326.1057) confirms the successful synthesis of the compound (24).

***Synthesis of 5-carboxy-1-(3-ethoxy-3-oxopropyl)-2,3,3-trimethyl-3H-indol-1-ium (5):*** Yield 59% with 99% purity as confirmed by HPLC. FAB-mass (measured 318.1698; calculated 318.1700) confirms the successful synthesis of the compound (25).

***Synthesis of symmetrical squaraine dyes***

Symmetrical SQ Dyes (SQ-1-4) were synthesized using corresponding carboxy functionalized trimethyl-indolium iodide salt 2-5 ((2 equiv.) and squaric acid (1 equiv.)) in 1-butanol: benzene mixture. The reaction mixture was refluxed for 18 h using Dean-Stark trap for azeotropic removal of water. After completion of the reaction, the reaction mixture was cooled, the solvent was evaporated and the product was purified by silica gel column chromatography using chloroform: methanol as eluting solvent. The physical and spectroscopic data of symmetrical SQ dyes are as follows;

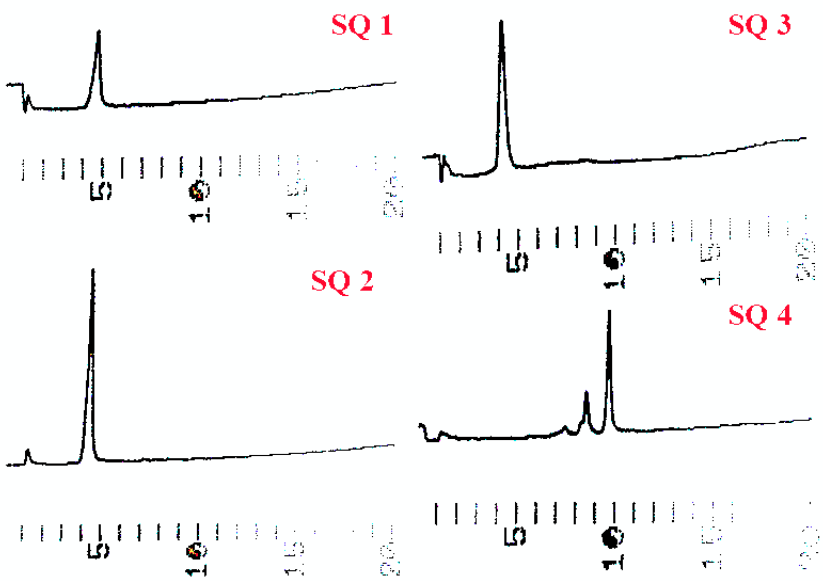


Figure 2. HPLC chromatogram of symmetrical squaraine dyes.

***Synthesis of N-butyl substituted squaraine dye SQ-1*:** Yield 64 % with HPLC purity 100 %. MALDI-TOF-mass (calculated 596.29 and observed 597.25 $[M+H]^+$). HR-MS (calculated 596.288 and observed 596.296 $[M]^+$). 1H NMR (500 MHz, d6-DMSO): d/ppm = 12.85 (b, –COOH), 8.04 (dd, H-6), 7.96 (dd, H-4), 7.43 (dd, H-7), 5.90 (s, H-10), 4.13 (q, 2H, H-13), 1.76 (m, 2H, H-14), 1.70 (s, 6H, H11 + 12), 1.40 (m, 2H, H-15), 0.95 (t, 3H, H-16) confirms the successful synthesis of the dye.

***Synthesis of N-Trifluorobutyl substituted squaraine dye SQ-2*:** Yield 71 % with HPLC purity 100 %. FAB-mass (calculated 704.23 and observed 705.0 $[M+H]^+$) confirms the identity of the compound. 1H NMR (500 MHz, d6-DMSO): d/ppm = 8.03 (d, H-6), 7.96 (d, H-5), 7.98 (d, H-7), 7.96 (d, H-4), 5.92 (s, H-10), 4.23 (t, 2H, H-13), 1.93 (m, 2H, H-14), 1.71 (s, 6H, H11 + 12) confirms the synthesis of dye.

***Synthesis of N-sulfopropyl substituted squaraine dye SQ-3*:** Yield 42% with HPLC purity 100 %. FAB-mass (calculated 728.17 and observed 729.00 $[M+H]^+$) confirms the identity of the compound. 1H NMR (500 MHz, d6-DMSO): d/ppm = 7.94 (d, H-7), 7.88 (d, H-5), 7.47 (d, H-4), 5.85 (s, H-10), 4.19 (t, 2H, H-13), 2.48 (m, 2H, H-14), 1.94 (t, 2H, H-15), 1.2 (s, 6H, H11 + 12) confirms the synthesis of dye.

***Synthesis of N-butoxybutyl substituted squaraine dye SQ-4*:** Yield 42 % with HPLC purity > 80 %. FAB-mass (calculated 769.9040 and observed 769 $[M]^+$) confirms the identity of the

compound. 1H NMR (500 MHz, d6-DMSO): d/ppm = 8.04 (d, H-7), 8.02 (d, H-5), 7.99 (d, H-4), 6.01 (s, 2H, H-10), 4.14-4.16 (t, 4H, H-17), 1.58-1.61 (m, 4H, H-14), 1.48-1.51 (t, 4H, H-15), 1.24-1.27 (m, 2H, H-18), 0.90-1.01 (m, 6H, H-11+12) confirms the successful synthesis of the dye.

## 3.4. Results and Discussion

### *3.4.1. Photophysical Characterization*

The far-red sensitive dyes were subjected to photophysical investigations pertaining to the electronic absorption and fluorescence emission spectroscopy. The electronic absorbance and fluorescence emission spectroscopy data of the far-red sensitive Squaraine dyes are tabulated in table 1. Figure 3 depicts the solution state absorbance and fluorescence spectra of dyes in dimethylformamide (DMF) as the solvent.

**Table 1.** Photophysical properties of symmetrical squaraine dyes in DMF solution

| Sensitizing Dyes | $\lambda_{(max)}$ Absorption | $\lambda_{(max)}$ Emission | Stoke Shift | ($\varepsilon$) ($dm^3\ M^{-1}\ cm^{-1}$) |
|---|---|---|---|---|
| SQ-1 | 650 nm | 662 nm | 12 nm | 2.2×105 |
| SQ-2 | 652 nm | 664 nm | 12 nm | 1.4×105 |
| SQ-3 | 656 nm | 666 nm | 10 nm | 1.5×105 |
| SQ-4 | 655 nm | 672 nm | 17 nm | 2.3×105 |

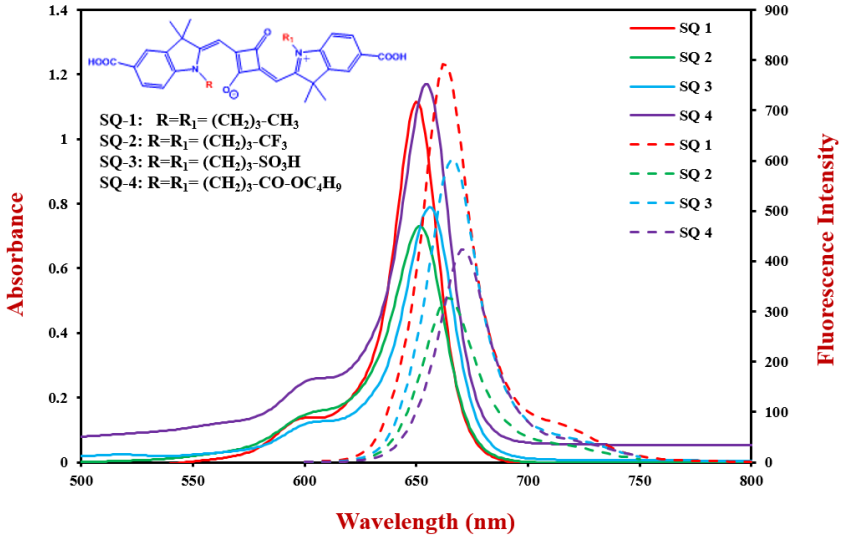


Figure 3. Electronic absorption (solid line) and fluorescence emission (dashed line) spectra of dyes in DMF solution (5 µM). The inset shows the molecular structure of squaraine dyes.

The N substituted alkyl group on the indole moiety plays a pronounced role on the absorbance maxima of the respective dyes where the value of $\lambda_{max}$ ranges from 650-656 nm with a high molar extinction coefficient ranging from $2.34 \times 10^5$ to $1.45 \times 10^5$ $dm^3\ M^{-1}\ cm^{-1}$. The high extinction coefficient is attributed to the strong $\pi$–$\pi^*$ electronic transitions. The fluorescence emission spectra were measured slightly below (about 12 to 16 nm) to the resultant $\lambda_{max}$ of absorption spectra. The peak maxima of the fluorescence emission band range from 662 to 672 nm with a small stoke shift of 10-17 nm. The stoke shift is depended on the conformational changes of the molecule after photoexcitation. A small stoke shift is attributed to the rigidity of the molecule where there is negligible conformational change after photoexcitation. Similarly, a fathomable stoke shift is due to the change in the molecular conformation upon photoexcitation.

### *3.4.2. Binding Assay of Squaraine dyes with BSA*

0.1 M PBS at almost neutral pH (7.4) and squaraine dyes solutions at 2 μM were used to employ the protein (BSA)-dye assay. To the concentration range of (0-10 μM) of PBS/BSA, 100 μl of 0.1 M DMF dye solution was added and stirred thoroughly at room temperature before recording their absorbance and emission spectra. Titrations of dyes were carried out at $25^0$C, to compare the interactions between protein and dyes. Hence, the apparent binding constants ($K_a$) was calculated using equation 1. (26)

$$\frac{1}{(F_x - F_0)} = \frac{1}{(F_\infty - F_0)} + \frac{1}{K_a[BSA]} \frac{1}{(F_\infty - F_0)} \quad (1)$$

Where, $F_0$, $F_X$, and $F_\infty$ are the fluorescence intensities of dyes in the absence, the presence of BSA and at a concentration of complete interaction, respectively, while [BSA] is the protein concentration. Equation [1] can be modified as

$$\frac{(F_\infty - F_0)}{(F_x - F_0)} = 1 + \frac{1}{K_a[BSA]} \quad (2)$$

The binding/association constant ($K_a$) values for the interaction between the BSA and Squaraine dyes were calculated from the slopes of the corresponding plots between the $(F_\infty - F_0)/(F_X - F_0)$ as a function of $[BSA]^{-1}$ as per the equation (2).

## Interactions of dyes with BSA

The interaction of squaraine dye with model proteins like bovine serum albumin (BSA), human serum albumin (HSA), avidin and ovalbumin helps in determination of the protein sensing of the dye. PBS was used as a buffer to investigate the interactions between dyes and protein which have a wide application in imaging and sensing applications for ligand binding mechanism and protein folding (27). When it comes to the investigation of the interactions between dye and protein molecule, noncovalent labeling of biomolecules is par excellent than the covalent part. There are reports that BSA interacts non-covalently with proteins leading a distinct color change of the solution. Thus non-covalent labeling technique was employed to circumvent the purification steps and chemical interaction of biomolecules with dyes towards the application of optical imaging (28). Figure 4 shows the binding sites of BSA and possible interaction of dye.

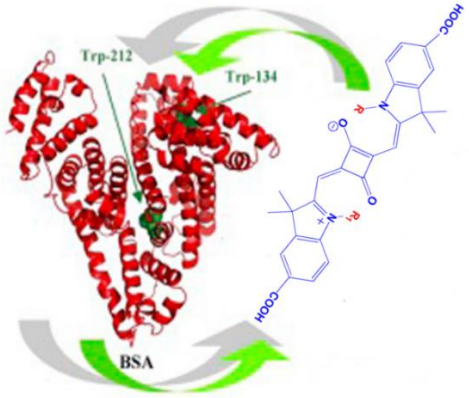


Figure 4. 3D structure of BSA and its binding sites.

Frank Welder et al have studied the noncovalent labeling of both Bovine Serum Albumin (BSA) and Human Serum Albumin (HSA) with NIR Squarylium dyes using absorption detection techniques (29). Bovine serum albumin (BSA) is a globular protein which has been prominently used as protein model to investigate the interactions between dye and protein owing to its high homology with HSA in the amino acid sequences (30). Therefore, dyes used in this work have been subjected to investigate their interaction with BSA as a model protein.

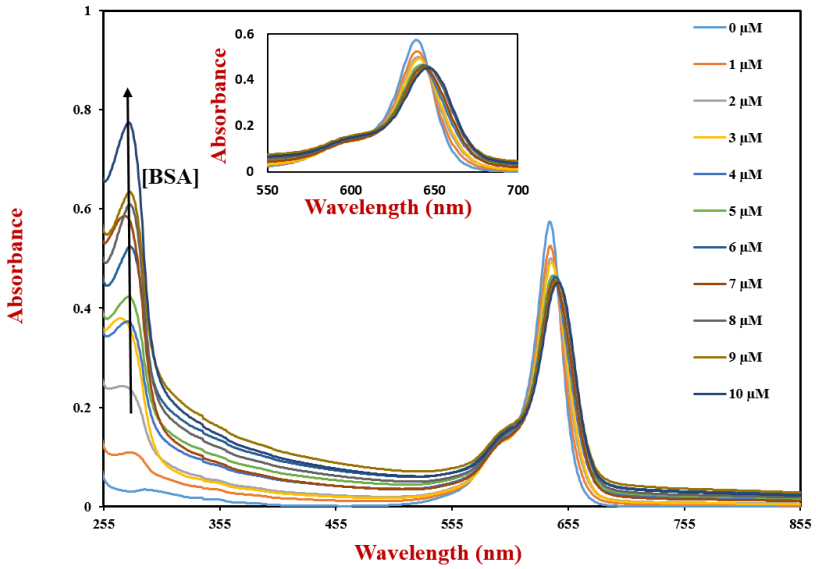


Figure 5. Electronic absorption spectra of SQ-1 in 0.1 M PBS at different concentrations of BSA for fixed dye concentration of 2 µM.

Figure 5 shows the absorption spectra of SQ-1, a representative of Squaraine dyes, in presence and absence of BSA. There are two distinct electronic absorption bands in the wavelength region of 250-300 nm and 620-680 nm corresponding to the absorption of BSA and the dye respectively. A gradual increase in the intensity of absorption between 250-300 nm was observed on the gradual increase in the BSA concentration. A red shift of 10 nm from 639 nm to 649 nm is observed on the interaction of BSA with the dye which is contributed by the increased concentration of BSA and formation of aggregates. There was initial decrease (hypochromism) in absorption intensity which continues up to 4-6 µM along with the presence of isosbestic point and then remains constant upon the further addition of BSA. The equilibrium between the free and bound protein is simple in all dyes which are clearly indicated by the presence of isosbestic point. The red shift could be attributed due to the presence of hydrophobic environment provided by BSA to the dye SQ-1 which indicates the development of dye-BSA conjugate pair. It is well known that squaraine dyes are prone to dye aggregate formation in the solution owing to their flat molecular structure. Upon interaction with BSA, first of all there, is dye-BSA conjugate formation leading to disruption of dye aggregates resulting into red-shifted absorption maximum. At the same time, compaction of the effective π-electron density decreases due to dye-BSA conjugate formation leading to the hypochromicity. Once the conjugate formation is finished, further increase in the BSA (> 6 µM) does not affect the decrease in the intensity of SQ-dye rather than only red-shift. This is

attributed to the fact that now added additional BSA is involved mainly in the prevention of dye aggregation rather than conjugate formation. Similar study of interaction between the HSA and Squaraine dye has also been investigated by Jisha et al. (31)

It is worth to mention that similar behavior has also been observed for the other squaraine dyes such as (**SQ-2, SQ-3, and SQ-4**). Figure 6 depicts the absorption spectra of dye SQ-2 with BSA. The dye SQ-2 also exhibits an initial decrease in absorption intensity up to 6µM and was random on further addition of BSA. The hydrophobicity of molecule is responsible to show high binding ability towards the protein.

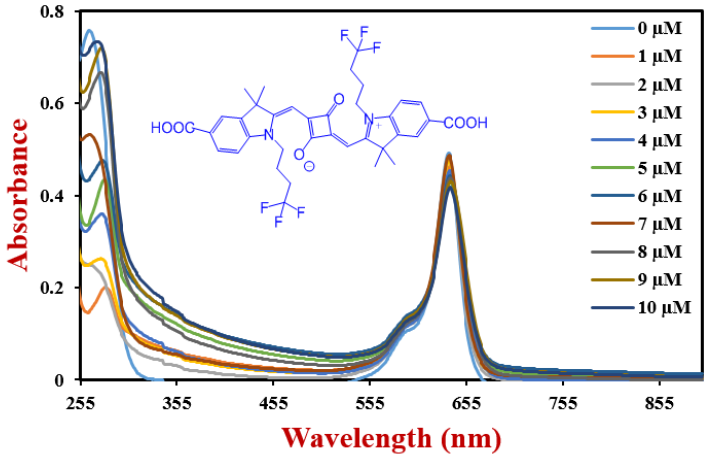


Figure 6. Electronic absorption spectra of SQ-2 in 0.1 M PBS at different concentrations of BSA for fixed dye concentration of 2 µM.

The enhanced hydrophilicity or least hydrophobicity of SQ-3 is a key factor to exhibit insignificant interaction with the protein. SQ-3 display random increase and a decrease in absorption till 5µM and were constant upon further addition of BSA. Figure 7 represents the absorption interaction of SQ-3 with different concentrations of BSA. Upon the interaction with BSA, SQ-3 showed enhanced side vibronic shoulder associated with the dye-aggregation owing to its strong hydrophilic nature due to the presence of two highly hydrophobic -$SO_3H$ groups in the side chain.

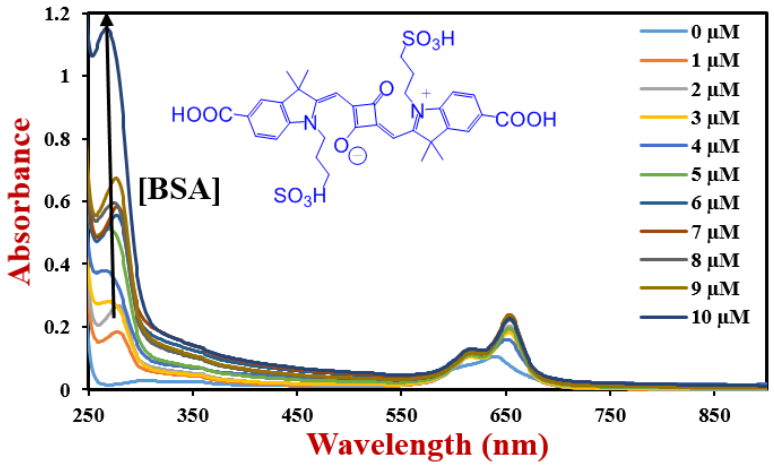


Figure 7. Electronic absorption spectra of SQ-3 in 0.1 M PBS at different concentrations of BSA for fixed dye concentration of 2 µM.

The mild hydrophobicity of dye SQ-4 ester is responsible for the binding with BSA. The interactions of SQ-4 is random and similar to that of SQ-3. Figure 8 displays the absorption interactions of dye SQ-4 with varied concentrations of BSA.

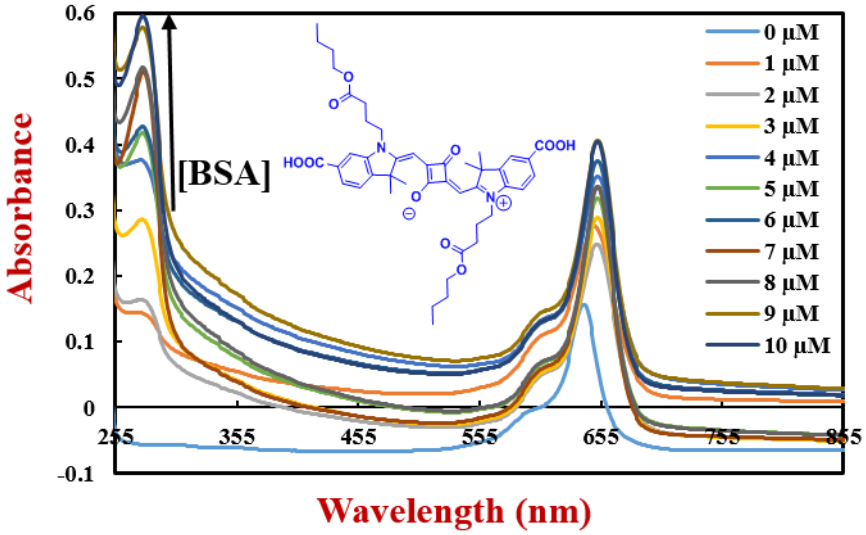


Figure 8. Electronic absorption spectra of SQ-4 in 0.1 M PBS at different concentrations of BSA for fixed dye concentration of 2 µM.

The fundamental basis for fluorescence bio-imaging is to observe changes in the fluorescence behavior of dyes on interactions with biomolecules. The spectroscopic behavior of squaraine dyes has been reported to be highly sensitive to the environmental conditions due to their self-aggregation (32). It was suggested that Squarylium dyes occupy a common hydrophobic site on protein to form a dye-protein complex, which enhances the fluorescence signal and be used

for the determination of proteins (33-34). In general, fluorophores are bound to protein either covalently or non-covalently. And noncovalent labeling technique basically promotes hydrophobic binding sites. Thus it is a wide potential application to monitor the change in conformation of the protein and their binding with drugs in biomedical field (28). The fluorescence emission spectra of dyes SQ-1, 2, 3 and 4 associated with different concentrations of BSA are shown in figure 9.

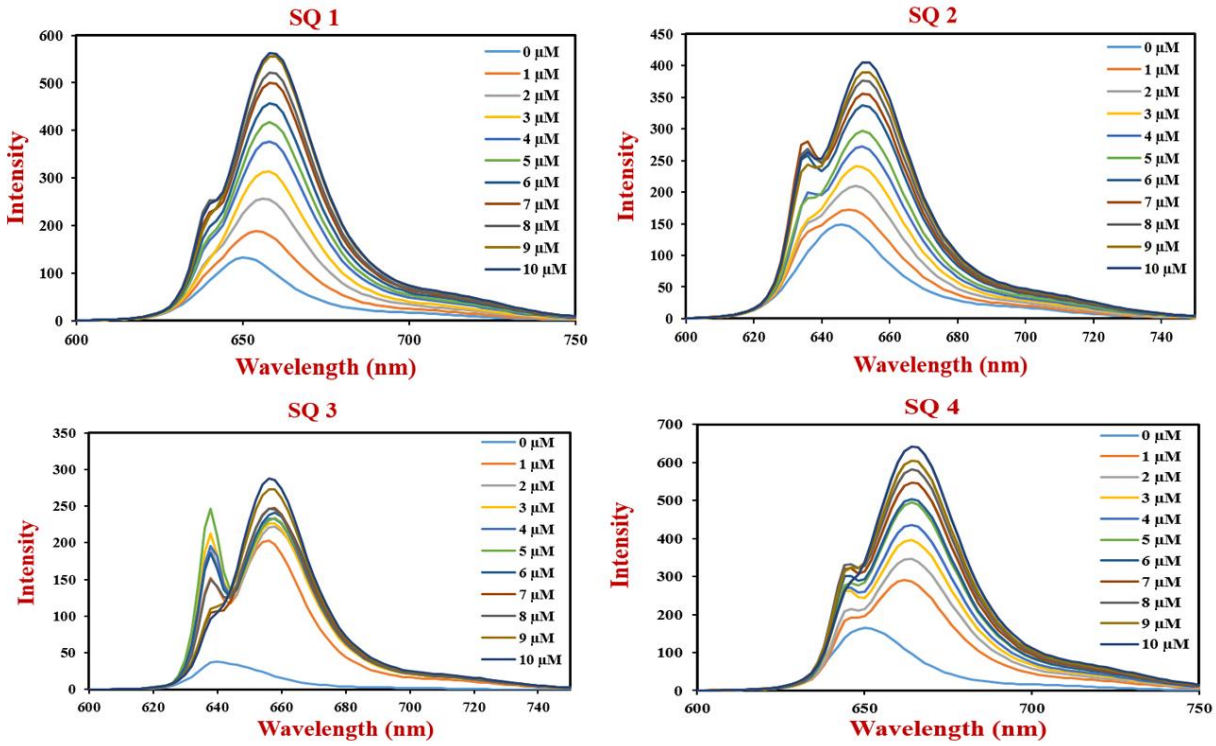


Figure 9. Fluorescence emission spectra of SQ-1-4 with varying concentrations of BSA for a fixed dye concentration of 2 µM.

Figure 9 shows that the addition of increasing amounts of BSA leads to the increase in fluorescence intensity along with a red shift of peak maxima. The reason for this bathochromic shift could be possibly due to the noncovalent interactions between the dye and the BSA. The bathochromic shift of SQ-1, 2, 3 and 4 of 10, 6, 16, 14 nm clearly presents that the BSA micro-atmosphere are less likely polar than that of the PBS alone which is solely because of the hydrophobic interior surface and the exterior surface of BSA. It can be argued that why there was continues increase in the fluorescence intensity of dye upon the addition of BSA where absorption maximum saturates up to 6 µM of BSA concentration. As discussed earlier, BSA is

not only involved in the dye-BSA conjugate formation but also prevention of dye aggregation. It has also been reported that there is quenching in the fluorescence upon the dye aggregate formation (35). This is the reason why the addition of the BSA with concentration > 6 μM leads to further enhancement in the fluorescence intensity of dye by preventing the dye aggregation. Among the dyes, SQ-3 shows relatively suppressed fluorescence intensity. It can be explained on the basis of dye aggregation which is prominent in case of SQ-3. H aggregate provides a supplementary pathway for non-radioactive decay which is the primary cause for low intensity. However, the addition of 10 μM BSA to SQ-4 amicably increased the fluorescence intensity by 3 folds. Interestingly, the addition of only 1 μM BSA to SQ-3 increased the same by 5 folds.

The dependency of BSA concentration with the fluorescence intensity of the different symmetrical squaraines dyes has been plotted in figure 10. It prominently shows a linear correlation between the fluorescent intensity and the BSA concentration that is there is an increase in fluorescence intensity when the concentration of BSA is increased was observed till 6 μM and attained saturation. Though, these dyes exhibit interactions on further addition of BSA, the emission intensity seems to follow nonlinearity, where the change in fluorescence intensity is comparatively less as it attained saturation at 6 μM of BSA. The reason for this linear behavior is the aspect of the non-covalent interaction between the dyes and proteins as a result of the formation of BSA- dye conjugate. It has been genuinely accepted worldwide that the drugs or probes interact uniquely with the protein which is basically confined on the protein concentration (36). The main feature of the dyes to implement it as a probe is its ability not to disturb the protein structure as the protein structure monitors its function and activity. The space in the protein where the probe is positioned is more likely to undergo its conformational change. Thus to avoid the deterioration of the protein structure, a minimum and optimized concentration of dye as 2 μM is probed to study the dye-BSA synergy.

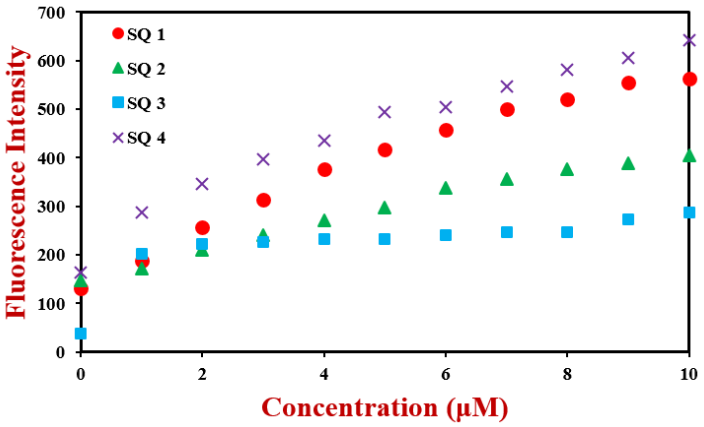


Figure 10. Plot of florescence emission intensity at peak maxima for Squaraine dyes as a function of BSA concentration. Dye concentration was constant (2 μM) for each of the dyes.

The apparent binding constant ($K_a$) for the synergy of the dyes with BSA was computed using equation (2) by plotting $(F_\infty - F_0)/(F_X - F_0)$ versus the inverse of BSA concentration as displayed in figure 11. The binding constant value ($K_a$) was obtained from the slopes of the curve. For SQ-1, SQ-2, SQ-3, SQ-4, the $K_a$ value deduced thus were be 6.2 x $10^6$ $M^{-1}$, 8.0 x $10^6$ $M^{-1}$, 0.3 x $10^6$ $M^{-1}$ and 3.9 x $10^6$ $M^{-1}$ respectively. Comparing the binding constants of all the dyes concerned, the dye having the N-trifluorobutyl in the indole moiety was supreme with $K_a$ value about an order of magnitude higher than the rest of the reported dyes (37). The reason for the high binding potency and hence high ($k_a$) of SQ-2 is due to the optimum hydrophobicity/hydrophilicity. Implying the same condition of optimum hydrophobicity/hydrophilicity for high binding ability, for SQ-3 the Binding constant is the lowest which may be due to enhanced hydrophilicity or least hydrophilicity and the secondary reason could be the high dye aggregation preventing it to interact with the protein.

BSA possess distinct hydrophobic and hydrophilic active sites site I and Site-II (38). The relative hydrophobicity of ligands (drug or dyes) controls its interaction with BSA, more generally with Site-I. The dyes under study have similar π-conjugation framework and the –COOH substituent at the 5$^{th}$ position. They differ only in the substituent at the N position of the indole moiety. The relative hydrophobicity of the dyes follows the trend **SQ-4 > SQ-1 > SQ-2 > SQ-3** which is confirmed from the retention time in HPLC. The one having more hydrophobicity has more retention time. Thus in one word, the binding affinity of the dye with BSA is controlled by the moderate (balanced) hydrophilic and hydrophobic interactions with Site-I and Site-II.

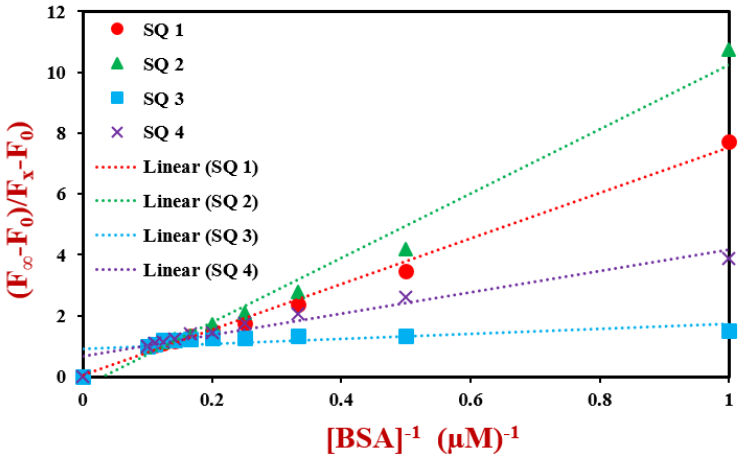


Figure 11. Plot of $(F_\infty - F_0) / (F_X - F_0)$ as function $[BSA]^{-1}$ at a fixed dye concentration of 2 µM.

## 3.5. Conclusions

Carboxy functionalized symmetrical squaraines with varying substituents were synthesized with satisfactory yields and characterized. The dyes were subjected to photophysical investigations in order to explore their applicability as fluorescent probes. Interactions of these dyes with BSA as a protein model suggested the formation of dye-BSA conjugates, which led to the enhancement in fluorescence intensity along with the bathochromic shift of emission maxima. The interaction between dyes with protein was found to be (**SQ-2 > SQ-1 > SQ-4 > SQ-3**) while hydrophobicity of the dyes was found to be in the order (**SQ-4> SQ-1 > SQ-2 > SQ-3**) as confirmed by HPLC retention time. The dye SQ-2 showed highest binding ability with BSA hence showed high binding constant ($K_a$) which can be attributed to its possible interactions with both the binding sites of BSA owing to its moderate hydrophilicity as well as hydrophobicity. The above photophysical characterization reveals that Squaraine dyes can be used as good fluorophores for designing NIR-FRET systems.

## 3.6. References:


1) K.Y. Law, Squaraine chemistry. Design, synthesis and xerographic properties of a highly sensitive unsymmetrical fluorinated squaraine, Chemistry of materials, 4 (1992) 605-611.
2) H. Chen, M.S. Farahat, K.-Y. Law, D.G. Whitten, Aggregation of surfactant squaraine dyes in aqueous solution and microheterogeneous media: correlation of aggregation behavior with molecular structure, Journal of the American Chemical Society, 118 (1996) 2584-2594.
3) H.-Y. Ahn, S. Yao, X. Wang, K.D. Belfield, Near-Infrared Emitting Squaraine Dyes with High 2PA Cross Sections for Multiphoton Fluorescence Imaging, ACS applied materials & interfaces, 4 (2012) 2847.
4) L. Hu, Z. Yan, H. Xu, Advances in synthesis and application of near-infrared absorbing squaraine dyes, RSC Advances, 3 (2013) 7667-7676.
5) R.W. Bigelow, H.-J. Freund, An MNDO and CNDO/S (S+ DES CI) study on the structural and electronic properties of a model squaraine dye and related cyanine, Chemical physics, 107 (1986) 159-174.
6) L. Beverina, P. Salice, Squaraine compounds: Tailored design and synthesis towards a variety of material science applications, European journal of organic chemistry, 2010 (2010) 1207-1225.
7) J.J. McEwen, K.J. Wallace, Squaraine dyes in molecular recognition and self-assembly, Chemical Communications, (2009) 6339-6351.
8) J.V. Ros-Lis, B. García, D. Jiménez, R. Martínez-Máñez, F. Sancenón, J. Soto, F. Gonzalvo, M.C. Valldecabres, Squaraines as fluoro− chromogenic probes for thiol-containing compounds and their application to the detection of biorelevant thiols, Journal of the American Chemical Society, 126 (2004) 4064-4065.
9) T.M. Kolev, D.Y. Yancheva, S.I. Stoyanov, Synthesis and spectral and structural elucidation of some pyridinium betaines of squaric acid: potential materials for nonlinear optical applications, Advanced Functional Materials, 14 (2004) 799-805.
10) J.R. Johnson, N. Fu, E. Arunkumar, W.M. Leevy, S.T. Gammon, D. Piwnica-Worms, B.D. Smith, Squaraine rotaxanes: superior substitutes for Cy-5 in molecular probes for near-infrared fluorescence cell imaging, Angewandte Chemie International Edition, 46 (2007) 5528-5531.

11) J. Gassensmith, E. Arunkumar, L. Barr, J.M. Baumes, K.M. DiVittorio, J.R. Johnson, B.C. Noll, B.D. Smith, Self-assembly of fluorescent inclusion complexes in competitive media including the interior of living cells, Journal of the American Chemical Society, 129 (2007) 15054.
12) W. Wang, A. Fu, J. Lan, G. Gao, J. You, L. Chen, Rational design of fluorescent bioimaging probes by controlling the aggregation behavior of squaraines: a special effect of ionic liquid pendants, Chemistry-a European Journal, 16 (2010) 5129-5137.
13) J. Thomas, D.B. Sherman, T.J. Amiss, S.A. Andaluz, J.B. Pitner, Synthesis and biosensor performance of a near-IR thiol-reactive fluorophore based on benzothiazolium squaraine, Bioconjugate chemistry, 18 (2007) 1841-1846.
14) C.-T. Chen, S.R. Marder, L.-T. Cheng, Syntheses and linear and nonlinear optical properties of unsymmetrical squaraines with extended conjugation, Journal of the American Chemical Society, 116 (1994) 3117-3118.
15) S.A. Odom, S. Webster, L.A. Padilha, D. Peceli, H. Hu, G. Nootz, S.-J. Chung, S. Ohira, J.D. Matichak, O.V. Przhonska, Synthesis and two-photon spectrum of a bis (porphyrin)-substituted squaraine, Journal of the American Chemical Society, 131 (2009) 7510-7511.
16) M. Suzuki, K. Hanabusa, Polymer organogelators that make supramolecular organogels through physical cross-linking and self-assembly, Chemical Society Reviews, 39 (2010) 455-463.
17) S. De Feyter, F.C. De Schryver, Two-dimensional supramolecular self-assembly probed by scanning tunneling microscopy, Chemical Society Reviews, 32 (2003) 139-150.
18) A. Herz, Aggregation of sensitizing dyes in solution and their adsorption onto silver halides, Advances in Colloid and Interface Science, 8 (1977) 237-298.
19) T. Kobayashi, J-aggregates, World Scientific, 2012.
20) M. Bednarz, V. Malyshev, J. Knoester, Temperature dependent fluorescence in disordered Frenkel chains: interplay of equilibration and local band-edge level structure, Physical review letters, 91 (2003) 217401.
21) W. Pham, W.-F. Lai, R. Weissleder, C.-H. Tung, High efficiency synthesis of a bioconjugatable near-infrared fluorochrome, Bioconjugate chemistry, 14 (2003) 1048-1051.

22) S.S. Pandey, T. Inoue, N. Fujikawa, Y. Yamaguchi, S. Hayase, Substituent effect in direct ring functionalized squaraine dyes on near infra-red sensitization of nanocrystalline TiO 2 for molecular photovoltaics, Journal of Photochemistry and Photobiology A: Chemistry, 214 (2010) 269-275.
23) S.S. Pandey, T. Inoue, N. Fujikawa, Y. Yamaguchi, S. Hayase, Alkyl and fluoro-alkyl substituted squaraine dyes: A prospective approach towards development of novel NIR sensitizers, Thin Solid Films, 519 (2010) 1066-1071.
24) N.G. Zhegalova, S. He, H. Zhou, D.M. Kim, M.Y. Berezin, Minimization of self-quenching fluorescence on dyes conjugated to biomolecules with multiple labeling sites via asymmetrically charged NIR fluorophores, Contrast media & molecular imaging, 9 (2014) 355-362.
25) J.T. Wojtyk, P.M. Kazmaier, E. Buncel, Modulation of the spiropyran− merocyanine reversion via metal-ion selective complexation: trapping of the "transient" cis-merocyanine, Chemistry of materials, 13 (2001) 2547-2551.
26) Y.Z. ZHANG, Q.F. YANG, H.Y. DU, Y.L. TANG, G.Z. XU, W.P. YAN, Spectroscopic investigation on the interaction of a cyanine dye with serum albumins, Chinese Journal of Chemistry, 26 (2008) 397-401.
27) V.S. Jisha, K.T. Arun, M. Hariharan, D. Ramaiah, Site-selective binding and dual mode recognition of serum albumin by a squaraine dye, Journal of the American Chemical Society, 128 (2006) 6024-6025.
28) G. Patonay, J. Salon, J. Sowell, L. Strekowski, Noncovalent labeling of biomolecules with red and near-infrared dyes, Molecules, 9 (2004) 40-49.
29) F. Welder, B. Paul, H. Nakazumi, S. Yagi, C.L. Colyer, Symmetric and asymmetric squarylium dyes as noncovalent protein labels: a study by fluorimetry and capillary electrophoresis, Journal of Chromatography B, 793 (2003) 93-105.
30) V.D. Suryawanshi, L.S. Walekar, A.H. Gore, P.V. Anbhule, G.B. Kolekar, Spectroscopic analysis on the binding interaction of biologically active pyrimidine derivative with bovine serum albumin, Journal of Pharmaceutical Analysis, 6 (2016) 56-63.
31) V.S. Jisha, K.T. Arun, M. Hariharan, D. Ramaiah, Site-selective interactions: squaraine dye− serum albumin complexes with enhanced fluorescence and triplet yields, The Journal of Physical Chemistry B, 114 (2010) 5912-5919.

32) O. Redy, E. Kisin-Finfer, E. Sella, D. Shabat, A simple FRET-based modular design for diagnostic probes, Organic & biomolecular chemistry, 10 (2012) 710-715.
33) B. Wang, J. Fan, S. Sun, L. Wang, B. Song, X. Peng, 1-(Carbamoylmethyl)-3H-indolium squaraine dyes: Synthesis, spectra, photo-stability and association with BSA, Dyes and Pigments, 85 (2010) 43-50.
34) F. Meadows, N. Narayanan, G. Patonay, Determination of protein–dye association by near infrared fluorescence-detected circular dichroism, Talanta, 50 (2000) 1149-1155.
35) B.Z. Packard, D.D. Toptygin, A. Komoriya, L. Brand, [2] Design of profluorescent protease substrates guided by exciton theory, Methods in enzymology, 278 (1997) 15-23.
36) D. Oushiki, H. Kojima, Y. Takahashi, T. Komatsu, T. Terai, K. Hanaoka, M. Nishikawa, Y. Takakura, T. Nagano, Near-infrared fluorescence probes for enzymes based on binding affinity modulation of squarylium dye scaffold, Analytical chemistry, 84 (2012) 4404-4410.
37) N. Nizomov, Z.F. Ismailov, S.N. Nizamov, M.K. Salakhitdinova, A.L. Tatarets, L.D. Patsenker, G. Khodjayev, Spectral-luminescent study of interaction of squaraine dyes with biological substances, Journal of Molecular structure, 788 (2006) 36-42.
38) M.C. Jiménez, M.A. Miranda, I. Vayá, Triplet excited states as chiral reporters for the binding of drugs to transport proteins, Journal of the American Chemical Society, 127 (2005) 10134-10135.

## 3.7. Appendix

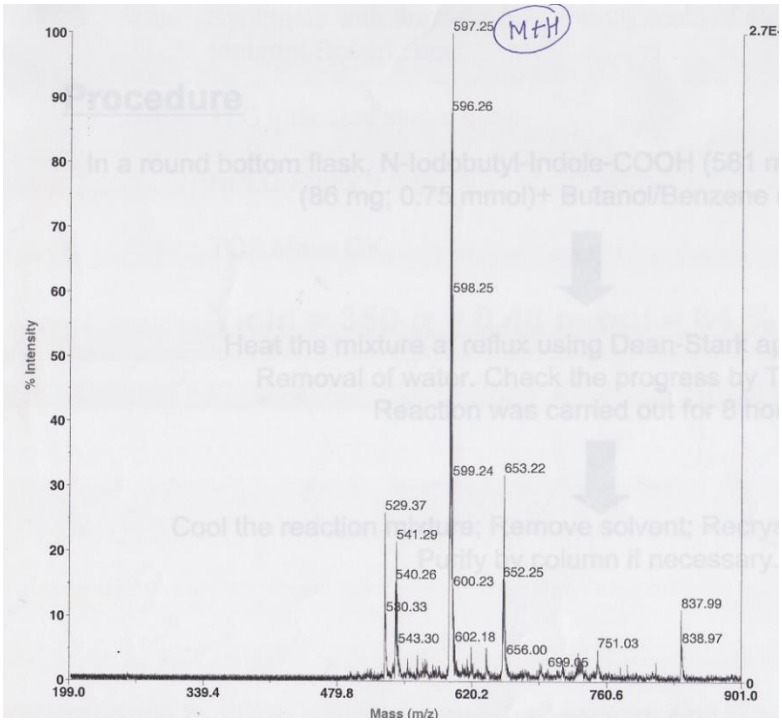


Figure 1: TOF Mass of SQ-1.

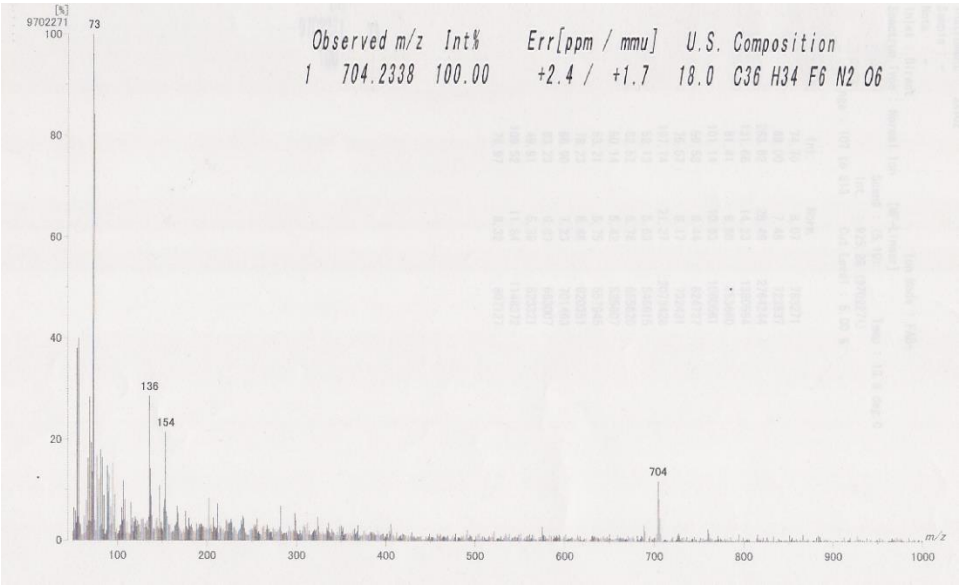


Figure 2 FAB Mass of SQ-2.

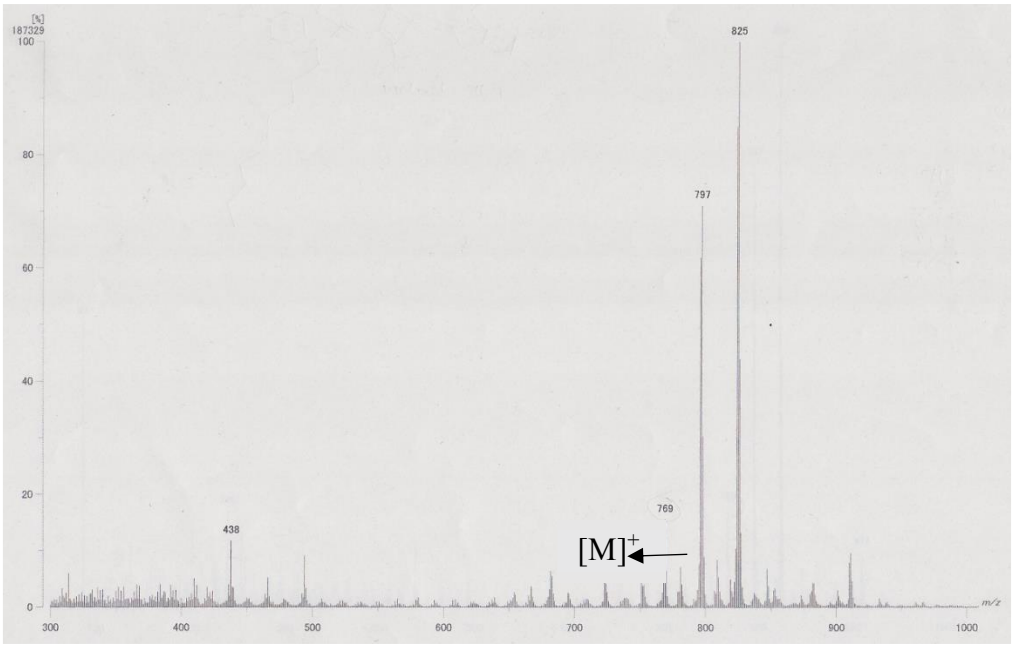


Figure 3. FAB Mass of SQ-4.

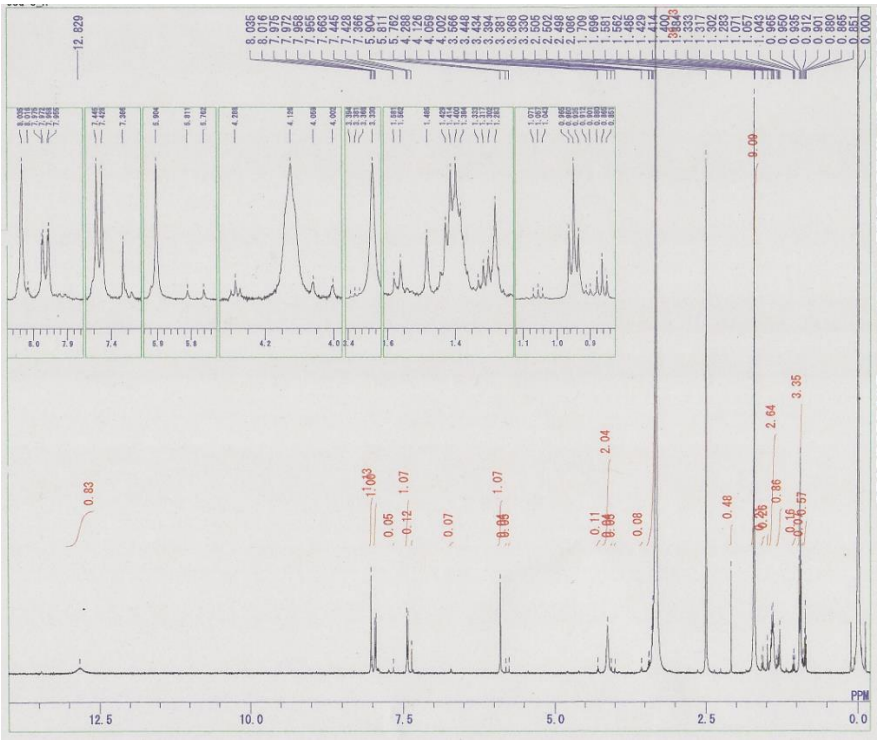


Figure 4. H-NMR of SQ-1.

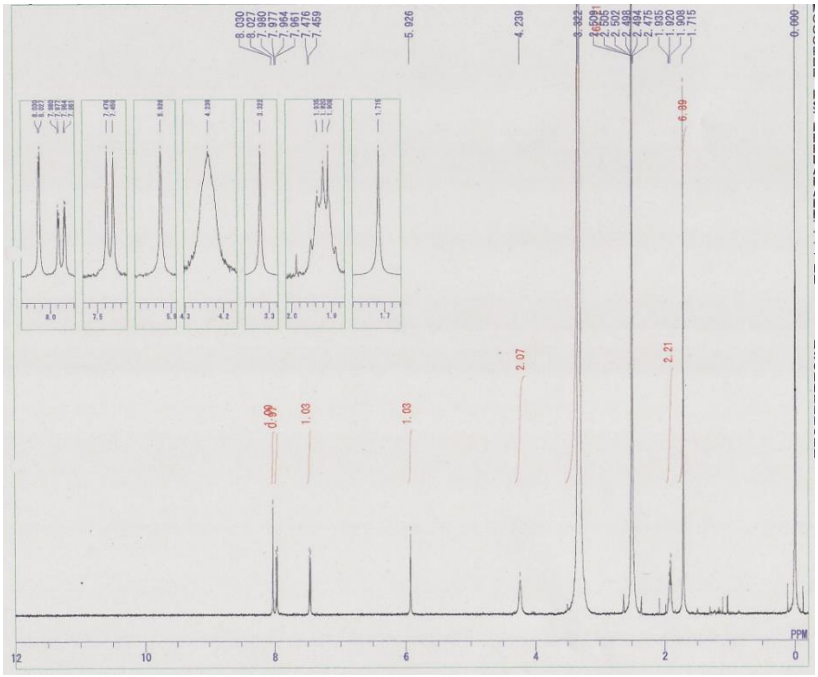


Figure 5. H-NMR of SQ-2.

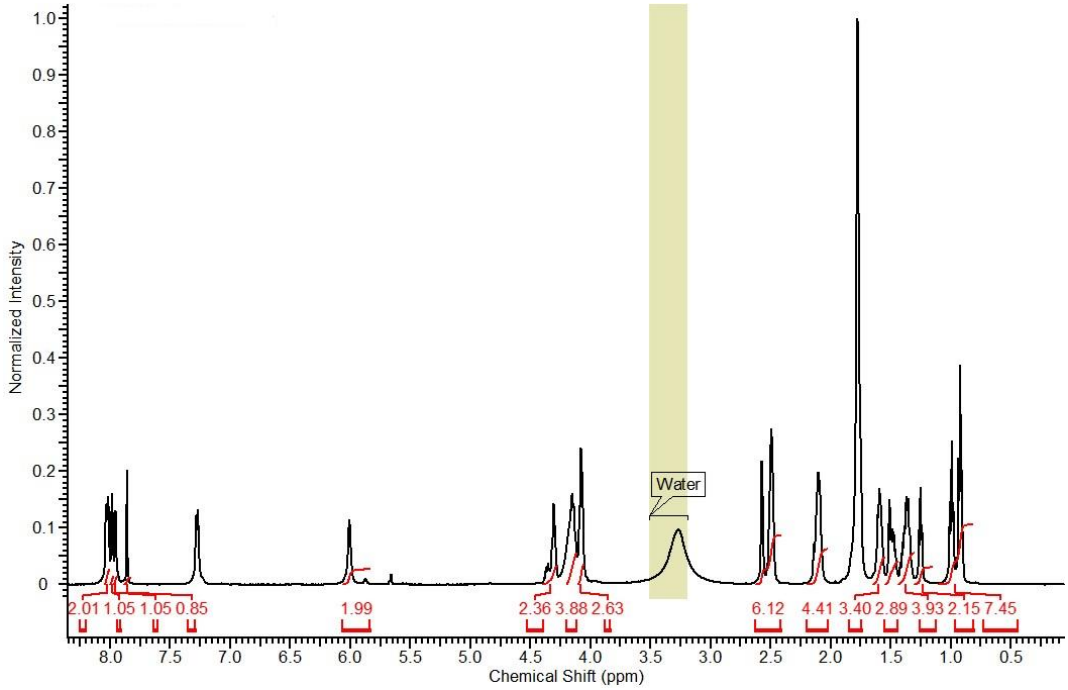


Figure 6. H-NMR of SQ-4.

# Chapter 4: Synthesis, Photophysical Characterization and Binding Interactions of Unsymmetrical Cyanine Dyes with BSA

**Abstract:** A series of model NIR sensitive unsymmetrical cyanine dyes bearing direct –COOH functionalized indole ring were efficiently synthesized, characterized and subjected to photophysical investigations. These unsymmetrical cyanine dyes were then subjected to investigate their interaction with bovine serum albumin (BSA) as a model protein in Phosphate buffer solutions (PBS). These dyes exhibit intense near infra-red light absorption and emission with high molar extinction coefficients and exhibit a blue shift in PBS solution owing to their enhanced dye aggregation. Interaction of these dyes with BSA leads to not only enhanced emission intensity but also bathochromically shifted absorption maximum due to the formation of the dye-BSA conjugate. These dyes bind strongly with BSA having an order of magnitude high binding constant as compared to the typical values reported for typical cyanine dyes. Amongst the unsymmetrical cyanine dyes used for present investigation one having substituents like Iodo and carboxylic acid in the terminal Indole ring (UCD-4) exhibited the highest association with the BSA having very high binding constant 1.01 x $10^7$ $M^{-1}$. Ligand displacement investigation with one of the cyanine dye UCD-4 having highest binding constant using dansylproline and dansylamide revealed they have the nearly equal binding capability (66 %) with both of the site-I and site-II of the BSA.

## 4. Introduction

### 4.1. Cyanine Dyes Structure

The photophysical properties of near-infrared (NIR) dyes within different types of media resulted in their use in potential applications such as photodynamic therapy, silver halide sensitizers, laser diodes, and optical data storage (1). Cyanine dyes are a unique class of charged chromophores with conjugated polymethene framework consisted of two quaternized nitrogen-containing heterocyclic rings linked together with an intermediate polymethene bridge (2). Varying the nature of the heterocyclic structure or increase in Polymethine Bridge results in dye absorption and fluorescence maxima extending into longer wavelengths. NIR polymethene class of cyanine dyes have attracted a great attention owing to their very high molar extinction coefficients, small Stokes shift and tunability of optical absorption and emission from visible to IR wavelength region by judicious molecular design (3). Their fluorescence can be readily

detected from deep tissues by commercially available imaging modalities making them the strong contender for the bio-imaging applications (4-6). Therefore, application of NIR sensitive organic dyes in optical imaging and bio-diagnosis has emerged as a potential candidate due to its low energy radiation, non-invasive nature and high sensitivity (7-9). In biological applications, NIR fluorescence can be particularly advantageous due to the absence of background interference because dye absorption bands are well removed from those most bio-macromolecules (3). Figure 1 depicts the typical absorption range of organic compounds used in the study of bio-molecules.

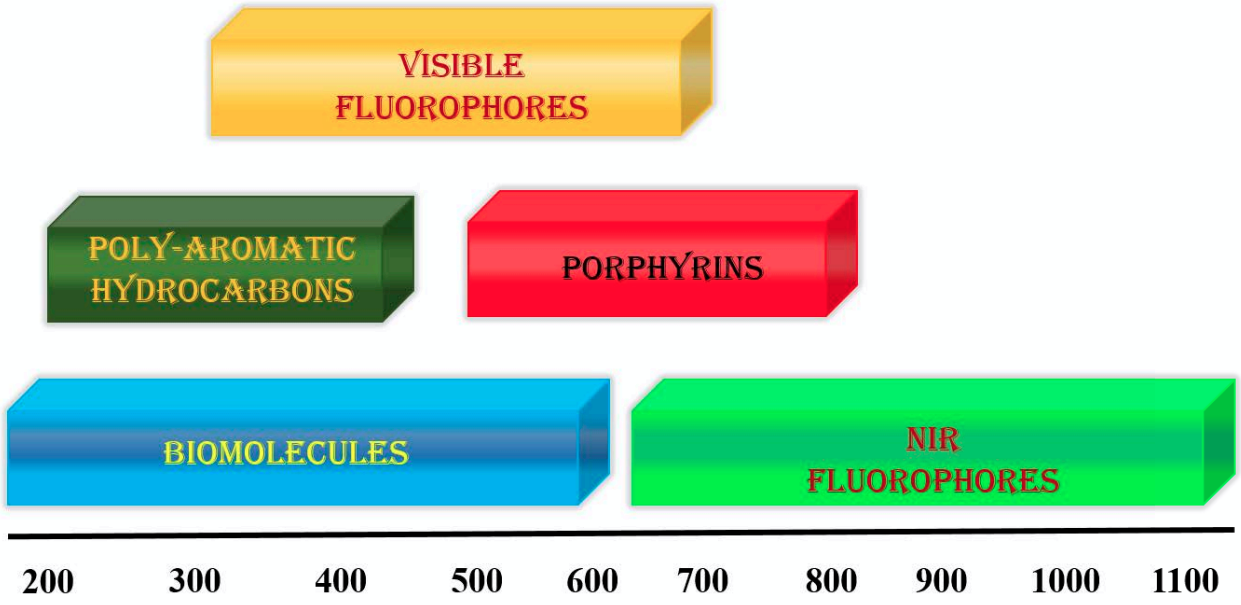


Figure 1. Typical absorption range of organic compounds used for the analysis of Bio-molecules.

Cyanine dyes have been extensively used in biological research during the last several decades. When examining the published literature, it is significant to note that this research has continuously been dictated by the availability of dye. Because visible dyes were made available much prior than their longer wavelength chromophores, a significant part of the literature focuses only on dyes exhibiting spectral characteristics (absorption and emission) in the visible region of the electromagnetic spectrum. In spite of the abundant advantages of using near-infrared (NIR) dyes, the limitations of former detection methods made the use of the longer wavelength range less attractive. Since then a large number of research groups have been dynamically employing the NIR spectral region for a broad range of biological applications.

Polymethine cyanine dyes, owning a huge number of conjugated systems which commonly absorb in NIR region. These dyes are potentially used in medical and biological application due to their solubility in water. In recent years, NIR dyes have been extensively used to study proteins in solution phase due to their absorption regions lying far beyond the absorption region of most of the bio-molecules. Cyanine dyes have been used in varied applications such as fluorescent probes in luminescent materials for labeling (11), analyte-responsive fluorescent probes (12) and in optoelectronics (13). Wavelength tunable fluorescence emission and good fluorescence quantum yield enable the cyanine dyes to detect low concentrations of analytes (14). Recent investigations on cyanine dyes have demonstrated that unsymmetrical cyanine dyes are more pronounced and gained much interest due to their excellent nucleic acid staining properties (15). Synthetic versatility due to variable central methene units and availability of a huge number of aromatic and heterocyclic terminal functionalities, considerable quantum yield, good tissue penetration, lower noise due to autofluorescence and the possibility of simultaneous multicolor and multi-target imaging enables the cyanine dyes for the utmost interest as fluorescent probes/labels (16-17).

Polymethine cyanine dyes are characterized by a chain of methine groups, that is of a structure of conjugated double bonds (18). The carbon atoms of the methine groups can be substituted by other groups than hydrogen, or they can be parts of carbocyclic or heterocyclic ring systems. The polyenes chain which ends with alkyl or other groups, do not influence the electronic excitation of the dye. In polymethine dyes, the chain of methine groups ends typically with an electron donor D and an electron acceptor A. The structural backbone of polymethine dyes is represented in figure 2. Polymethines can be classified by the number of methine groups where n = 0, 1, 2, etc. corresponding to mono-, tri-, penta-methines. In addition, polymethines can be further divided with respect to the structure of the electron donor-acceptors. For example, in the largest group of cationic polymethine dyes the donor and acceptor moieties contain nitrogen. And depending on whether or not both or one of the nitrogen's are components of a ring moiety, they are named cyanine or hemi-cyanine.

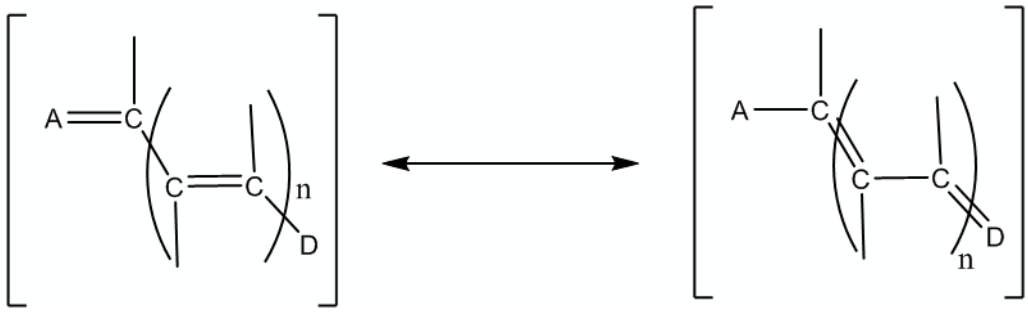


Figure 2. Structural backbone of Polymethine Cyanine dyes

## The relationship between dye structure and Spectra

The monomethine cyanine's typically get absorbed in the visible region, and with each extension of the chromophore by one vinylene moiety (CH=CH) a bathochromic shift of about 100 nm is achieved (1, 11, 19). Substituents at the chromophore lead to additional shifts in absorption. Remarkable spectral changes are witnessed with strongly electron withdrawing or strongly electron donating substituents on the chain. The extensive conjugation may increase the instability which can result in photo-bleaching or shorten the shelf life of the label. This instability may be compensated with appropriate dye design such as phthalocyanines or combining the polymethine chain into a cyclic structure. Patonay and Strekowski's research groups synthesize heptamethine cyanine dyes. In their procedure, two heterocyclic moieties are linked by Vilsmeier- Haack reagent which comprises a heptamethine chain. Polymethine cyanine's are weakly fluorescent owing to its conformational flexibility. In common, the quantum yield of cyanine dyes passes through a maximum value with the extension of the polymethine chain. The fluorescence efficiency of NIR polymethines is also improved or enhanced upon immobilization in complexes with biomolecules.

## 4.2. Cyanine Dyes Aggregation

Cyanine dyes forms aggregate quite readily in aqueous solution. These aggregates display absorption bands which are different from the monomeric species (11). The aggregate bands which are bathochromically shifted in relative to the monomeric band are termed as J-aggregates (20-23). Bands which are hypsochromically shifted when compared to the monomeric peak are recognized as to H-aggregates. The tendency of dye molecules to form aggregates be influenced by the structure of the dye and the environment (11). Aggregation of dyes is mainly promoted by strong van der Waals interactions and/or hydrogen bonding. The

strong stacking of cyanine dye structure can be promoted by van der Waals interactions due to the delocalized positive charge on the molecule. Environmental aspects of aggregation include ionic strength, pH, solvent polarity, concentration, temperature and micellar.

Cyanine dye aggregation can be defined by the exciton coupling model as displayed in figure 3 (11). Both H- and J-aggregates are composed of parallel dye molecules arranged in end to end and plane to plane to produce a two-dimensional crystal structure. According to this model, the dye molecule is termed as a point dipole and exciton state of the dye aggregate separates into two levels due to the interaction of transition dipoles. The molecules may aggregate in a head to tail (end to end) or parallel way (plane to plane stacking) to form J- and H-aggregates respectively.

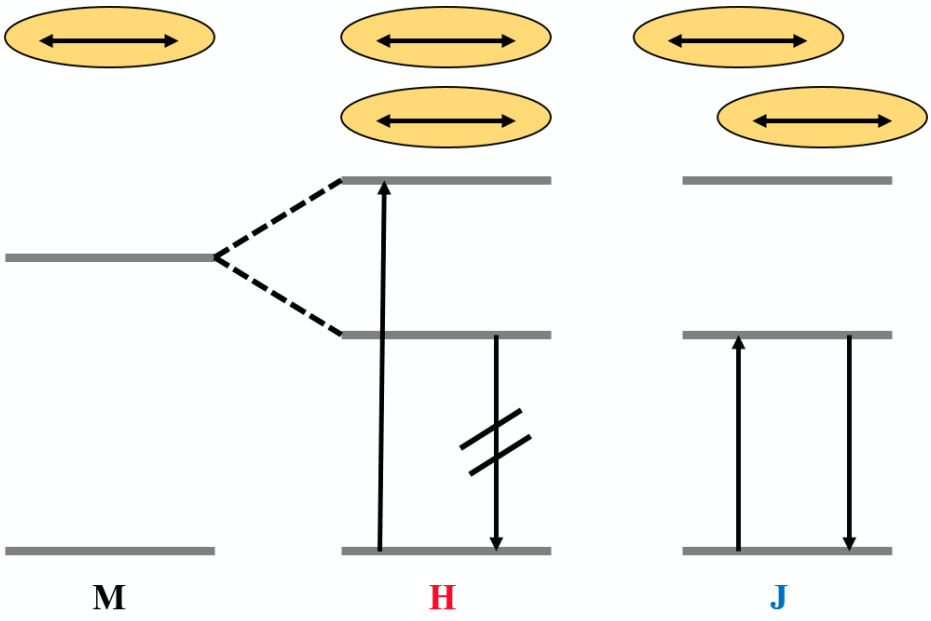


Figure 3. Exciton coupling model of Polymethine cyanine dye aggregation

H-aggregates are designated to be in a brickwork formation and J-aggregates are assumed to be more of a staircase confirmation. In H-aggregates, dipoles are fully coupled and are promoted to higher energy excited states. Whereas in the staircase conformation, dipoles are partially coupled and are only excited to the lowest energy excited states. Only J-aggregates are potential and capable of producing fluorescence with a large quantum yield (24). Meanwhile, fluorescence only takes place from the lowest energy excited state (Kasha's rule),

only J-aggregates will fluoresce. H-aggregates normally possess low quantum yields and molar extinction coefficients when compared to their monomeric absorption bands (25-27).

## 4.3. Experimental

### 4.3.1. Materials and Methods

All the chemicals for synthesis and photophysical characterization are of analytical or spectroscopic grade and used as received. Synthesized unsymmetrical cyanine dyes and dye intermediates were analyzed by MALDI-TOF/FAB-mass spectroscopy in positive ion monitoring mode and nuclear magnetic resonance spectroscopy (NMR 500MHz) for structural elucidation. Electronic absorption spectroscopic investigations in solution state were made using UV-visible-NIR spectrophotometer (JASCO V-530 UV/VIS spectrophotometer). At the same time, fluorescence emission spectrum was also recorded using fluorescence emission spectroscopy (JASCO FP-6600 spectrophotometer).

### 4.3.2. *Synthesis of Cyanine dyes and dye intermediates*

Most cyanine dyes have conventionally been synthesized by a condensation reaction between an unsaturated bis-aldehyde or its equivalent as Schiff base in the presence of a catalyst and a heterocyclic base containing an activated methyl group (28). The most widely used catalyst in this type of reaction is sodium acetate. Narayanan and Patonay reported a unique method for the synthesis of heptamethine cyanine dyes. The potential of these polymethine cyanine dyes as precursors for creating functionalized near-infrared biomolecular labels was also reported. The reaction basically involves heating a mixture of *N*-alkyl-substituted quaternary salts derived from 2,3,3-trimethylbenzoindole or 2,3,3-trimethyl indole and 2-chloro-1-formyl-3 (hydroxymethylene)cyclohex-1-ene to reflux in a mixture of benzene and 1-butanol as a solvent. An important characteristic of this method is that the slower rate of the reaction permits one to prepare asymmetric dyes from two different heterocycles in a single pot with satisfactorily yield. These cyanine dyes under investigation can be readily used for various covalent protein labeling applications since they bear –COOH group on the terminal of the indole ring.

Model NIR sensitive unsymmetrical cyanine dyes (UCD-1-4) used in the present study has been synthesized as per the scheme-1 and reported literature procedures.

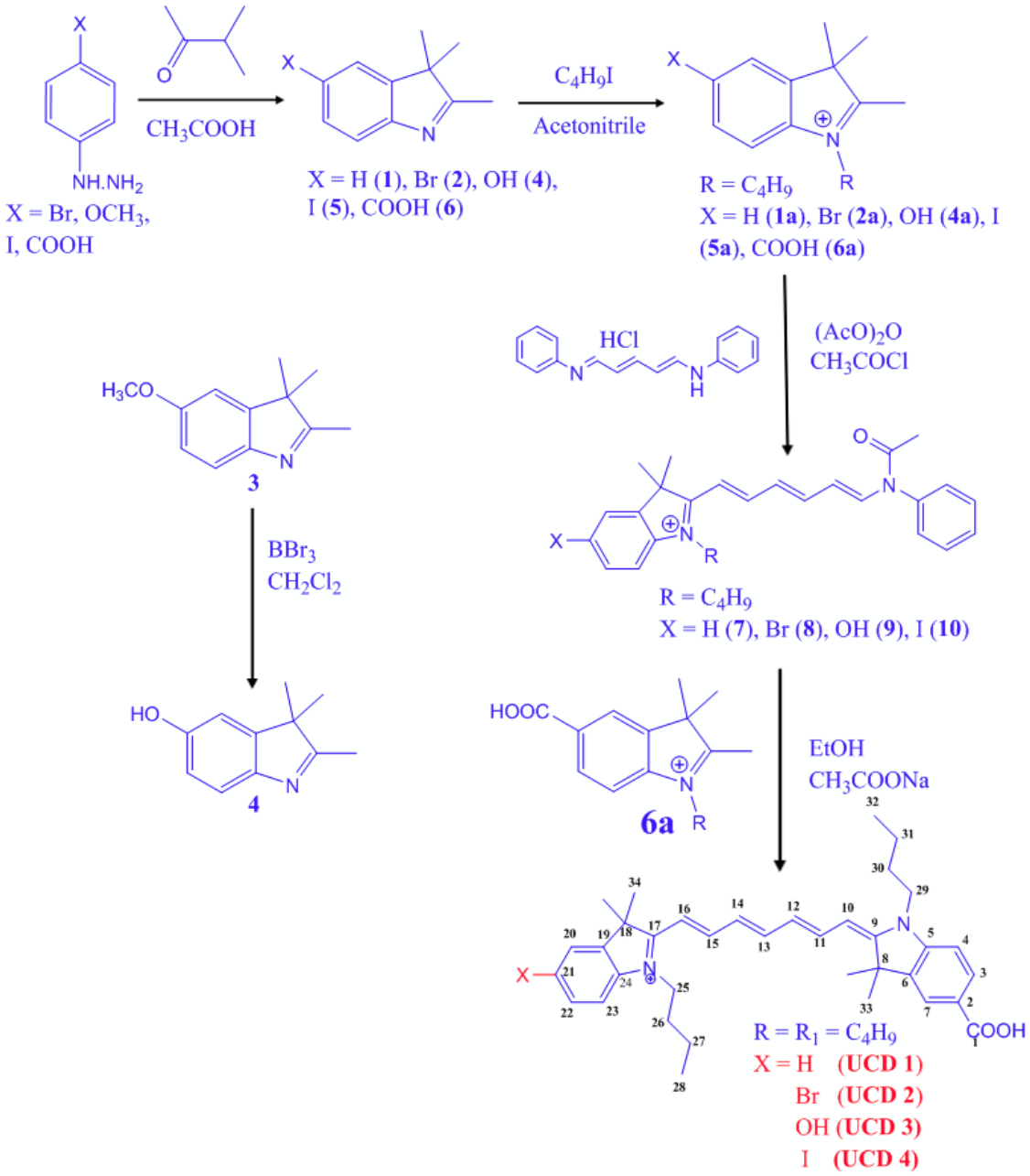


Scheme 1: Synthesis of Unsymmetrical NIR Cyanine Dyes.

***Synthesis of substituted indole derivatives (2-6):***

The derivatives *5-bromo-2,3,3-trimethyl-3H-indole (**2**)*, *5-methoxy-2,3,3-trimethyl-3H-indole (**3**)*, *5-iodo-2,3,3-trimethyl-3H-indole (**5**)* and *2,3,3-trimethyl-3H-indole-5-carboxylic acid (**6**)* were synthesized following the methodology reported by Barbero N *et al* (29), Li H *et al* (30), Klotz E J *et al* (31) and Inoue T *et al* (32) respectively.

***Synthesis of 2,3,3-trimethyl-3H-indol-5-ol (4):***

To a solution of compound **3** in dichloromethane (30 mL) at 0 °C was added dropwise 2 equivalents of 1 M BBr3 in dichloromethane and the mixture was stirred at room temperature for 12 hours. Upon the completion of reaction as monitored by TLC, the reaction mixture was washed with a saturated aqueous solution of sodium bicarbonate and the organic extracts were dried over $Na_2SO_4$, filtered, and evaporated to afford **4** as a brown solid in 79% yield (33).

***Synthesis of Alkyl-3H-indolium iodides (1a-6a):***

The derivatives *1-butyl-2,3,3-trimethyl-3H-indol-1-ium iodide (**1a**)*, *5-bromo-1-butyl-2,3,3-trimethyl-3H-indol-1-ium (**2a**)*, *1-butyl-5-hydroxy-2,3,3-trimethyl-3H-indol-1-ium (**4a**)*, *1-butyl-5-iodo-2,3,3-trimethyl-3H-indol-1-ium (**5a**)* and *1-butyl-5-carboxy-2,3,3-trimethyl-3H-indol-1-ium (**6a**)* were synthesized by following the procedure reported by Pisoni *et al* (34), Levitz A *et al* (35), Oshikawa Y *et al* (36), Gerowska M *et al* (37) and Pandey S S *et al* (38) respectively.

***Synthesis of Hemi cyanines (7-10):***

In a round bottom flask one equivalent of corresponding alkyl-3H-indolium iodides (**1a, 2 a, 4a, 5a**) and glutaconaldehyde dianil monohydrochloride, along with the catalytic amount of acetyl chloride were dissolved in acetic anhydride. The reaction mixture was refluxed at $140^0$C. After the completion of reaction as monitored by TLC, the reaction mixture was poured on to crushed ice to precipitate the desired compound as black solid. This was filtered, dried and purified by silica gel column chromatography (Ethyl acetate: Hexane = 1:1). The title compound was obtained as green solid (39).

*1-butyl-3,3-dimethyl-2-((1E,3E,5E)-6-(N-phenylacetamido)hexa-1,3,5-trien-1-yl)-3H-indol-1-ium chloride (**7**)* was obtained in 60% yield. MALDI TOF – mass (measured 414.33 $[M+H]^+$; calculated 413.58), *5-bromo-1-butyl-3,3-dimethyl-2-((1E,3E,5E)-6-(N-phenylacetamido)hexa-1,3,5-trien-1-yl)-3H-indol-1-ium chloride (**8**)* obtained in 20% yield. MALDI TOF – mass (measured 492.33 $[M]^+$; calculated 492.48), *1-butyl-5-hydroxy-3,3-dimethyl-2-((1E,3E,5E)-6-(N-phenylacetamido)hexa-1,3,5-trien-1-yl)-3H-indol-1-ium chloride (**9**)* obtained in 26% yield ESI – mass (measured 429.25 $[M]^+$; calculated 429.58), *1-butyl-5-iodo-3,3-dimethyl-2-((1E,3E,5E)-6-(N-phenylacetamido)hexa-1,3,5-trien-1-yl)-3H-*

*indol-1-ium chloride (**10**)* obtained in 20% yield confirmed the successful synthesis of intermediate hemi-cyanine's.

***Synthesis of Unsymmetrical cyanine dyes (UCD-1 - 4):***

In a round bottom flask, one equivalent of corresponding hemi cyanine (**7-10**) was dissolved in 20 ml of ethanol. To the above solution one equivalent of Compound **6a,** 2 equivalents of sodium acetate were added. The reaction mixture was refluxed at $95^0$C. Upon the completion of reaction as monitored by TLC, the solvent was evaporated under reduced pressure and the residue was dissolved in chloroform and washed with water to remove excess sodium acetate. The organic layer was dried over anhydrous sodium sulfate and evaporated under reduced pressure. The crude was purified by silica gel column chromatography (Chloroform: Methanol = 9:1) to afford the respective compounds as blue green solid (40).

1-butyl-2-((1E,3E,5E)-7-((E)-1-butyl-5-carboxy-3,3-dimethylindolin-2-ylidene)hepta-1,3,5-trien-1-yl)-3,3-dimethyl-3H-indolium chloride (**UCD-1**) was obtained in 10% yield. High resolution (HR)-FAB mass (measured 537.3453 $[M]^+$; calculated 537.3476). $^1$H NMR (500 MHz $CDCl_3$): 0.99 (6 H, t), 1.26-1.68 (8 H, m), 1.71 (6 H, s), 1.78 (6 H, s), 3.65-4.10 (4H, t), 6.21-6.99 (7 H, m), 7.45 (1 H, s), 7.49 (1 H, s), 7.81 (1 H, s), 7.91 (1 H, s), 8.05-8.13 (3 H, m). $^{13}$C NMR (500 MHz, DMSO: δ180.59 (C-17), δ167.16 (C-9), δ166.92 (C-1), δ146.65 (C-6), δ145.67 (C-24), δ142.01 (C-19), δ141.77 (C-5), δ140.30 (C-7), δ136.16 (C-15), δ131.50 (4C, C-11,12,13,14), δ127.60 (C-3, 22), δ125.04 (C-21), δ123.57 (C-20), δ123.06 (C-2), δ122.61 (C-23), δ121.87 (C-4), δ112.34 (C-16), δ109.17 (C-10), δ49.74 (C-8), δ47.21 (C-18), δ43.26 (C-29), δ43.23 (C-25), δ29.52 (C-30), δ28.96 (C-26), δ26.76 (C-33), δ24.12 (C-34), δ19.5 (C-27), δ19.44 (C-31), δ13.78 (C-32), δ13.56 (C-28). FTIR (KBr, $cm^{-1}$): 2958-m (OH), 1694-s (C=O), 1604-s (C= C), 1515-s (C= C (Ar)), 1417-s ($CH_2$ bend), 1365-m (C-N), 1316-w (C-O), 833-w (P-substitution), 782-m 714-s (C-H (oop)).

*5-bromo-1-butyl-2-((1E,3E,5E)-7-((E)-1-butyl-5-carboxy-3,3-dimethylindolin-2-ylidene)hepta-1,3,5-trien-1-yl)-3,3-dimethyl-3H-indol-1-ium chloride* (UCD-2) obtained in 9% yield. FAB – mass (measured 615.2581 $[M]^+$; calculated 615.2557). FTIR (KBr, cm-1): 2957-m (OH), 1710-s (C=O), 1609-m (C= C), 1508-s (C= C (Ar)),

1417-m (CH2 bend), 1347-m (C-N), 1267-w (C-O (carboxyl)), 1086-m (C-O), 824-w (p-substitution), 723-w (m-substitution), 652-m (C-H (oop)).

1-butyl-2-((1E,3E,5E)-7-((E)-1-butyl-5-carboxy-3,3-dimethylindolin-2-ylidene)hepta-1,3,5-trien-1-yl)-5-hydroxy-3,3-dimethyl-3H-indolium chloride (UCD-3) obtained in 5% yield. (HR)-ESI - TOF mass (measured 553.3415 [M] +; calculated 553.3425). 1H NMR (500 MHz CDCl3): 0.97 (6 H, t), 1.12-1.58 (8 H, m), 1.65 (6 H, s), 1.69 (6 H, s), 3.99 (2 H, m), 4.44 (2 H, m), 6.10-6.99 (7 H, m), 7.2 (3 H, m), 7.99 (2 H, m), 8.33 (1 H, s). 13C NMR (500 MHz, DMSO: δ177.17 (C-17), δ170.09 (C-9), δ166.18 (C-1), δ153.49 (C-6), δ149.34 (C-24), δ144.94 (C-19), δ140.79 (C-5), δ132.49 (C-15), δ131.75 (C-11,12,13,14), δ129.92 (C-3, 22), δ126.99 (C-7), δ123.57 (C-21), δ122.11 (C-20), δ120.89 (C-2), δ104.77 (C-23), δ98.67 (C-4), δ95.74 (C-10), δ93.05 (C-16), δ58.26 (C-18), δ48.73 (C-25), δ44.34 (C-8), δ42.38 (C-29), δ29.69 (C-26), δ28.22 (C-30), δ25.54 (C-33), δ24.80 (C-34), δ20.41 (C-27), δ20.16 (C-31), δ15.29 (C-32), δ14.55 (C-28).FTIR (KBr, cm-1): 2964-m (OH), 1695-m (C=O), 1605-s (C= C), 1521-m (C= C (Ar)), 1417-m (CH2 bend), 1360-s (C-N), 1291-w (C-O (carboxyl)), 1091-s (C-O), 831-w (p-substitution), 716-s (m-substitution), 658-w (C-H (oop)).

1-butyl-2-((1E,3E,5E)-7-((E)-1-butyl-5-carboxy-3,3-dimethylindolin-2-ylidene)hepta-1,3,5-trien-1-yl)-5-iodo-3,3-dimethyl-3H-indolium chloride (**UCD-4**) obtained in 11 % yield. $^{1}$H NMR (500 MHz $CDCl_3$): 0.97 (6 H, t), 1.1-1.58 (8 H, m), 1.65 (6 H, s), 1.69 (6 H, s), 4.0-4.10 (4H, m), 6.2-7.2 (7 H, m), 7.55 (1 H, s), 7.63 (2 H, d), 7.99 (1 H, s), 8.09 (2 H, d). $^{13}$C NMR (500 MHz, DMSO: δ176.20 (C-17), δ173.70 (C-9), δ168.09 (C-1), δ154.23 (C-5), δ147.10 (C-24), δ146.47 (C-19), δ145.07 (C-6), δ140.91 (C-15), δ133.14 (C-14), δ132.69 (C-13), δ131.68 (C-12), δ129.62 (C-11), δ125.78 (C-7), δ124.06 (C-3, 22), δ123.70 (C-21), δ122.37 (C-20), δ121.87 (C-2), δ119.29 (C-23), δ113.63 (C-4), δ112.14 (C-10), δ86.92 (C-16), δ69.18 (C-18), δ63.35 (C-25), δ48.29 (C-8), δ44.65 (C-29), δ29.89 (C-26), δ29.87 (C-30), δ27.98 (C-33), δ24.44 (C-34), δ20.36 (C-27), δ20.13 (C-31), δ14.35 (C-32), δ14.20 (C-28). FTIR (KBr, $cm^{-1}$): 2958-m (OH), 1699-m (C=O), 1605-m (C= C), 1506-s (C= C (Ar)), 1415-s ($CH_2$ bend), 1360-s (C-N), 1309-w (C-O (carboxyl)), 816-w (p-substitution), 714-s (m-substitution), 649-m (C-H (oop)), 554-w (C-I).

## 4.4. Results and Discussion

### *4.4.1. Photophysical Characterization*

After the successful synthesis and purification, these NIR sensitive dyes were subjected to photophysical investigations pertaining to the electronic absorption and fluorescence emission spectroscopy. Results thus obtained pertaining to the photophysical parameters have been summarized in table 1. Figure 4 exhibits the solution state electronic absorption and fluorescence emission spectra of the unsymmetrical cyanine dyes in the dimethylformamide (DMF) solution.

**Table 1.** Spectral properties of dyes in DMF and 0.1 M PBS solution at pH 7.4.

| DYE | DMF solution | | PBS solution | | Stoke Shift | | (ε) ($dm^3\ M^{-1}\ cm^{-1}$) |
|---|---|---|---|---|---|---|---|
| | λ (max) Absorption | λ (max) Emission | λ (max) Absorption | λ (max) Emission | DMF | PBS | |
| **UCD -1** | 764 nm | 788 nm | 750 nm | 770 nm | 24 nm | 20 nm | $1.1\times10^5$ |
| **UCD -2** | 769 nm | 792 nm | 755 nm | 774 nm | 23 nm | 19 nm | $1.2\times10^5$ |
| **UCD -3** | 769 nm | 792 nm | 753 nm | 772 nm | 23 nm | 19 nm | $0.8\times10^5$ |
| **UCD -4** | 774 nm | 798 nm | 758 nm | 770 nm | 24 nm | 12 nm | $1.4\times10^5$ |

It can be observed that position of maxima ($\lambda_{max}$) for the electronic absorption and fluorescence emission in DMF are not much affected by the different substituents (bromo, hydroxyl and iodo) present in main π-conjugated polymethene framework. The $\lambda_{max}$ of unsymmetrical cyanine dyes ranges from 764 to 774 nm with high molar extinction coefficients ($\varepsilon \approx 10^5\ dm^3\ M^{-1}\ cm^{-1}$). This sharp and intense light absorption in this class of dyes is associated with the π–π* electronic transitions. The fluorescence emission spectra for each of dyes were measured slightly below (about 15-20 nm) to the corresponding $\lambda_{max}$ of absorption spectrum as the excitation wavelength. For all of the unsymmetrical cyanine dyes, one main emission band can be observed which is ranging from 788 nm to 798 nm, with a small Stokes shift of 23 and 24 nm. This small Stokes shift represents the rigidity of the molecules without having any conformational changes after the photoexcitation.

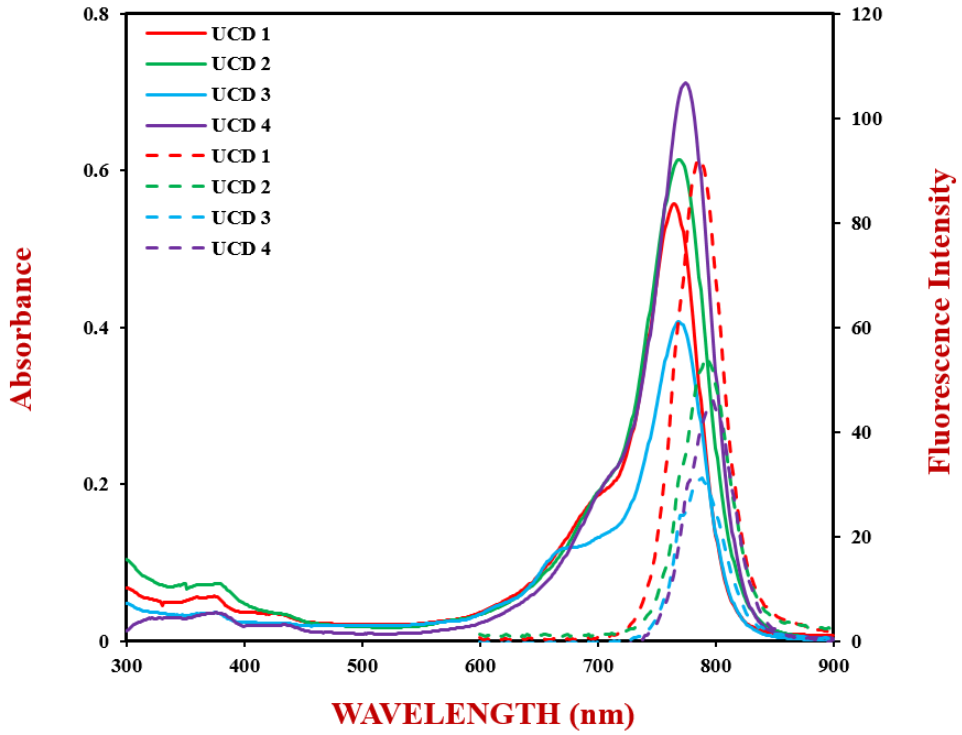


Figure 4. Electronic absorption (solid line) and fluorescence emission (dashed line) spectra of UCD-1-4 in DMF solution (5 μM).

To investigate the interactions between the dyes and the biomolecules for imaging applications, Phosphate buffer solution (PBS) has been most commonly used. Keeping this in mind, electronic absorption spectra of these dyes were also measured in the 0.1 M PBS solution at pH 7.4 which has been shown in figure 5. It is worth mentioning that the absorption spectra of cyanine dyes in PBS exhibited slightly blue shifted $\lambda_{max}$ compared to that observed in DMF. This behaviour of blue shifted $\lambda_{max}$ could be attributed to the enhancement in the aggregation of dye, promoted by the hydrogen bonding between the dye molecules due to the presence of –COOH groups. It is well known that cyanine dyes exhibit dye aggregation owing to their flat molecular structure (41). Apart from the main π–π* electronic transition, cyanine and squaraine dyes also exhibit a vibronic shoulder just before the main absorption peak and the vibronic shoulder has been reported to be the marker of molecular aggregation (42). A higher value of the ratio of absorbance for the vibronic shoulder with respect to the absorbance corresponding to the main π–π* transition indicates an enhanced dye aggregation (43-44).

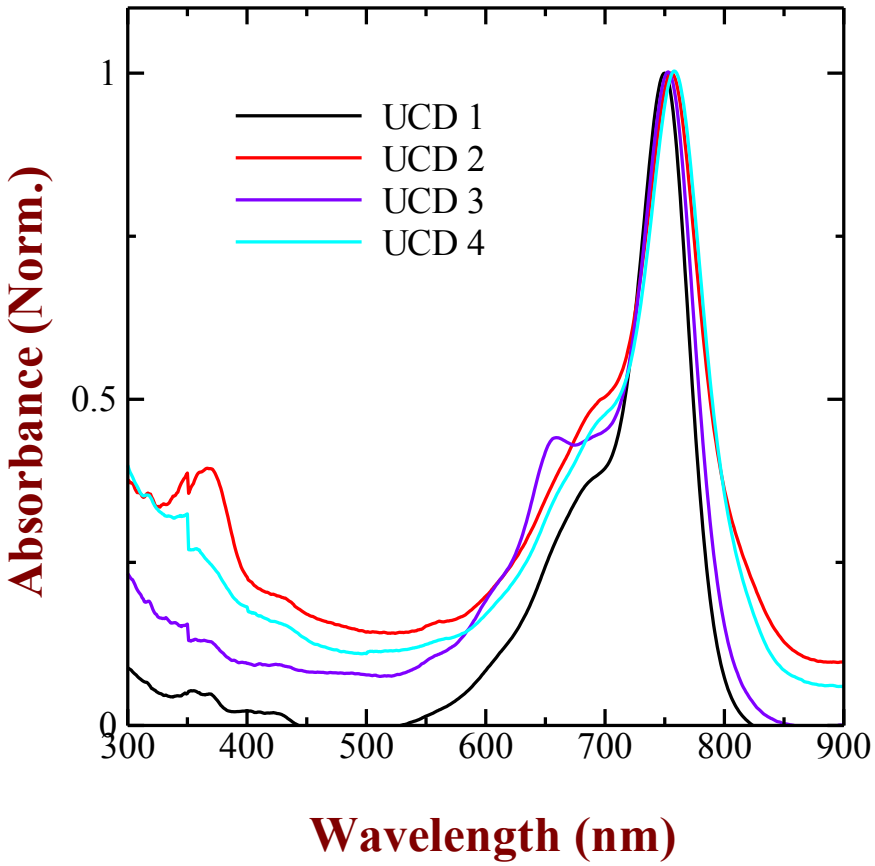


Figure 5. Electronic absorption spectra for unsymmetrical cyanine dyes UCD-1 to 4 in 0.1 M PBS.

An interesting feature that the fluorescence emission of cyanine dyes in PBS showed slightly red shifted curves with stoke shift less than those observed in organic solvents which are displayed in figure 6, can also be credited to the aggregation of dyes. The emission intensities of these cyanine's in PBS solution are relatively high at similar concentration and experimental conditions than those reported by Pisoni *et al* (34). Therefore the dyes UCD-1-4 can be used as potential applicants as quenching probes for the design and development of NIR fluorescence resonance energy transfer systems.

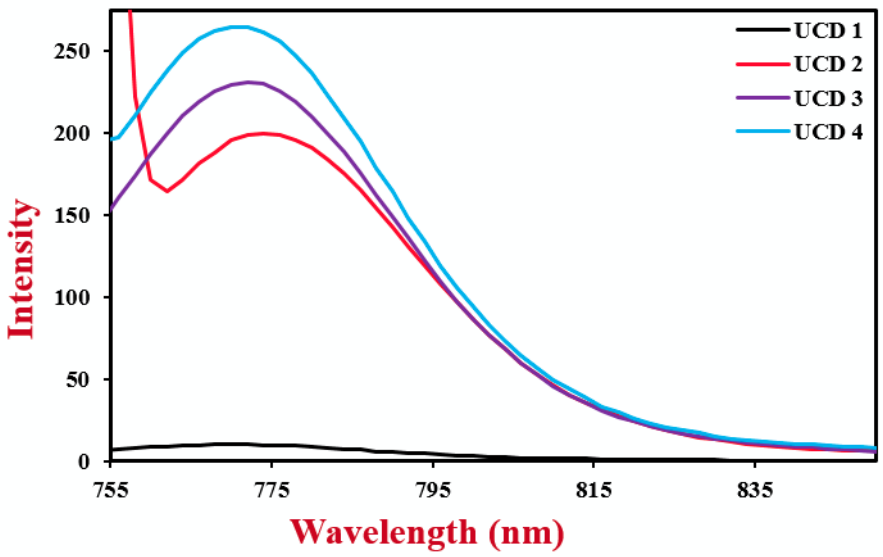


Figure 6. Fluorescence emission spectra for unsymmetrical cyanine dyes UCD-1-4 in 0.1 M PBS.

### *4.4.2. Quantum Yield of Cyanine Dyes*

Cyanine dyes are considered to be a vast area of chemical research owing to its wide applications in biomedical, analytical, biological and various other research fields. Near-infrared absorbing cyanine dyes have drawn much attention because of their optimal spectral, biological and chemical properties along with their excellent safety profile (45). The potential advantages of NIR fluorophores are the ability to penetrate deep into biological tissue as slight NIR absorption and emission exist in natural biosystems and the pronounced decrease in autofluorescence which is constantly encountered in the visible region (46). Cyanine dyes can be regarded as the leading class of NIR fluorescent probes towards biological applications at the current situation because of their unique, broad wavelength tunability, moderate-to-high fluorescence quantum yields and high molar extinction coefficients (45). Most polymethine cyanine's possess the disadvantage that their Stoke shifts are less than 20 nm. A small Stokes‟ can leads to self-quenching and measurement error by scattered light and excitation light. Both of these key features are responsible for decreasing the detection sensitivity to a greater extent.

Fluorescence quantum yield ($\phi$) is an important parameter towards the development of fluorescent probes and is an indicator of the capability of a fluorescent probe to convert absorbed photons into the emitted one in a particular environment. In combination with molar

extinction coefficient (ε), it signifies the strength of fluorescence signal since the product of the ϕ and ε determines the brightness of fluorophore.

Fluorescence emission quantum yield of dyes was estimated based on the comparative method reported by Williams et al (47), which involves the use of well characterized standard samples with known $\Phi_F$ values. Basically, the same number of photons can be expected to absorb when the solutions of the standard and test samples with matching absorbance at similar excitation wavelength are preferred. Therefore, a simple ratio of the integrated fluorescence intensities of the two solutions will give the ratio of the quantum yield values.

$$Q = Q_R \left[\frac{Grad}{Grad_R}\right]\left[\frac{\eta^2}{\eta_R^2}\right] \qquad [1]$$

Where $Q_R$ is the quantum yield of the known (reference) sample, Grad is the gradient obtained from the plot of integrated fluorescence intensity vs. absorbance, $Grad_R$ is the gradient of reference sample η is the refractive index of the solvent. The fluorescence emission quantum yield assay was done by using different concentrations of dyes ranging from 100 μM to 100 nm in the chloroform as the solvent. The electronic absorption and fluorescence emission spectra were recorded. The emission spectra were measured using the corresponding $\lambda_{max}$ of absorption spectra as the excitation wavelength. Integrated fluorescence intensity (area under the peak) was obtained and a graph between integrated fluorescence intensity vs. absorbance was plotted to obtain straight line with Gradient (m).

**Table 2.** Fluorescent quantum yield of cyanine dyes.

| Dye | Quantum Yield (ϕ) |
|---|---|
| **UCD-1** | 0.33 |
| **UCD-2** | 0.44 |
| **UCD-3** | 0.19 |
| **UCD-4** | 0.65 |

A perusal of Table 2 indicates that newly synthesized dyes in this work exhibits moderate the high ϕ values compared to that of the values reported for a variety of typical NIR cyanine dyes. Amongst the dyes used in this work, it can be seen that dye UCD-2 exhibit moderate value of ϕ (about 0.44), which can be attributed to the presence of donating group as well as low stoke

shift than unsubstituted dye and –OH substituted cyanine dye UCD-3 exhibits relatively hampered value of ϕ (about 0.20) as compared to the unsubstituted UCD-1 (0.33). This could be attributed the fact that UCD-3 exhibits pronounced aggregate formation and aggregate assisted non-radiative fluorescence decay leading to the hampered ϕ. The dye UCD-4 exhibit high value of ϕ (about 0.65), due to the presence of heavy metal on the terminus of the indole ring. The dyes under investigation display's high quantum yield and the stoke shift is greater than 20 nm which greatly reduces the defects such as self-quenching and measurement error due to scattered and excited light there by enhancing the detection sensitivity.

### *4.4.3. Fluorescence Life time Measurement*

The average amount of time the molecule spends in its excited state can be precisely defined as the fluorescent life time of a molecule (48). When the molecule absorbs a photon, one of the electrons gets promoted to an excited state and descends to the first excited state vibrational orbital through intersystem crossing. The molecule can stay in this state for a quite long period of time, which ranges from hundreds of picoseconds to tens of nanoseconds. The fluorescence lifetime depends not only on the structure in the excited state, but also rigidity is the most important factor, and its environment, such as oxygen concentration, viscosity, polarity, temperature and pH (49). Meanwhile, all these parameters are biologically significant and their defects often accompanying with to diseases, application of fluorescent lifetime as an imaging modality in medical biology is promptly developing. The heightened interest in the use of NIR fluorescent dyes for in vivo and in-cellular imaging studies motivated researchers to evaluate the FLT of NIR fluorescent polymethine dyes. This class of dyes are particularly used in a variety of biological applications due to their excellent biocompatibility and spectral properties (50-52).

The fluorescence lifetime of the dyes in chloroform as a solvent was estimated to provide insights on excited state decay pathway. It is generally accepted that the photo-isomerization decay pathway is dependent on solvent whereas internal conversion is the solvent independent process. There is no clear information about which properties of the solvent including hydrogen bonding, viscosity and polarity play an important role in decay pathway. The research conducted by M Y Berezin et al concluded that cyanine dyes are highly sensitive to solvent polarity (49, 53).

The study conducted by H Lee and group in 2008 had synthesized structurally diverse NIR polymethine dyes and their fluorescence life time was evaluated in relation to their structural properties. Comparative life time study based on modification of heterocyclic system and methine chain length showed that indolium or benzoindolium polymethine cyanine dyes display longer life time when compared to benzoindolium trimethine dye. This particular study had also revealed that the fluorescence life time of polymethine dyes increases from polar to non-polar solvents. The dyes displayed enhanced lifetime values in chloroform as the solvent.

**Table 3.** Life time fluorescence measurement of unsymmetrical cyanine dyes.

| Dye | Lifetime (τ) |
|---|---|
| **UCD-1** | 1.39 ns |
| **UCD-2** | 1.40 ns |
| **UCD-3** | 1.40 ns |
| **UCD-4** | 1.42 ns |

Keeping this in view, the fluorescence lifetime of dyes under present investigation was executed in chloroform solvent. The constant dye solution of concentration 5 μM was prepared using chloroform and the lifetime measurement were recorded by employing the emission maxima of corresponding dyes at 20 ns time of scale. The lifetime values displayed by these unsymmetrical dyes are shown in table 3 and are comparable to the dyes reported by H Lee (54). Figure 7 displays the lifetime measurement of unsymmetrical cyanine dyes which are high when compared to the dyes reported. There is no significant change in life time fluorescence displayed by these dyes though different electron withdrawing, donating and heavy metal ion substituents are incorporated in the terminus of the indolium ring.

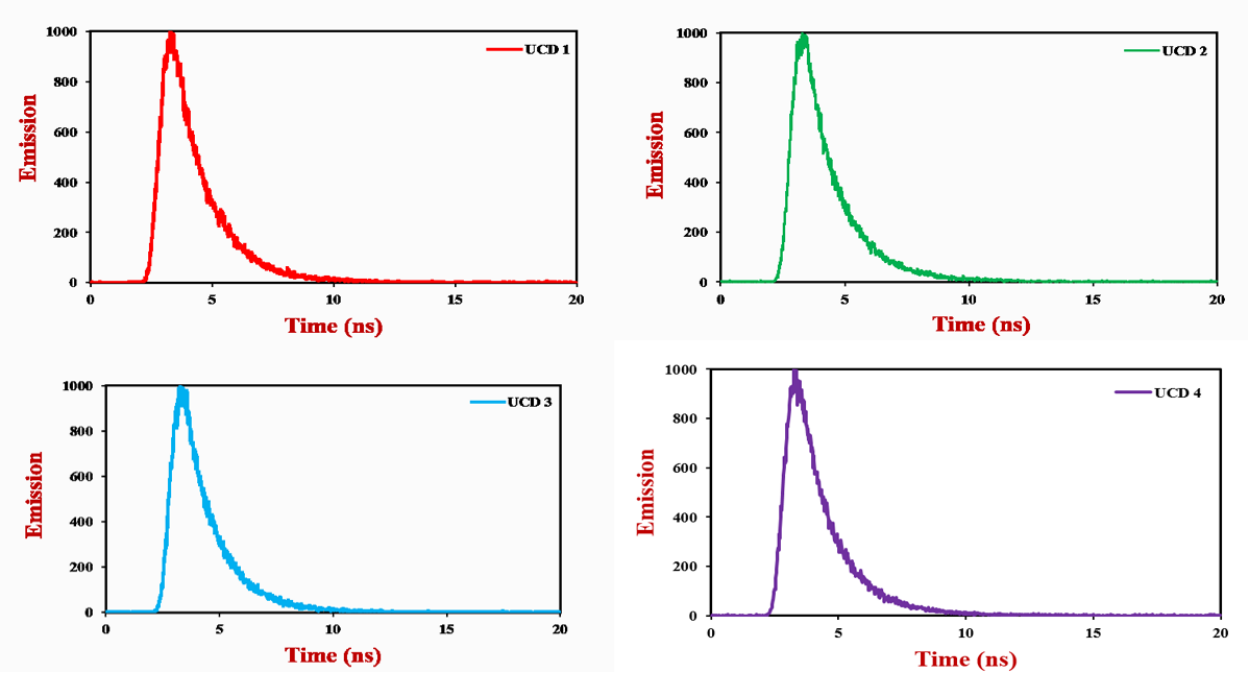


Figure 7. Life time fluorescence measurement of unsymmetrical cyanine dyes.

### *4.4.4. Binding Assay of Cyanine Dyes with BSA*

BSA is a globular protein made of three main domains that contain two subdomains each: IIA and IIIA (34). The sub domains are stabilized by 17 disulfide bridges which serve the purpose as specific binding pockets with the ligands. Both the sub domains comprise of intrinsic fluorescent residues Tyr 411 and Trp 214 in IIIA and IIA respectively. Trp 214 exhibits the most fluorescence in the molecule, Tyr displays reasonable fluorescence and is quenched in the presence of tryptophan residue, amino groups, and carboxyl groups (55). These hydrophobic residues are the binding sites of interest for noncovalent interactions with cyanine dyes. Furthermore, as Pisoni and coworkers point out, steric interferences can also affect dye and protein binding interactions (34).

The protein-dye binding interactions were executed using PBS (0.1 M at pH 7.4) and cyanine dye solutions (2μM), prepared by the addition of 100 μl of 0.1 M dye solution in DMF to the various concentrations of PBS/BSA solutions in the concentration range of (0-10 μM). The methodology adopted was similar to that discussed in chapter 3. This study aims to characterize a series of unsymmetrical NIR cyanine dyes and their binding behavior with BSA. Specifically, to study the effect of substitution on the terminal of the indolium ring with various groups such as electron withdrawing, electron donating and heavy ion was taken into

consideration while evaluating their absorption and emission properties and their changes upon interaction with BSA. It is expected that the dye with most hydrophobic moieties will show preference in binding with BSA thus supporting their potential use for the applications towards noncovalent labelling of proteins.

In order to avoid the purification steps in labelling of biomolecules with dyes towards the application of optical bio imaging, noncovalent methods have been frequently used (19). Patonay and co-workers were among the first to study the noncovalent labelling of the human serum albumin (HSA) with near-infrared dyes by using high-performance liquid chromatography (HPLC) and absorption detection (56). At the same time, bovine serum albumin (BSA) is a globular protein which has been prominently used as protein model to investigate the interactions between dye and protein owing to its high homology with HSA in the amino acid sequences (57). Therefore, dyes used in this work have also been subjected to investigate their interaction with the BSA as a model protein. Figure 8 depicts the absorption spectra of one of the representative cyanine dyes (UCD-1) in the presence and absence of BSA. It can be seen that there are two different sets of prominent electronic absorption bands in the wavelength region of 250 nm - 300 nm and 700 nm - to 800 nm associated with the absorption of BSA and dye UCD-1, respectively. Increase in the BSA concentration led to the gradual increase in the intensity of absorption between 250 nm - 300 nm, which was associated with electronic absorption of the protein BSA.

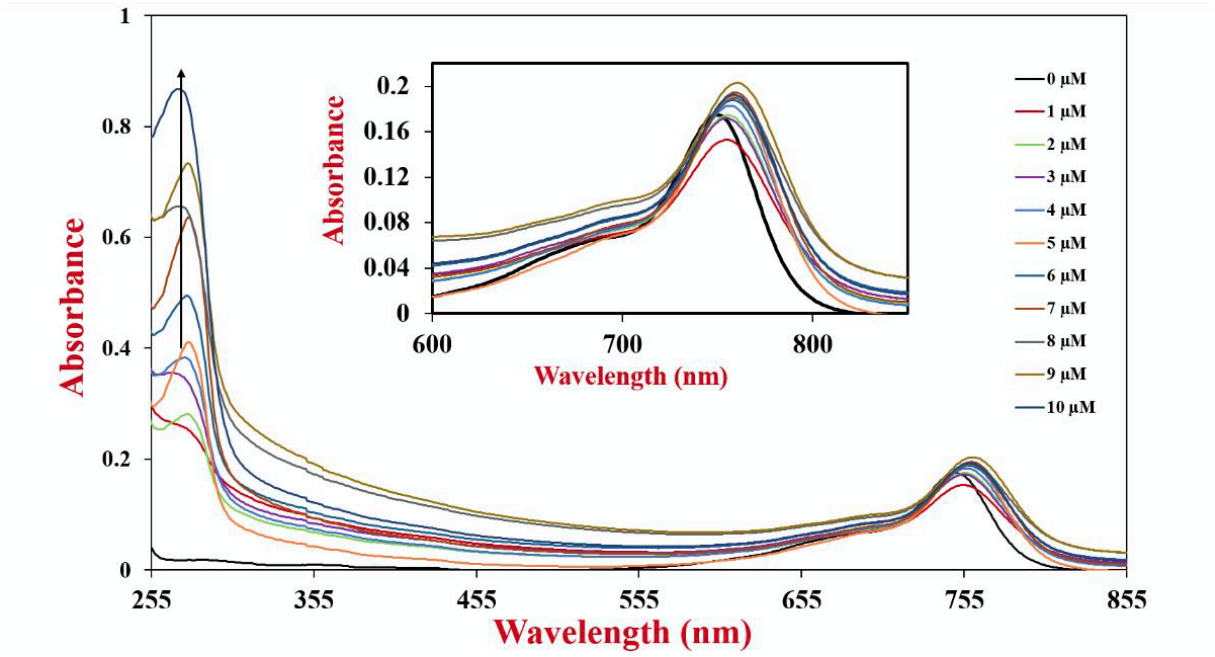


Figure 8. Electronic absorption spectra of UCD-1 in 0.1 M PBS at different concentrations of BSA for fixed dye concentration of 2 µM.

However, there was random increase and the decrease of absorption intensity associated with dye in NIR region of 600 nm - 800 nm, a behavior similar to that observed by Pisoni et al also (33). At the same time, random increase and decrease without any isosbestic point indicate that the equilibrium between the free and bound protein is not simple in all the dyes under investigation. Interestingly, $\lambda_{max}$ associated with UCD-1 which was around 750 nm in the absence of BSA was found to be bathochromically shifted by 5-10 nm in the presence of BSA. This could be attributed to the suppression of dye aggregation due to the interactions between the protein and dye molecules. A similar type of behavior has also been observed for the other cyanine dyes (UCD-2 and UCD-3and UCD-4) and results have been provided in figure 9.

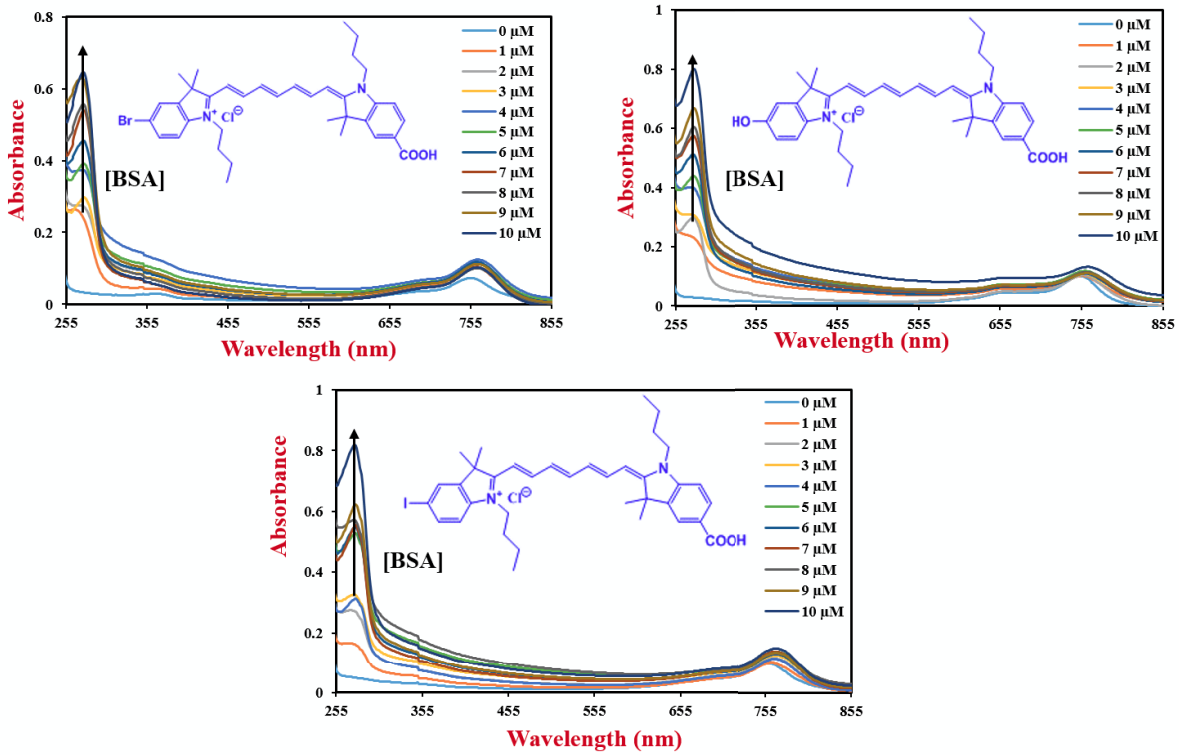


Figure 9. Electronic absorption spectra of UCD (2-4) in 0.1 M PBS at different concentrations of BSA for fixed dye concentration of 2 µM.

The fluorescence emission spectra of UCD-1 in the presence and absence of BSA is shown in figure 10. It can be seen that dye exhibits increase in fluorescence intensity near the $\lambda_{max}$ along with the slight red shift of peak maxima upon the addition of increasing amounts of BSA. The increase in fluorescence intensity could be attributed to the possible interaction between the UCD-1 and BSA.

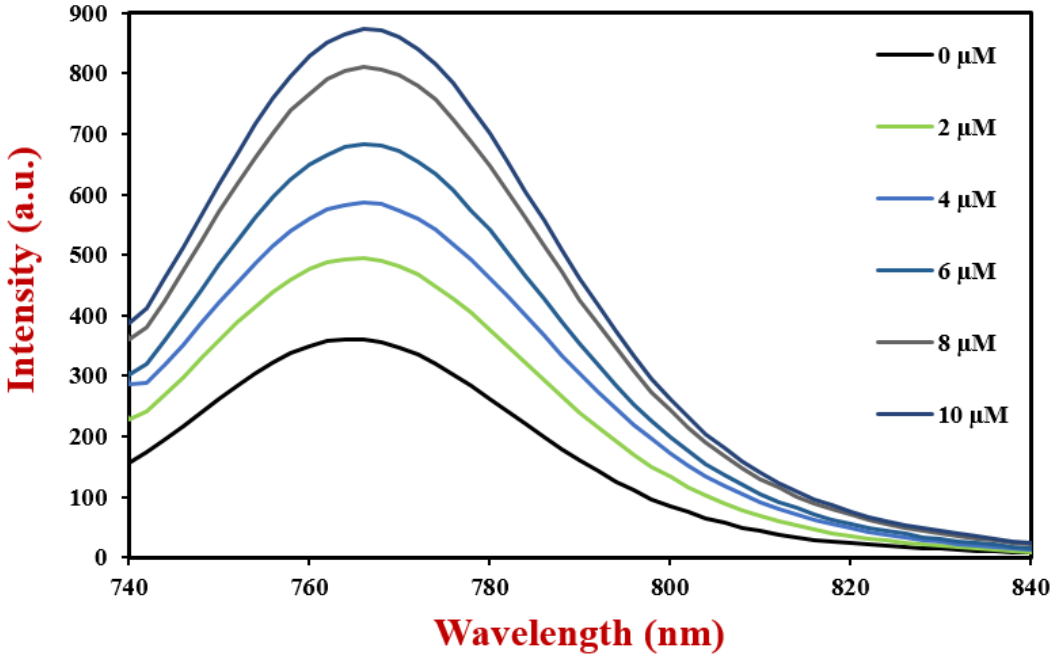


Figure 10. Fluorescence emission spectra of UCD-1 with varying concentrations of BSA for a fixed dye concentration of 2 µM.

This interaction may lead to the strengthening of the planar configuration of the dye molecules especially in the excited state ultimately enhancing the molecular rigidity after formation of a complex between UCD-1 and BSA. It seems quite probable that –COOH functionality of dye is expected to the hydrogen bond assisted dye aggregate formation in PBS leading to the blue-shifted emission maximum (Table 1). In the presence of BSA in the PBS, this aggregate formation is hampered due to the dye-BSA complex formation leading to bathochromically shifted emission. For the other dyes under investigation also electronic absorption and fluorescence emission spectra in the presence and absence of BSA were also measured and shown in figure 11.

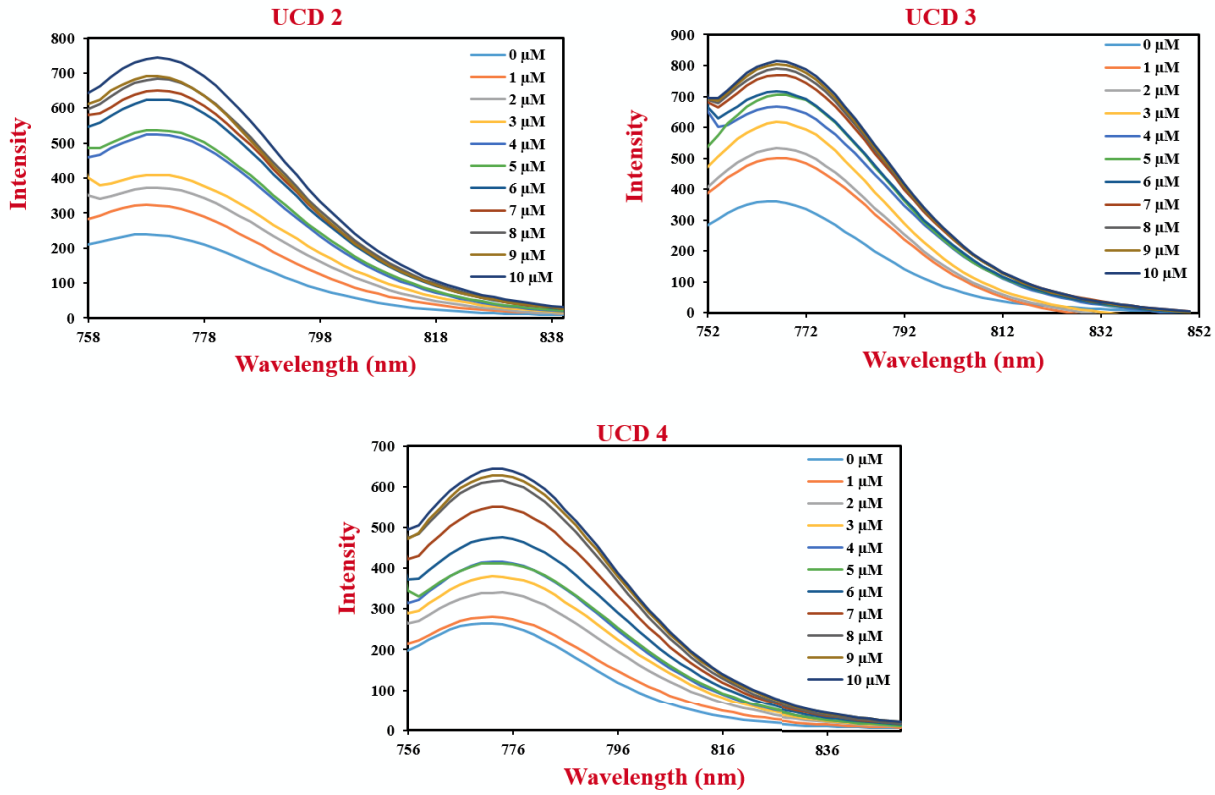


Figure 11. Fluorescence emission spectra of UCD (2-4) with varying concentrations of BSA for a fixed dye concentration of 2 µM.

BSA concentration dependence of the fluorescence intensity for various unsymmetrical cyanine dyes have been shown in figure 12. A linear correlation between the fluorescent intensity of dyes as a function of BSA concentration was observed. This increase in fluorescent intensity along with the red shift of $\lambda_{max}$ can be attributed to the non-covalent interaction between dyes and protein for the formation of BSA-dye conjugates.

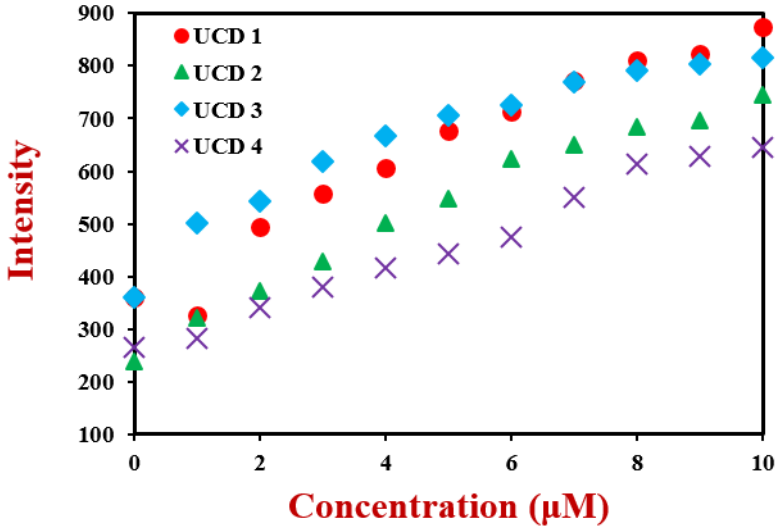


Figure 12. Plot of florescence emission intensity at peak maxima for cyanine dyes (UCD-1-4) as a function of BSA concentration. Dye concentration was constant (2 µM) for each of the dyes.

It has been widely accepted that drugs or probes interact differently with the protein under consideration and their ability to bind depends on protein concentration (33). It can be clearly seen that ability to bind with fluorescent dyes utilized in this work were enhanced upon the addition of increasing concentration of BSA. At the same time, amongst the dyes utilized dye-BSA interaction studies, UCD-4 was found to exhibit the highest binding affinity BSA. In order to successfully implement fluorescent dyes as a probe, it is necessary that the dye should bind to the protein without causing any damage to its three-dimensional conformation which basically governs the protein function and activity. The conformational changes in protein may occur at the point where the probe is located. As the dye concentration increases, there may be more damage in its activity. Keeping this mind, a very low dye concentration of (2 µM) has been used for investigation of the dye-BSA interaction with all of the unsymmetrical NIR cyanine dyes. Thanks to high ε and good ϕ of the dyes, it possible to investigate the interaction satisfactorily even at lower dye concentration.

To compare the ability of binding and relative association of dyes with BSA quantitatively, apparent binding constant ($K_a$) was calculated using equation [2] by plotting $(F\infty - F_0)/(F_X - F_0)$ as a function of the inverse of BSA concentration as shown

in figure 13. The value of $K_a$ was calculated from the slopes of these curves which was found to be 7.08 x $10^6$ $M^{-1}$, 7.06×$10^6$ $M^{-1}$, 3.7 x $10^6$ $M^{-1}$ and 10.13 x $10^6$ $M^{-1}$ with the cyanine dyes UCD-1, UCD-2, UCD-3 and UCD-4, respectively. Therefore, unsymmetrical cyanine dye bearing 5-Iodoindole exhibits highest binding affinity with the BSA and estimated $K_a$ is about an order of the magnitude higher as compared to that obtained for the typical cyanine dyes (36). This could be attributed to the presence of direct ring substituted hydrophilic carboxylic acid (–COOH) functional group promoting hydrogen bonding with binding sites of BSA. On the other hand enhanced aggregation and competitive interactions due to the presence of two functional groups –OH and –COOH on the two opposite ends of the chromophore in the dye UCD-3 could be attributed to the least association with the BSA.

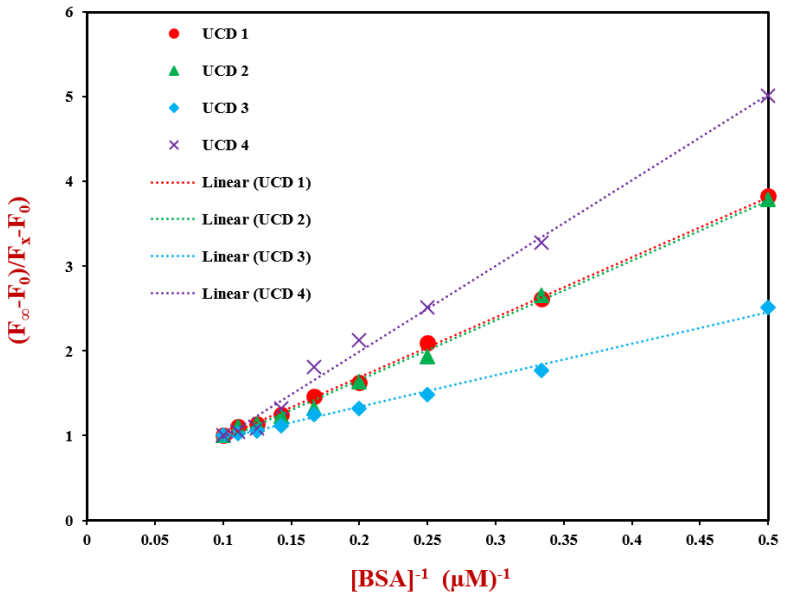


Figure 13. Plot of $(F\infty - F_0)/(F_X - F_0)$ as function $[BSA]^{-1}$ at a fixed dye concentration of 2.0 × $10^{-6}$ M.

## 4.5. Conclusions

Direct ring carboxy functionalized NIR sensitive unsymmetrical cyanine dyes having different substituents (-Br, -OH and -I) have been successfully synthesized and characterized. These dyes were subjected to the photophysical investigations in order to explore their applicability as fluorescent probes. Interactions of these dyes with BSA as a protein model suggested the formation of dye-BSA conjugates, which led to the enhancement in fluorescence intensity along with the bathochromic shift of emission maxima. Amongst the various dyes utilized, one with mild electron withdrawing iodo group (UCD-4) has been found to exhibit the highest affinity towards the association with BSA. This high binding constant observed in the case of UCD-4 could be associated with the presence of relatively bulkier iodo group along with the –COOH group directly attached to the indole ring.

## 4.6. References


1) J. Fabian, H. Nakazumi, M. Matsuoka, Near-infrared absorbing dyes, Chemical Reviews, 92 (1992) 1197-1226.
2) J.O. Escobedo, O. Rusin, S. Lim, R.M. Strongin, NIR dyes for bioimaging applications, Current opinion in chemical biology, 14 (2010) 64-70.
3) G. Patonay, M.D. Antoine, Near-infrared fluorogenic labels: new approach to an old problem, Analytical Chemistry, 63 (1991) 321A-327A.
4) J.V. Frangioni, In vivo near-infrared fluorescence imaging, Current opinion in chemical biology, 7 (2003) 626-634.
5) D.J. Hawrysz, E.M. Sevick-Muraca, Developments Toward Diagnostic Breast Cancer Imaging Using Near-Infrared Optical Measurements and Fluorescent Contrast Agents1, Neoplasia, 2 (2000) 388-417.
6) V. Ntziachristos, C. Bremer, R. Weissleder, Fluorescence imaging with near-infrared light: new technological advances that enable in vivo molecular imaging, European radiology, 13 (2003) 195-208.
7) S. Yagi, Y. Nakasaku, T. Maeda, H. Nakazumi, Y. Sakurai, Synthesis and near-infrared absorption properties of linearly π-extended squarylium oligomers, Dyes and Pigments, 90 (2011) 211-218.
8) X. Yang, C. Shi, R. Tong, W. Qian, H.E. Zhau, R. Wang, G. Zhu, J. Cheng, V.W. Yang, T. Cheng, Near IR heptamethine cyanine dye–mediated cancer imaging, Clinical Cancer Research, 16 (2010) 2833-2844.
9) K.Y. Law, Squaraine chemistry. Design, synthesis and xerographic properties of a highly sensitive unsymmetrical fluorinated squaraine, Chemistry of materials, 4 (1992) 605-611.
10) A. Mishra, R.K. Behera, P.K. Behera, B.K. Mishra, G.B. Behera, Cyanines during the 1990s: a review, Chemical reviews, 100 (2000) 1973-2012.
11) L. Yuan, W. Lin, K. Zheng, L. He, W. Huang, Far-red to near infrared analyte-responsive fluorescent probes based on organic fluorophore platforms for fluorescence imaging, Chemical Society Reviews, 42 (2013) 622-661.
12) R.M. El-Shishtawy, Functional dyes, and some hi-tech applications, International Journal of Photoenergy, 2009 (2009).
13) C. Benzi, C.A. Bertolino, I. Miletto, P. Ponzio, C. Barolo, G. Viscardi, S. Coluccia, G. Caputo, The design, synthesis and characterization of a novel acceptor for real time

polymerase chain reaction using both computational and experimental approaches, Dyes and Pigments, 83 (2009) 111-120.

14) A.S. Tatikolov, S.l.M. Costa, Complexation of polymethine dyes with human serum albumin: a spectroscopic study, Biophysical chemistry, 107 (2004) 33-49.
15) M.V. Reddington, Synthesis and properties of phosphonic acid containing cyanine and squaraine dyes for use as fluorescent labels, Bioconjugate chemistry, 18 (2007) 2178-2190.
16) M.S.T. Gonçalves, Fluorescent labeling of biomolecules with organic probes, Chemical reviews, 109 (2009) 190.
17) H. Zollinger, Color chemistry: syntheses, properties, and applications of organic dyes and pigments, John Wiley & Sons, 2003.
18) G. Patonay, J. Salon, J. Sowell, L. Strekowski, Noncovalent labeling of biomolecules with red and near-infrared dyes, Molecules, 9 (2004) 40-49.
19) E.E. Jelley, Spectral absorption and fluorescence of dyes in the molecular state, Nature, 138 (1936) 1009-1010.
20) E.E. Jelley, Molecular, Nematic and Crystal States of I: I-Diethyl--Cyanine Chloride, Nature, 139 (1937) 631-632.
21) G. Scheibe, Variability of the absorption spectra of some sensitizing dyes and its cause, Angew. Chem, 49 (1936) 563.
22) G. Scheibe, Über die Veränderlichkeit der Absorptionsspektren in Lösungen und die Nebenvalenzen als ihre Ursache, Angewandte Chemie, 50 (1937) 212-219.
23) H. Yao, K. Domoto, T. Isohashi, K. Kimura, In situ detection of birefringent mesoscopic H and J aggregates of thiacarbocyanine dye in solution, Langmuir, 21 (2005) 1067-1073.
24) J.S. Kim, R. Kodagahally, L. Strekowski, G. Patonay, A study of intramolecular H-complexes of novel bis (heptamethine cyanine) dyes, Talanta, 67 (2005) 947-954.
25) S. Yarmoluk, S. Lukashov, T.Y. Ogul'Chansky, M.Y. Losytskyy, O. Kornyushyna, Interaction of cyanine dyes with nucleic acids. XXI. Arguments for half-intercalation model of interaction, Biopolymers, 62 (2001) 219-227.
26) T.Y. Ogul'chansky, M.Y. Losytskyy, V. Kovalska, V. Yashchuk, S. Yarmoluk, Interactions of cyanine dyes with nucleic acids. XXIV. Aggregation of monomethine cyanine dyes in presence of DNA and its manifestation in absorption and fluorescence

spectra, Spectrochimica Acta Part A: Molecular and Biomolecular Spectroscopy, 57 (2001) 1525-1532.

27) N. Narayanan, G. Patonay, A new method for the synthesis of heptamethine cyanine dyes: synthesis of new near-infrared fluorescent labels, The Journal of Organic Chemistry, 60 (1995) 2391-2395.

28) N. Barbero, C. Magistris, J. Park, D. Saccone, P. Quagliotto, R. Buscaino, C. Medana, C. Barolo, G. Viscardi, Microwave-assisted synthesis of near-infrared fluorescent indole-based squaraines, Organic letters, 17 (2015) 3306-3309.

29) H. Li, M. Pang, B. Wu, J. Meng, Synthesis, crystal structure and photochromism of a novel spiro [indoline–naphthaline] oxazine derivative, Journal of Molecular Structure, 1087 (2015) 73-79.

30) E.J. Klotz, T.D. Claridge, H.L. Anderson, Homo-and hetero-[3] rotaxanes with two π-systems clasped in a single macrocycle, Journal of the American Chemical Society, 128 (2006) 15374-15375.

31) T. Inoue, S.S. Pandey, N. Fujikawa, Y. Yamaguchi, S. Hayase, Synthesis and characterization of squaric acid based NIR dyes for their application towards dye-sensitized solar cells, Journal of Photochemistry and Photobiology A: Chemistry, 213 (2010) 23-29.

32) D. Oushiki, H. Kojima, Y. Takahashi, T. Komatsu, T. Terai, K. Hanaoka, M. Nishikawa, Y. Takakura, T. Nagano, Near-infrared fluorescence probes for enzymes based on binding affinity modulation of squarylium dye scaffold, Analytical chemistry, 84 (2012) 4404-4410.

33) D.S. Pisoni, L. Todeschini, A.C.s.A. Borges, C.L. Petzhold, F.S. Rodembusch, L.F. Campo, Symmetrical and asymmetrical cyanine dyes. synthesis, spectral properties, and BSA association study, The Journal of organic chemistry, 79 (2014) 5511-5520.

34) A. Levitz, S.T. Ladani, D. Hamelberg, M. Henary, Synthesis and effect of heterocycle modification on the spectroscopic properties of a series of unsymmetrical trimethine cyanine dyes, Dyes and Pigments, 105 (2014) 238-249.

35) Y. Oshikawa, K. Furuta, S. Tanaka, A. Ojida, Cell surface-anchored fluorescent probe capable of real-time imaging of single mast cell degranulation based on histamine-induced coordination displacement, Analytical chemistry, 88 (2016) 1526-1529.

36) M. Gerowska, L. Hall, J. Richardson, M. Shelbourne, T. Brown, Efficient reverse click labeling of azide oligonucleotides with multiple alkynyl Cy-Dyes applied to the synthesis of HyBeacon probes for genetic analysis, Tetrahedron, 68 (2012) 857-864.
37) S.S. Pandey, T. Inoue, N. Fujikawa, Y. Yamaguchi, S. Hayase, Substituent effect in direct ring functionalized squaraine dyes on near infra-red sensitization of nanocrystalline TiO 2 for molecular photovoltaics, Journal of Photochemistry and Photobiology A: Chemistry, 214 (2010) 269-275.
38) M.Y. Berezin, K. Guo, B. Teng, W.B. Edwards, C.J. Anderson, O. Vasalatiy, A. Gandjbakhche, G.L. Griffiths, S. Achilefu, Radioactivity Synchronized Fluorescence Enhancement using a Radionuclide Fluorescence-Quenched Dye, Journal of the American Chemical Society, 131 (2009) 9198.
39) O. Redy, E. Kisin-Finfer, E. Sella, D. Shabat, A simple FRET-based modular design for diagnostic probes, Organic & biomolecular chemistry, 10 (2012) 710-715.
40) A.S. Tatikolov, Polymethine dyes as spectral-fluorescent probes for biomacromolecules, Journal of Photochemistry and Photobiology C: Photochemistry Reviews, 13 (2012) 55-90.
41) C. Peyratout, L. Daehne, Aggregation of thiacyanine derivatives on polyelectrolytes, Physical Chemistry Chemical Physics, 4 (2002) 3032-3039.
42) G. Behera, P. Behera, B.K. Mishra, Cyanine dyes: self-aggregation and behaviour in surfactants a review, Journal of Surface Science and Technology, 23 (2007) 1.
43) G.M. Shivashimpi, S.S. Pandey, A. Hayat, N. Fujikawa, Y. Ogomi, Y. Yamaguchi, S. Hayase, Far-red sensitizing octatrifluorobutoxy phosphorous triazatetrabenzocorrole: Synthesis, spectral characterization and aggregation studies, Journal of Photochemistry and Photobiology A: Chemistry, 289 (2014) 53-59.
44) S.A. Hilderbrand, K.A. Kelly, R. Weissleder, C.-H. Tung, Monofunctional near-infrared fluorochromes for imaging applications, Bioconjugate chemistry, 16 (2005) 1275-1281.
45) J. Widengren, P. Schwille, Characterization of photoinduced isomerization and back-isomerization of the cyanine dye Cy5 by fluorescence correlation spectroscopy, The Journal of Physical Chemistry A, 104 (2000) 6416-6428.
46) A.T.R. Williams, S.A. Winfield, J.N. Miller, Relative fluorescence quantum yields using a computer-controlled luminescence spectrometer, Analyst, 108 (1983) 1067-1071.

47) M.Y. Berezin, S. Achilefu, Fluorescence lifetime measurements and biological imaging, Chemical reviews, 110 (2010) 2641.
48) M.Y. Berezin, H. Lee, W. Akers, K. Guo, R.J. Goiffon, A. Almutairi, J.M. Fréchet, S. Achilefu, Engineering NIR dyes for fluorescent lifetime contrast, in: Engineering in Medicine and Biology Society, 2009. EMBC 2009. Annual International Conference of the IEEE, IEEE, 2009, pp. 114-117.
49) V. Ntziachristos, A. Yodh, M. Schnall, B. Chance, Concurrent MRI and diffuse optical tomography of breast after indocyanine green enhancement, Proceedings of the National Academy of Sciences, 97 (2000) 2767-2772.
50) S. Bloch, F. Lesage, L. McIntosh, A. Gandjbakhche, K. Liang, S. Achilefu, Whole-body fluorescence lifetime imaging of a tumor-targeted near-infrared molecular probe in mice, Journal of biomedical optics, 10 (2005) 054003-054003-054008.
51) M. Gurfinkel, A.B. Thompson, W. Ralston, T.L. Troy, A.L. Moore, T.A. Moore, J.D. Gust, D. Tatman, J.S. Reynolds, B. Muggenburg, Pharmacokinetics of ICG and HPPH-car for the Detection of Normal and Tumor Tissue Using Fluorescence, Near-infrared Reflectance Imaging: A Case Study¶, Photochemistry and Photobiology, 72 (2000) 94-102.
52) M.Y. Berezin, H. Lee, W. Akers, G. Nikiforovich, S. Achilefu, Fluorescent lifetime of near infrared dyes for structural analysis of serum albumin, in: Biomedical Optics (BiOS) 2008, International Society for Optics and Photonics, 2008, pp. 68670J-68670J-68611.
53) H. Lee, M.Y. Berezin, M. Henary, L. Strekowski, S. Achilefu, Fluorescence lifetime properties of near-infrared cyanine dyes in relation to their structures, Journal of Photochemistry and Photobiology A: Chemistry, 200 (2008) 438-444.
54) M. Anraku, K. Yamasaki, T. Maruyama, U. Kragh-Hansen, M. Otagiri, Effect of oxidative stress on the structure and function of human serum albumin, Pharmaceutical research, 18 (2001) 632-639.
55) R.J. Williams, M. Lipowska, G. Patonay, L. Strekowski, Comparison of covalent and noncovalent labeling with near-infrared dyes for the high-performance liquid chromatographic determination of human serum albumin, Analytical chemistry, 65 (1993) 601-605.
56) M.B.E. Turbay, V. Rey, N.M. Argañaraz, F.E.M. Vieyra, A. Aspée, E.A. Lissi, C.D. Borsarelli, Effect of dye localization and self-interactions on the photosensitized

generation of singlet oxygen by rose bengal bound to bovine serum albumin, Journal of Photochemistry and Photobiology B: Biology, 141 (2014) 275-282.

## 4.7. Appendix

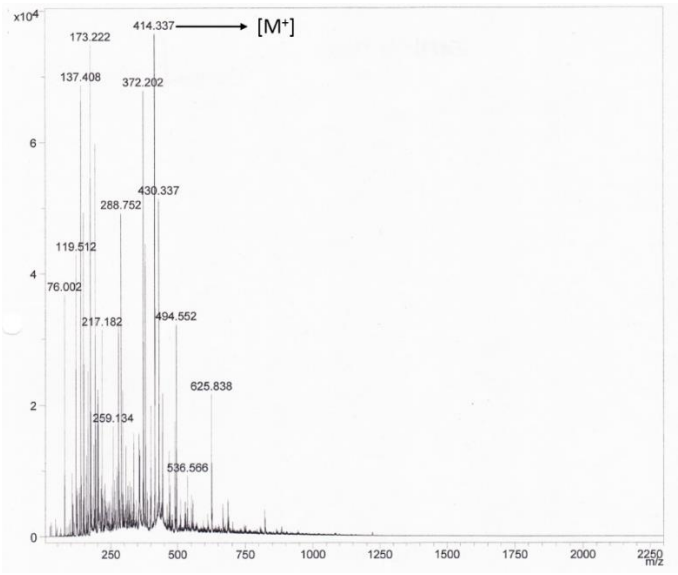


Figure 1. TOF Mass of 1-*butyl-3,3-dimethyl-2-((1E,3E,5E)-6-(N-phenylacetamido)hexa-1,3,5-trien-1-yl)-3H-indol-1-ium chloride (**7**)*.

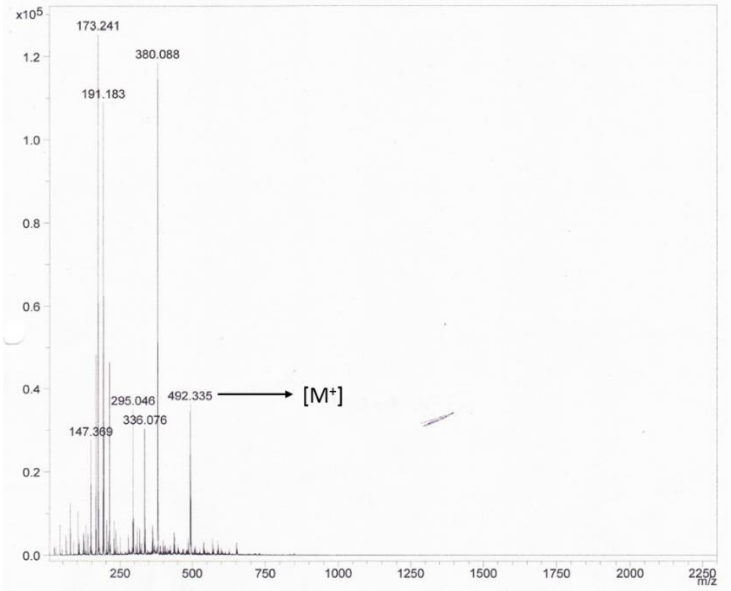


Figure 2. TOF Mass of *5-bromo-1-butyl-3,3-dimethyl-2-((1E,3E,5E)-6-(N-phenylacetamido)hexa-1,3,5-trien-1-yl)-3H-indol-1-ium chloride (**8**)*.

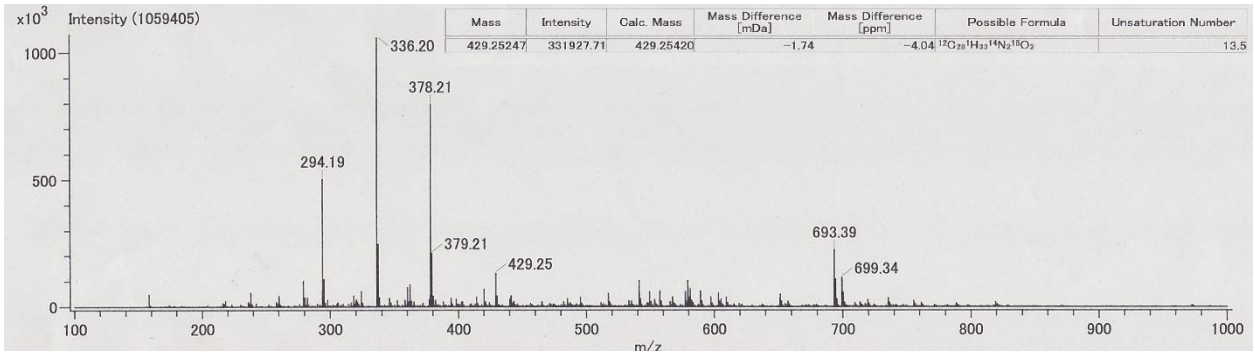


Figure 3. ESI Mass of *1-butyl-5-hydroxy-3,3-dimethyl-2-((1E,3E,5E)-6-(N-phenylacetamido)hexa-1,3,5-trien-1-yl)-3H-indol-1-ium chloride (**9**).*

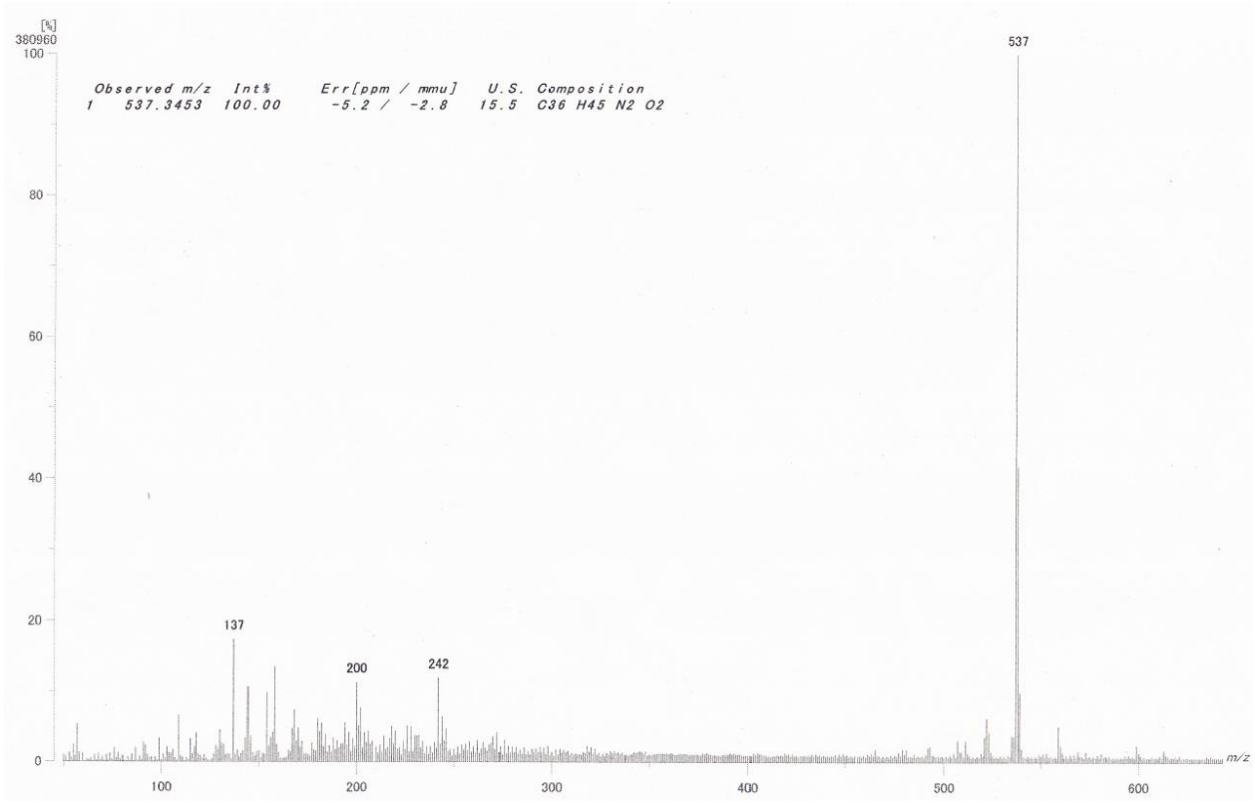


Figure 4. FAB Mass of dye UCD-1.

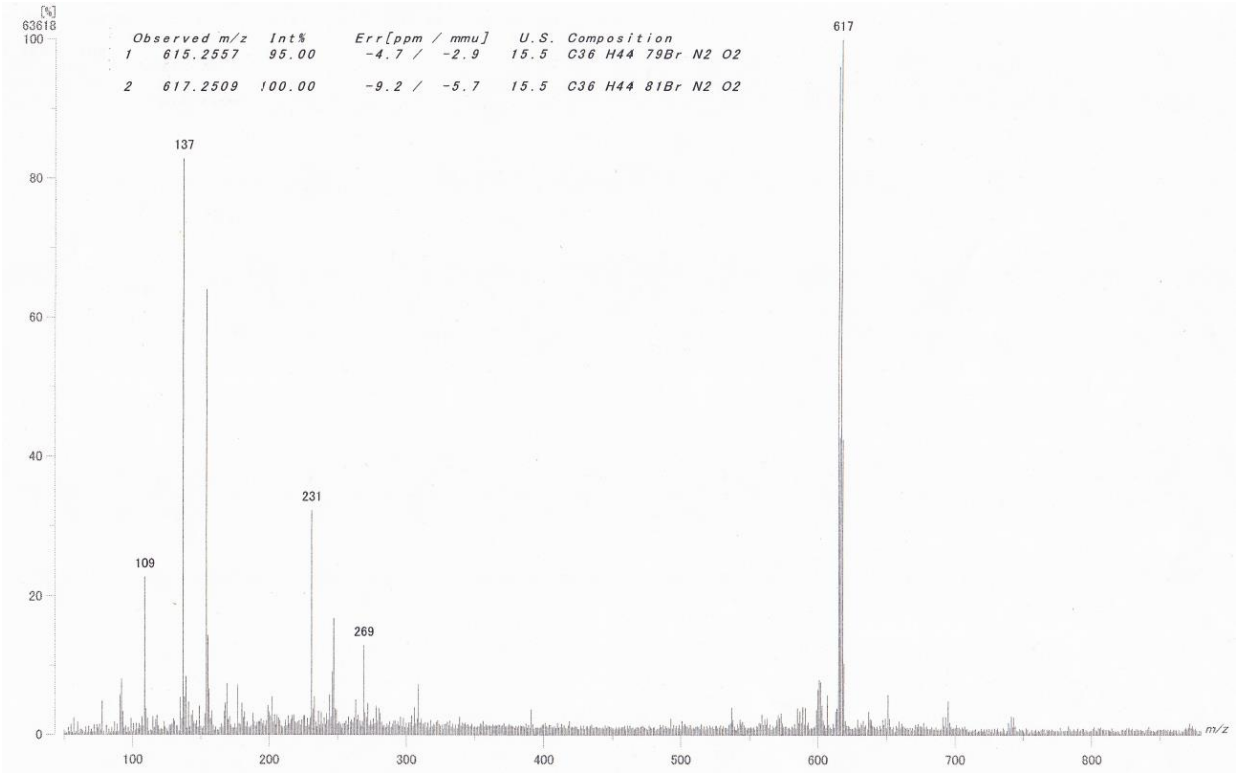


Figure 5. FAB Mass of dye UCD-2.

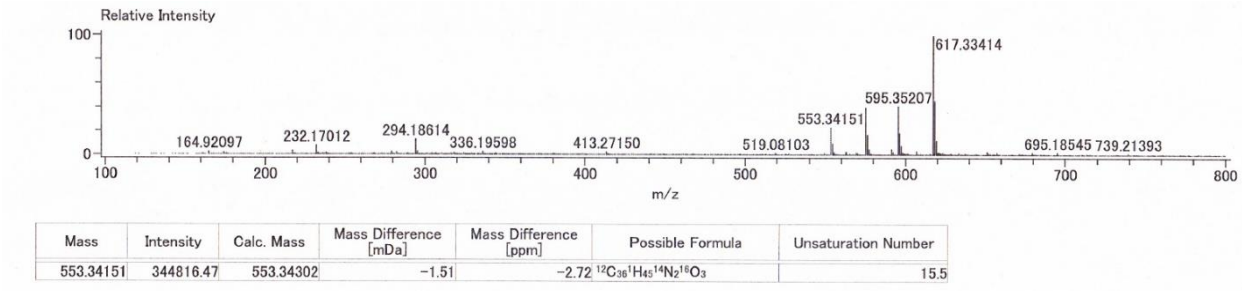


| Mass | Intensity | Calc. Mass | Mass Difference [mDa] | Mass Difference [ppm] | Possible Formula | Unsaturation Number |
|---|---|---|---|---|---|---|
| 553.34151 | 344816.47 | 553.34302 | -1.51 | -2.72 | $^{12}C_{36}{}^{1}H_{45}{}^{14}N_2{}^{16}O_3$ | 15.5 |

Figure 6. ESI Mass of dye UCD-3.

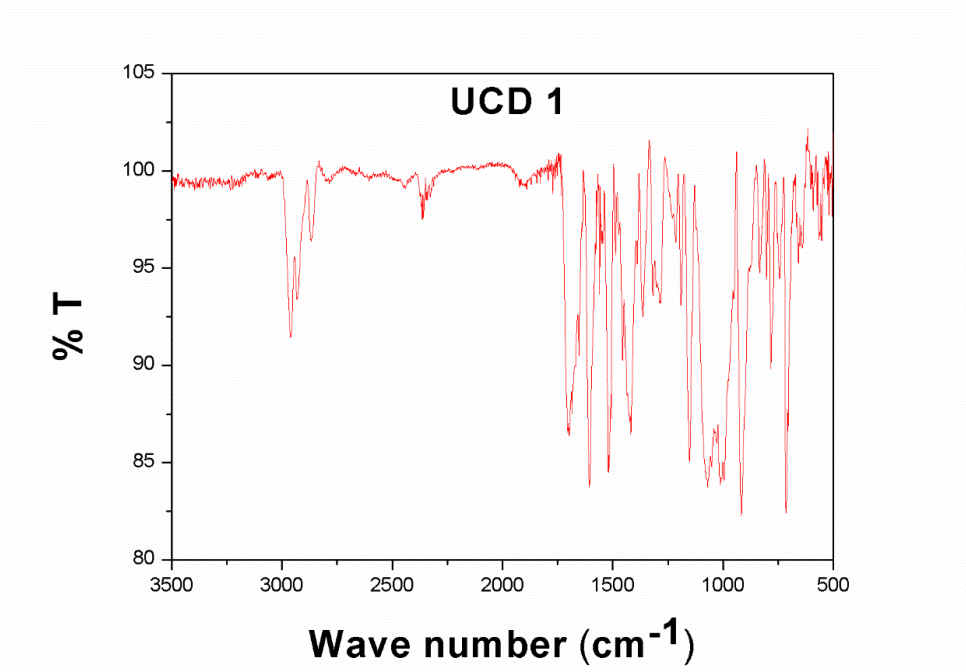


Figure 7. IR spectrum of dye UCD-1.

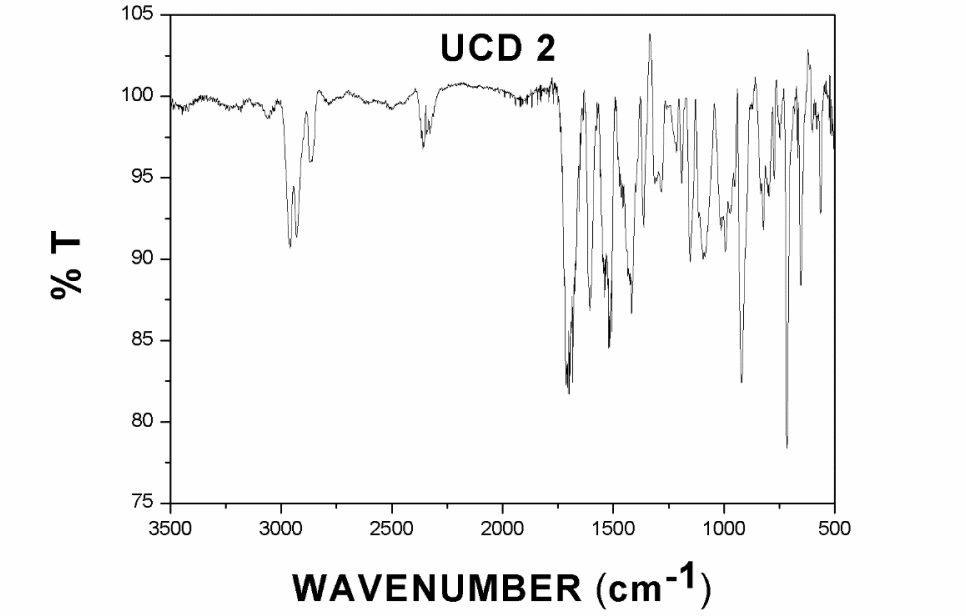


Figure 8. IR spectrum of dye UCD-2.

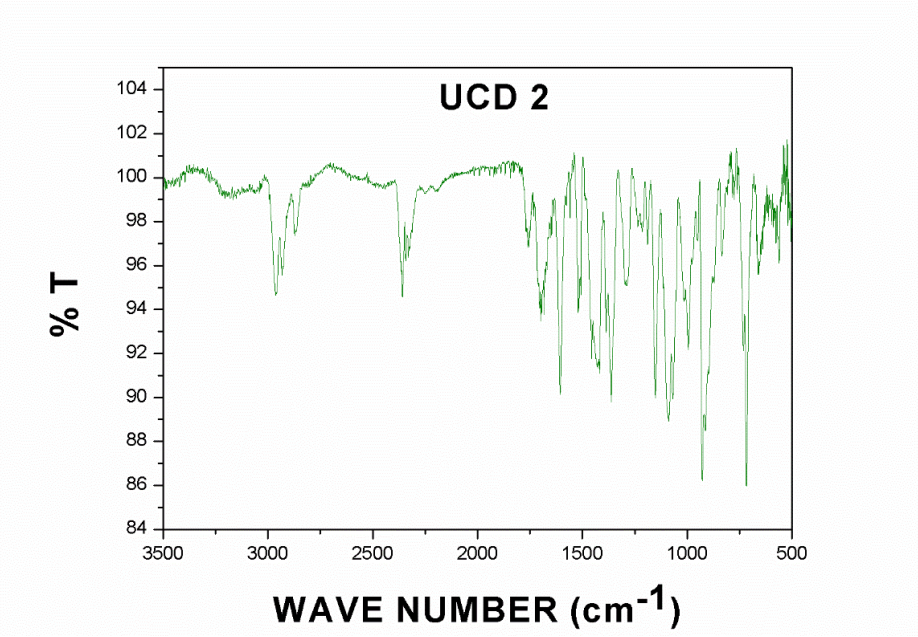


Figure 9. IR spectrum of dye UCD-3.

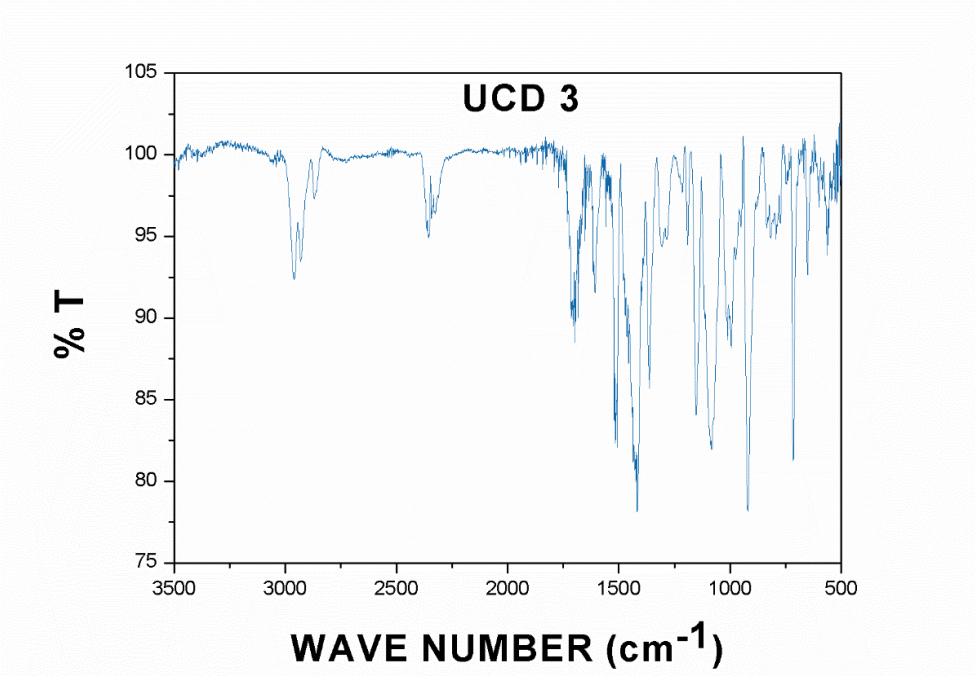


Figure 10. IR spectrum of dye UCD-4.

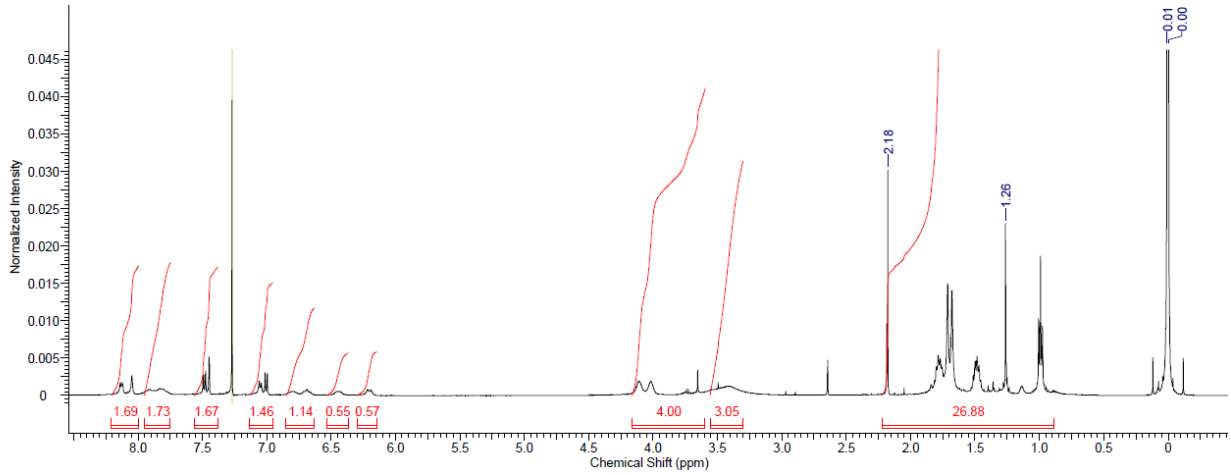


Figure 11. H-NMR of dye UCD-1.

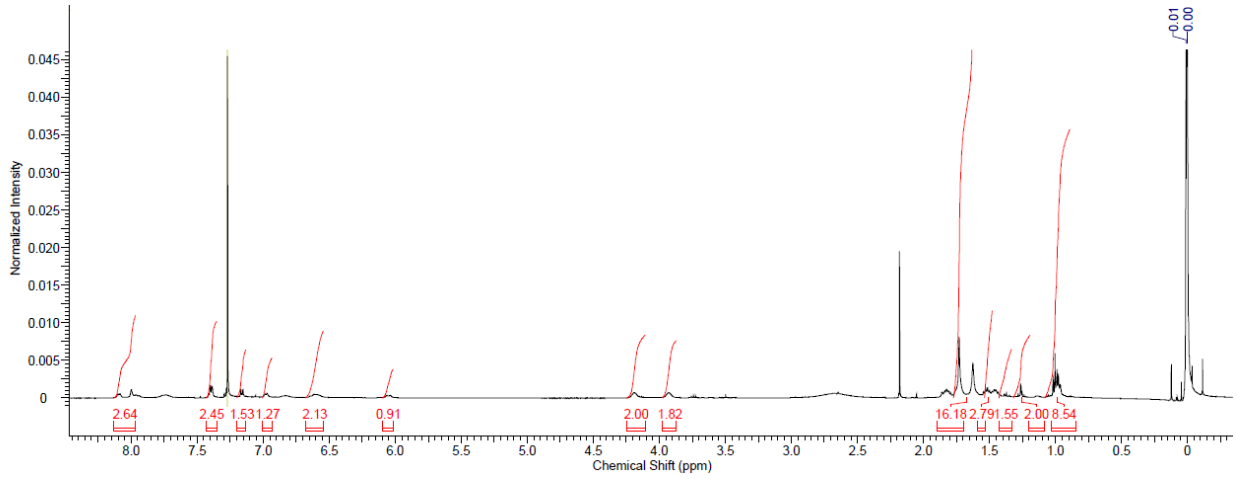


Figure 12. H-NMR of dye UCD-2.

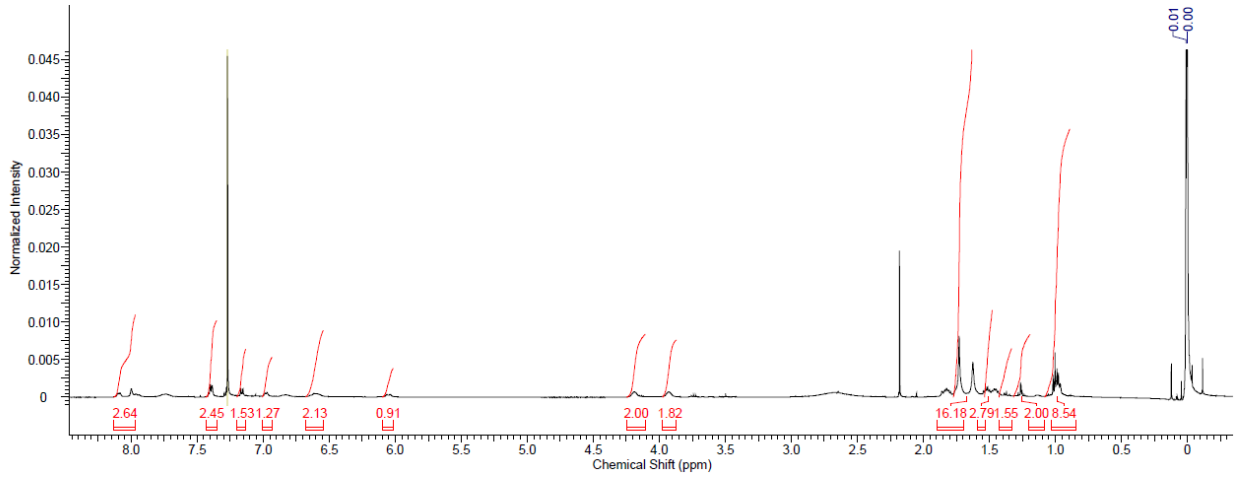


Figure 13. H-NMR of dye UCD-3.

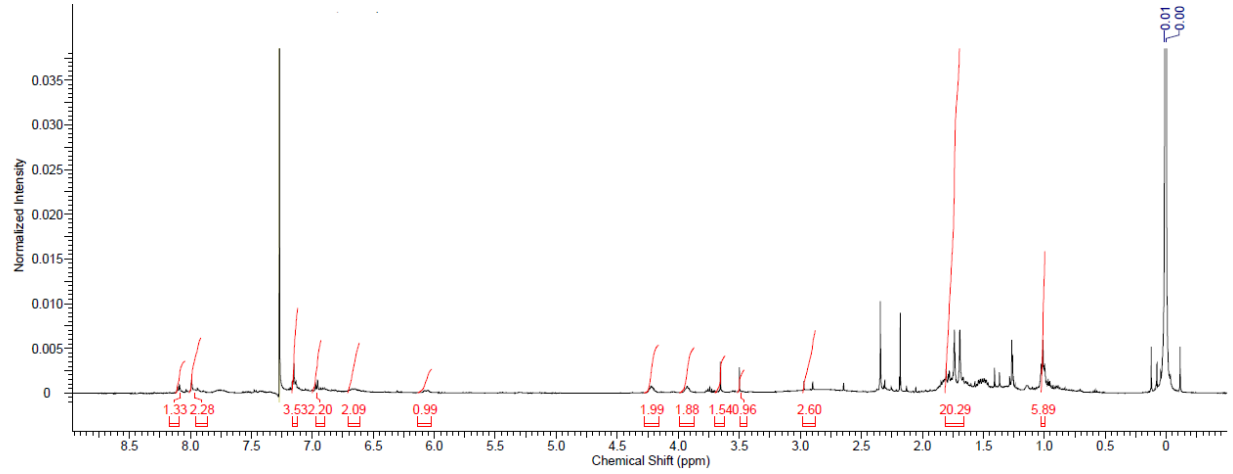


Figure 14. H-NMR of dye UCD-4.

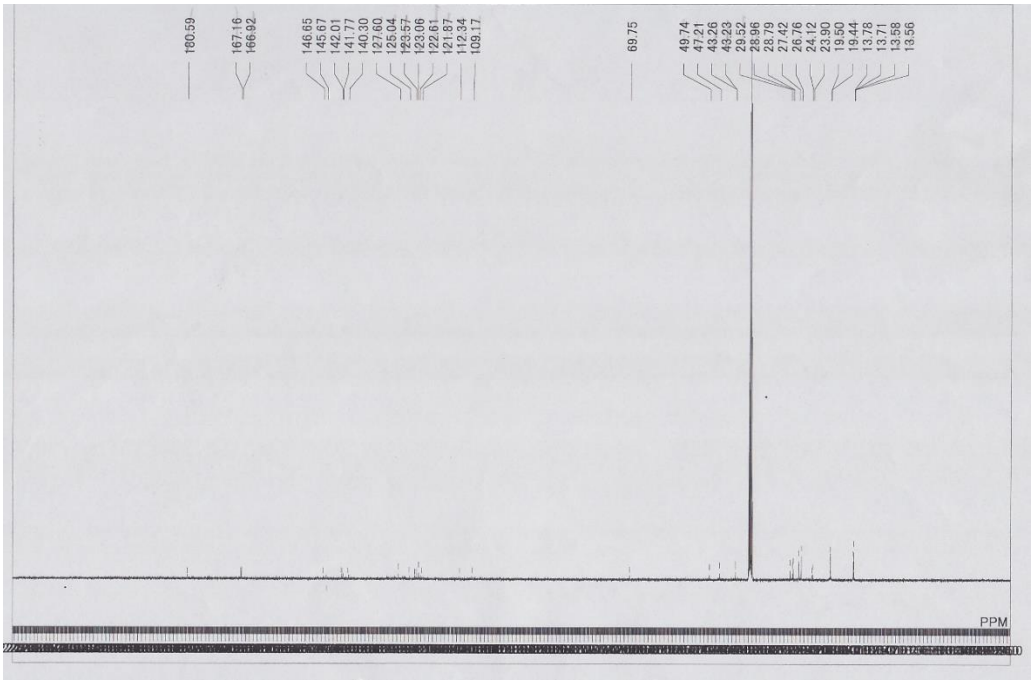


Figure 15. C-NMR of dye UCD-1.

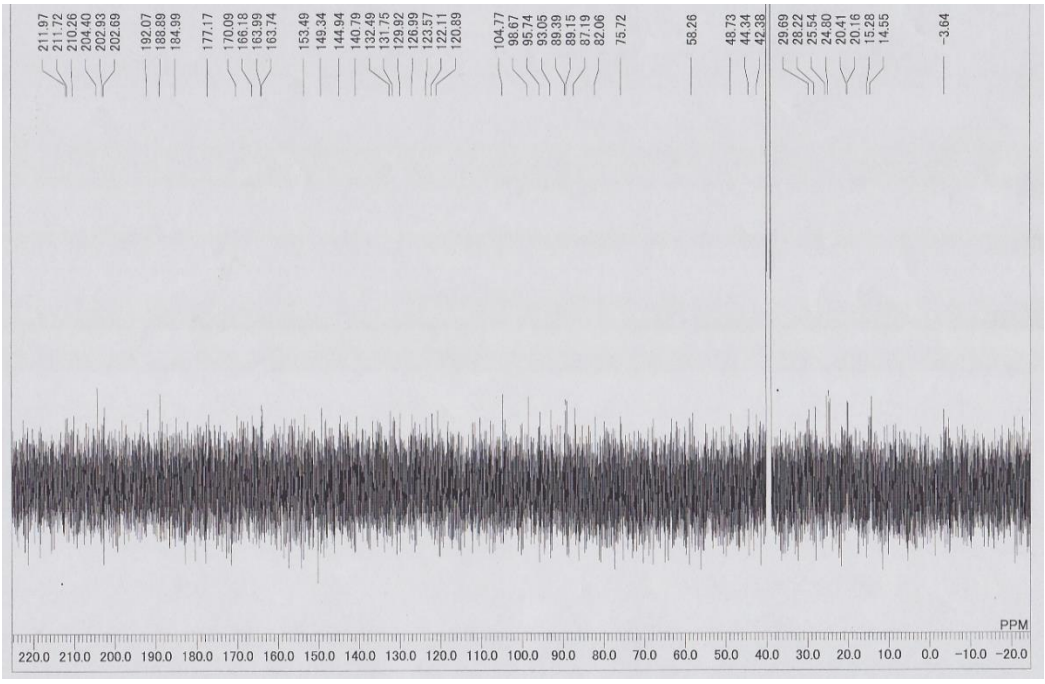


Figure 16. C-NMR of dye UCD-3.

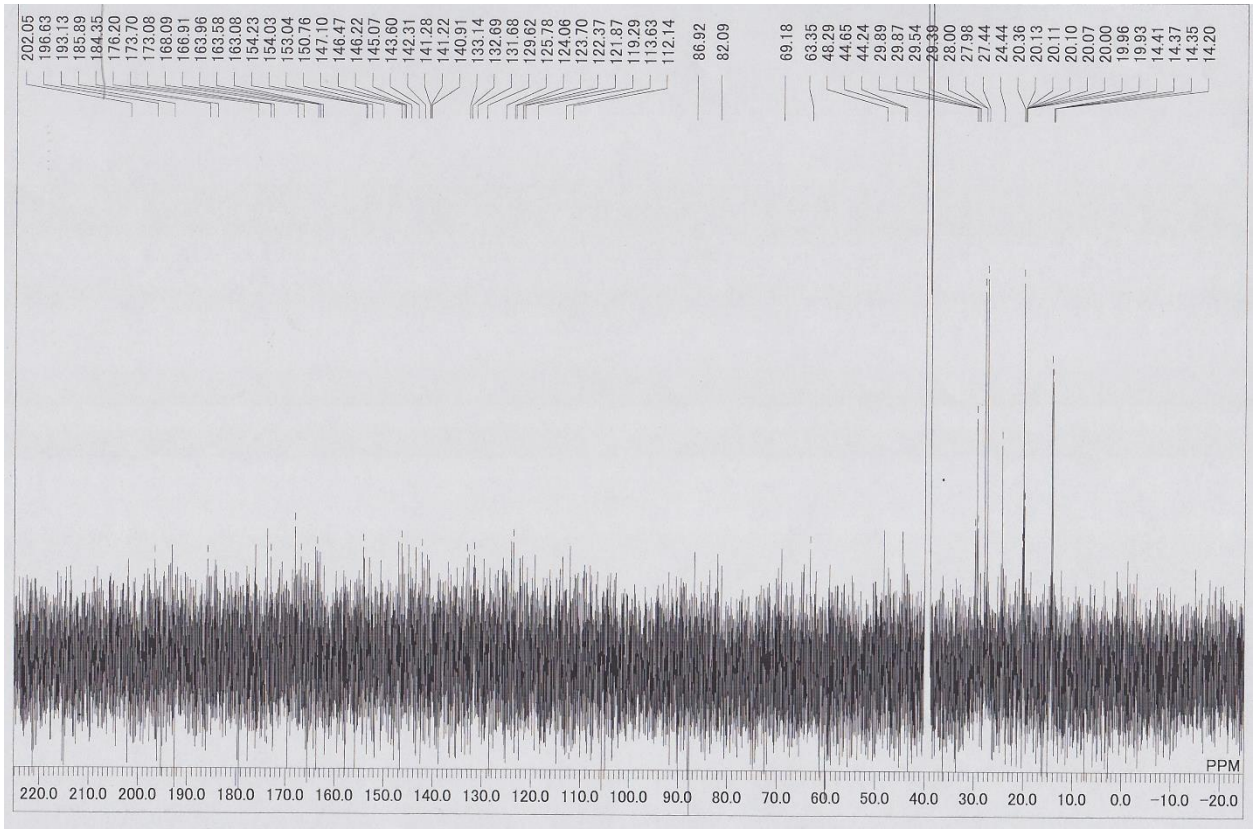


Figure 17. C-NMR of dye UCD-4.

# Chapter 5: Near Infrared Fluorescence Detection of Elastase Enzyme Activity Using Peptide-Bound Unsymmetrical Squaraine Dye

**Abstract**

Extended wavelength analyte-responsive fluorescent probes are highly desired for the imaging applications owing to their deep tissue penetration and minimum interference from autofluorescence by biomolecules. Near infra-red (NIR) sensitive and self-quenching fluorescent probe based on the dye-peptide conjugate (SQ 1 PC) was designed and synthesized by facile and efficient one-pot synthetic route for the detection of Elastase activity. In the phosphate buffer solution, there was an efficient quenching of fluorescence of SQ 1 PC (86 %) assisted by pronounced dye-dye interaction due to H-aggregate formation. Efficient and fast recovery of this quenched fluorescence of SQ 1 PC (> 50 % in 30 seconds) was observed on hydrolysis of this peptide-dye conjugate by elastase enzyme. Presently designed NIR sensitive self-quenching substrate offers the potential application for the detection of diseases related to proteases by efficient and fast detection of their activities.

## 5. Introduction

Growing demand for point-of-care testing (POCT) devices for home diagnostic and facile health care monitoring, biosensors have attracted tremendous attentions owing to utilization of small amount of biological samples, ease of handling and user-friendliness (1, 2). Although, biosensors are one of the strong contenders for POCT devices, due to the existing challenges like utilization of single analyte at a time, controlling the sensitivity in the presence of interfering agents, prior analyte processing for higher sensitivity and low throughput are needed to be considered for the further development of more efficient and versatile POCT devices. It is, therefore, necessary to develop biosensors that are sensitive and having the capability of high throughput detection along with their compatibility with imaging techniques for simultaneous multi-target analysis (3). The advent of Microarray technology has led the possibility of rapid profiling of huge number of proteins in a single experiment (4, 5). Working with protein arrays for biosensing applications is challenging and cumbersome to control polar and ionic interactions, unspecific adsorption of proteins and preservation of native form of protein along with their spatial orientations onto the surface after immobilization (6). The establishment of robust protein biosensing platforms, however, remains changeling. The recent advancements in microarray technology provide a tool that helps to identify genetic mutations

in healthy and diseased tissues (7) and are beneficial in clinics (8). The detection of low abundant protein in the typical mixtures of blood, saliva or urine will enable the early detection of potential medical conditions. This is the reason why more attentions are being paid for the development of peptide arrays for rapid and high throughput screening of complex protein functions including qualitative as well as quantitative estimation of proteases (9, 10). Proteases are an important class of physiological enzymes which hydrolyze the amide bond at specific sites of the polypeptide chain thereby playing a vital role in the regulation of a large number of physiological processes such as cell proliferation/differentiation, apoptosis, DNA replication, haemostasis and immune responses (11-13). The recent year`s study had seen enormous progress in design and study of molecular imaging towards biomedical applications. The activity and expression of specific enzymes including proteases can now be analyzed by various molecular imaging techniques (14) including optical imaging in NIR regions (15). Human Neutrophil Elastase (HNE) belongs to serine class of proteases and is a proteolytic enzyme stored in the azurophilic granules of polymorphonuclear cells (16). Although the proteolytic destruction of bacteria is one of the major roles of this enzyme, its hyperactivity leads to the pathogenesis of acute and chronic inflammations (17, 18). Excess release of HNE cleaves the cellular receptors, activates protogenetic mediators and intrinsically involved in the epithelial as well as endothelial membrane damage (19, 20). Therefore, knowledge of roles played by different serine protease along with their strict control and monitoring especially HNE activity has a great importance for therapeutic viewpoints.

In spite of fast growth and development of protease assay methods, methods based on immunoassay consisted of specific binding to the target protease with antibodies have been although commercialized and able to estimate the proteases quantitatively (21). However, they are not much suitable for mapping protease activity and stages of disease which are associated with protease activity rather than their quantity. In order to avoid these issues of immunoassay-based detection of proteases, several other methods such as utilization of suitable peptide substrates based on optical (absorbance/fluorescence) detection and appearance or quenching of fluorescence emanating from Forster resonance energy transfer (FRET) have been widely used (22-24). Interaction of proteases with these chromogenic or fluorogenic substrates leads to the selective proteolytic cleavage of the peptide bond resulting in changes of their absorption or fluorescent spectral behaviors which form the basis for the detection of protease activity. In this context, fluorogenic substrates are preferred over chromogenic substrates owing to their enhanced sensitivity and compatibility with the high throughput fluorescence mapping on

microarray-based platforms (25). A perusal of the fluorogenic substrates used for the protease assay reveals that the wide-spread use of fluorescent tags working mainly in the visible or low wavelength region. In this case, not only auto-fluorescence resulting from the biological analyte poses a limitation to attain good signal-to-noise (S/N) ratio but also photo-damage to biological species which cannot be avoided owing to the high energy excitations. In this context, utilization of fluorophores exhibiting emission in the near-infrared (NIR) wavelength region not only imparts much higher sensitivity owing to its highly diminished auto-fluorescence from the biological samples but also are capable of deep tissue penetration leading to efficient bio-imaging (26). Accordingly, various NIR fluorescent dyes had been designed and developed in past few years (27-31).

Tung, Ching-Hsuan, et al in 2002 (32) had reported the design and development of NIR fluorochromes which are modified by small molecules other than peptides and are used potentially for targeting receptor systems. The probe developed opened the door to more extensive medical and biological applications like detection of small tumors by endoscopy (33, 34), determination of efficacy of receptor targeted therapeutic agents and non-invasive measurements of receptors (35). Sreejith et al in 2008 (36) had demonstrated a method for the detection of low molecular weight aminothiol by employing a π-extended squaraine dye that exhibits NIR electronic transition. The probe was important in imaging and bio labeling applications. The probe was used successfully for the detection and estimation of aminothiols in human blood plasma to confirm the effect of smoking on increased levels of aminothiols in blood. Yuan, Lin, et al in 2012 (37) demonstrated a unique approach to construction of NIR fluorescent sensor based on NIR dyes for biological applications in living animals. NIR-$H_2O_2$ for endogenously produced $H_2O_2$ and NIR-thiol for endogenous thiols. These probes serve as a platform for the development of fluorescent sensors based on hydroxyl functionalized reactive sites. Zhang, Yongbin, et al in 2015 (38) had reported the development of a fluorescent probe for the detection of thiols in aqueous media. The probe displayed tremendous enhancement in fluorescence intensity selectively for Cys, Hcy and GSh thiols over other amino acids in analytes. The probe exhibited as a good cell membrane permeability and can be used to mark thiols in living cells. Yao, Defan et al in 2016 (39) reported an effective fluorogenic probe based on polarity sensitive NIR emission. The probe exhibited high selectivity and specificity for LPA based on specific recognition between the RDG ligand and integrin receptor. The probe developed was highly stable in aqueous media and exhibited low

toxicity in live cells. The probe outcome as an important tool for LPA imaging in NIR optical window for the application in early clinical detection of ovarian cancer and can be further applied in wide range of clinical diagnostics. On the other hand, the FRET-based assay requires the logical development of suitable fluorophore and quencher pair posing synthetic complications due to the need orthogonal protecting groups while their coupling with peptide substrate library.

The design of peptide substrates tagged with fluorescent moieties having the capability of self-quenching and re-appearance of the fluorescence after enzymatic hydrolysis has also been simplified for the solution of the relatively complicated fluorescence-peptide-quencher molecular system. This was demonstrated by designing the substrates after the incorporation of a multiple numbers of identical fluorophores leading to concentration-dependent quenching. Sato et al have demonstrated the concentration dependent fluorescence quenching for their fluorescein isothiocyanates (Fluorescent moiety) tagged peptide substrate for Trypsin enzyme and proteolytic cleave of the peptide bond led to the appearance of the fluorescence (40). Internally quenched fluorescence-based fluorescent dendritic peptide substrates have also been reported which exhibit fluorescence ON sensing of chymotrypsin enzyme due to increased fluorescence emission after the enzymatic hydrolysis of the designed substrates (41). Squaraine dye belongs to a class of intensely colored dyes having donor-acceptor-donor zwitterionic molecular framework containing squaric acid as central four-membered ring core surrounded by electron-rich aromatic moieties. Incorporation of immensely available and judiciously selected aromatic/heterocyclic systems with varying donor strength it is easily possible to design a variety of squaraine dyes with tunable light absorption and fluorescence emission encompassing from visible to IR wavelength region (42).

## 5.1. Experimental

### 5.1.1. Materials and Methods

1-iodoethane, 2-methyl-5,6-benzoquinoline, dibutoxy squarate and Elastase used in present work were purchased from Sigma. Reagent grade solvents, trimethylamine, benzyl bromide, *N,N′*-di-cyclohexylcarbodiimide (DCC), Pd/C were purchased from Wako chemical company and used as received. The amino acids, coupling reagents like Hydroxybenzotriazole (HOBT.$H_2O$), 2-(1*H*-benzotriazol-1-yl)-1,1,3,3-tetramethyluronium hexafluorophosphate

(HBTU), *N*-Hydroxysuccinimide (NHS ester) and de-protecting reagents such as 4N HCl/dioxane, 20% DMF/piperidine were purchased from Watanabe chemicals. Mass of the intermediates as well as final SQ dye and peptide sequence were confirmed by MALDI-TOF mass and ESI-Mass. The purity of the synthesized peptide sequence and intermediates were analyzed by high-performance liquid chromatography (HITACHI) equipped with chromolith analytical column (RP – 18e, φ 4.6 mm × 100 mm) using Acetonitrile-water solvent gradient.

**Preparation of buffer and stock solutions**

**Preparation of PBS buffer (0.1M, pH=7.4)**

The buffer solution was prepared by dissolving 1.76 g of $NaH_2PO_4.2H_2O$ and 5.49 g of $Na_2HPO_4$ in 500 ml of water. The pH was adjusted to 7.4 using HCl and NaOH.

**Preparation of Peptide conjugate and Elastase stock solution**

The 100 μM stock solution of peptide conjugate was prepared by dissolving 1.57 mg in 10 ml dimethylsulfoxide. The concentration of the peptide conjugate stock solution was determined by the molar extinction coefficient of SQ 1 dye ($\varepsilon = 0.5\times10^5$ $dm^3.mol^{-1}.cm^{-1}$). The molar extinction coefficient of peptide conjugate should be twice that of SQ 1 dye as 2 units of dye per mole is present in peptide conjugate. Therefore the molar extinction coefficient of SQ 1 PC is $1.05\times10^5$ $dm^3.mol^{-1}.cm^{-1}$. The 1 mM stock solution of elastase (Mol. Wt = 30,000 Daltons) enzyme was prepared by dissolving 15 mg of elastase in 0.5 ml of PBS buffer.

**Enzyme activity Assay**

The enzyme activity assay was executed by preparing different concentrations of Elastase enzyme (3, 9, 21 nmol) from the above-mentioned stock solution with a fixed concentration of dye-peptide conjugate (10 μM) in PBS. The overall solution used for analysis was 3ml (2.9 ml dye-peptide conjugate and 0.1 ml of elastase solution). Change in fluorescence intensity as a function of time with different concentrations of an enzyme was depicted in figure 3b and Fluorescence emission spectra of 0.1 M phosphate buffer solution of dye –peptide conjugate (10 μM) at pH 7.4 as a function of time after the addition of 21 nM of an enzyme was depicted in figure 3a. The self-quenching efficiency (43) was calculated by using the following equation.

$$\text{Self-quenching efficiency (\%)} = [1 - (F_{substrate}/F_{control})] \times 100$$

Where $F_{substrate}$ is emission intensity after complete hydrolysis of dye-peptide conjugate and $F_{control}$ is emission intensity of dye-peptide conjugate before hydrolysis.

### *5.1.2. Synthesis of SQ-1 dye and dye Intermediates*

***Synthesis of 5-Carboxy-2,3,3-trimethyl-1-ethyl-3H-indolium iodide (1)***

2,3,3-trimethyl-3H-indole-5-carboxylic acid was synthesized following the procedure reported by Pandey et al (44). 2,3,3-trimethyl-3H-indole-5-carboxylic acid (1 equiv.) and 1-iodoethane (3 equiv.) were dissolved in acetonitrile and reaction was refluxed for 24 h at $90^0$C. The reaction was monitored by TLC using chloroform: methanol system. Upon the completion of the reaction, the solvent was evaporated under reduced pressure and the product was precipitated with ample addition of ether. The solid was filtered and dried, yielded 79% with purity 98% as confirmed by HPLC. FAB-mass (measured 232.0 $[M]^+$; calculated 232.13).

***Synthesis of 3-methyl-N-ethyl-5,6-benzoquinoline iodide (2)***

In a round bottom flask fitted with a condenser, 3-methyl-5,6-benzoquinoline (1.93g; 10mmol) and iodoethane (3.06g; 20mmol) were dissolved in dichlorobenzene and the reaction was refluxed at $130^0$C for 48 hours. The reaction was monitored by TLC and HPLC. After the reaction, the solvent was evaporated under reduced pressure and ample amount of ether was added to precipitate the title compound. The solid compound was filtered, washed with ample ether and dried under vacuum yielded 86% with purity 97% as confirmed by HPLC. Maldi-Tof Mass (measured 222.0 $[M]^+$, 223.0 $[M+H]^+$; calculated 222.0).

***Synthesis of semi squaraine (3)***

In a round bottom flask with a condenser, 1-ethyl-3-methyl benzoquinolium iodide (2.8g; 8mmol), dibutoxy squarate (1.8g; 8mmol) and trimethylamine (2 ml) were added and dissolved in ethanol. The reaction mixture was then refluxed for 1 hour. The progress of the reaction was monitored by TLC. Upon the completion of the reaction as monitored by TLC, the solvent was removed under reduced pressure. The crude was then purified by silica gel column

chromatography yielded 60% with the purity of 98% as confirmed by HPLC. Maldi-Tof Mass (measured 373.65 $[M]^+$, 374.68 [M+H]+; calculated 373.16).

***Synthesis of unsymmetrical squaraine dye (SQ 1)***

Semi squaraine (3, 746mg; 2mmol) was taken in a round bottom flask and dissolved in 30 ml of ethanol. To this reaction mix, 40 % NaOH (0.6ml) was added and refluxed at $100^0$C for 30 minutes. The reaction progress was monitored by TLC. Upon the completion, the reaction mix was cooled and 1.2 ml of 20 % HCl was added. Upon cooling, the solvent was evaporated under reduced pressure, to this residue 5-Carboxy-2,3,3-trimethyl-1-ethyl-3H-indolium iodide (716 mg; 2mmol) and 1:1 ratio of benzene/butanol was added. The reaction mixture was then refluxed at $110^0$C for 18 hours. The reaction was monitored by TLC and HPLC. After the reaction, the solvent was evaporated and the crude was purified by employing silica gel column chromatography yielded 60% with 100 % purity as confirmed by HPLC. Maldi-Tof Mass (measured 530.11 $[M]^+$, 531.12 $[M+H]^+$; calculated 530.2) confirms the successful synthesis of SQ 1. Figure 1 depicts the synthetic scheme of SQ 1.

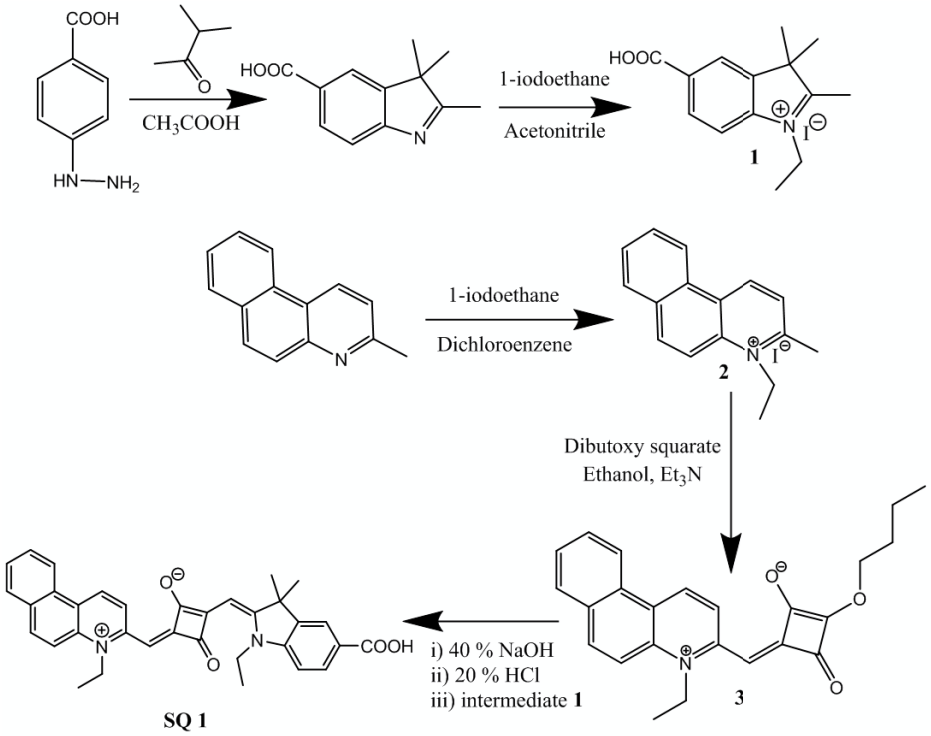


Scheme 1: Synthesis of unsymmetrical squaraine dye

### *5.1.3. Synthesis of fluorescent peptide sequence*

***Boc protection of amino acids on N-terminal (Boc-Ala-OH)***

In a round bottom flask, alanine (4.5g, 50mmol) was dissolved in 20 ml of water and cooled in ice bath. To this solution triethylamine (10ml, 75mmol) and $Boc_2O$ (12g, 60mmol) dissolved in dioxane was added and stirred at room temperature for overnight. Upon the completion of the reaction as confirmed by TLC, the solvent was evaporated. The reaction mixture was dissolved in ethyl acetate and extracted with 4% $NaHCO_3$, 10% citric acid and brine repeatedly for 3 times. The organic layer was then dried over $MgSO_4$, filtered and the solvent was concentrated under reduced pressure. The Boc protected amino acid was then crystallized using ether and petroleum ether yielding 97% with purity 93% as confirmed by HPLC.

***Protection of amino acids on C-terminus (Boc-Ala-OBzl)***

In a round bottom flask, Boc protected (Boc-Ala-OH) amino acid (11.4 g, 60mmol) was dissolved in DMF and placed over an ice bath. To this mixture, triethylamine (9ml, 72mmol) and benzyl bromide (18ml, 132mmol) was added. The above mixture was stirred at room temperature for overnight. Upon the completion of reaction as monitored by TLC, the solvent was evaporated and the residue was dissolved in ethyl acetate, washed with 4 % $NaHCO_3$ and brine. The organic layer was then dried over $MgSO_4$, filtered and concentrated. The final compound was crystallized with petroleum ether yielded 84% with purity 92% as confirmed by HPLC.

***De-protection of Boc from the amino acids (HCl.H-Ala-OBzl)***

In a round bottom flask with calcium guard tube, Boc protected (Boc-Ala-OBzl) amino acid (14g, 50mmol) and 40 ml of 4N HCl/dioxane was added and stirred at room temperature for 3 hours. After the reaction was monitored by TLC, the solvent was evaporated under reduced pressure and the compound was crystallized using ether. The solid compound was filtered and dried yielded 99% with purity 99% as confirmed by HPLC.

***Coupling of amino acids (Boc-Pro-Ala-OBzl)***

In a round bottom flask, HCl.H-Ala-OBzl (5g, 23mmol) was dissolved in DMF and placed over an ice bath. To this reaction mixture, triethylamine (4ml, 28mmol), Boc-Pro-OH (5.9g, 28mmol), HOBT.$H_2O$ (4.3g, 28mmol) and DCC (5.8g, 28mmol) was added and stirred at room temperature for overnight. Upon the completion of reaction as monitored by TLC, the solvent was evaporated, the residue was dissolved in ethyl acetate and 10% citric acid solution was added to precipitate DCU. The DCU was filtered, the filtrate was washed with 10% citric acid, brine, 4% $NaHCO_3$ and brine respectively for 3 times. Finally, the organic layer was dried over $MgSO_4$, filtered and dried yielding 75% of title compound with purity 100 % as confirmed by HPLC.

***Synthesis of Peptide sequence A (Boc-β-Ala-Ala-Pro-Ala-OBzl)***

By following the above-described protection, deprotection and coupling methods peptide elongation was repeated using β-Alanine, Alanine and Proline amino acids. The final compound *(Boc-β-Ala-Ala-Pro-Ala-OBzl)* was obtained in 98 % yield with purity 100 % as confirmed by HPLC.

***Synthesis of compound B ($H_2$N-Lys-(Boc)-OH)***

In a round bottom flask with *Fmoc-Lys-(Boc)-OH* (11.71g, 25mmol) was dissolved in DMF and placed over an ice bath. To this reaction mixture, triethylamine (7.7ml, 55mmol) and benzyl bromide (3.6ml, 30mmol) was added. The above mixture was stirred at room temperature for overnight. Upon the completion of reaction as monitored by TLC, the solvent was evaporated and the residue was dissolved in ethyl acetate, washed with 4 % $NaHCO_3$ and brine twice respectively. The organic layer was then dried over $MgSO_4$, filtered and concentrated. The titled compound (*Fmoc-Lys-(Boc)-OBzl)* was yielded in 75% with purity 90% as confirmed by HPLC and further used for the next step.

The compound obtained above, *Fmoc-Lys-(Boc)-OBzl* (10g, 17.9mmol) was dissolved in 20% DMF/Piperidine and stirred for 1.5 hours to remove the Fmoc residue. Upon completion of the reaction as monitored by TLC, the solvent was evaporated under reduced pressure, ethyl acetate was added to the residue and washed with saturated $Na_2CO_3$ twice. The organic layer

was then dried over $Na_2CO_3$, concentrated and dried under vacuum to obtain compound **B** *(H-Lys-(Boc)-OBzl)* in 96% yield with purity 91% ass confirmed by HPLC.

***Synthesis of compound C (H- β-Ala-Ala-Pro-Ala-Lys-OBzl)***

The peptide substrate **A** was dissolved in methanol and Pd/C was added to the mixture and stirred under $H_2$ gas for 1 hour. Upon the completion of reaction as monitored by TLC, the palladium-charcoal was filtered and the solvent was concentrated under reduced pressure and dried to obtain *(Boc- β-Ala-Ala-Pro-Ala-OH)* in 94% yield with purity >90% as confirmed by HPLC. The obtained compound was further used for the next step, the coupling reaction with **B**.

In a round bottom flask, above obtained compound, *Boc- β-Ala-Ala-Pro-Ala-OH* (6g, 14mmol) and compound **B** (5.2g, 16.8mmol) was coupled using the above-mentioned coupling method. The compound *(Boc-β-Ala-Ala-Pro-Ala-Lys-(Boc)-OBzl)* was obtained in 92% yield with purity 92% as confirmed by HPLC. The compound was further used in the next step to remove the Boc residues.

The compound *Boc-β-Ala-Ala-Pro-Ala-Lys-(Boc)-OBzl* (1.2g, 1.6mmol) was treated with 4N HCl/dioxane in a round bottom flask with calcium chloride guard tube for overnight. Upon the completion of the reaction as monitored by TLC, the solvent was evaporated and the peptide substrate *(H-β-Ala-Ala-Pro-Ala-Lys-OBzl)* was crystallized using ether. The titled compound **C** was then filtered and dried under vacuum, yielded in 98% with purity 85% as confirmed by HPLC. Scheme 2 represents the synthetic strategy of peptide substrate **C**. ESI-Mass (measured 569.3057 $[M+Na]^+$; calculated 546.66) which confirms the successful synthesis of **C**.

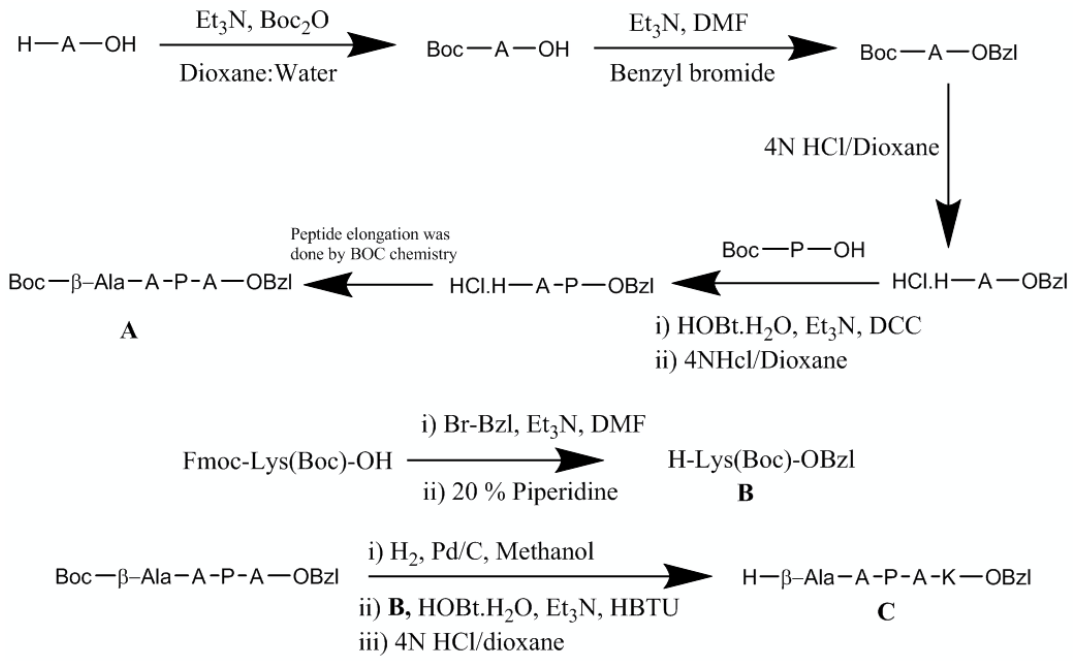


Scheme 2: Synthetic strategy of peptide sequence

### *5.1.4. One pot synthesis of dye-peptide conjugate (SQ 1 PC)*

In a round bottom flask fitted with condenser SQ 1 (50mg, 0.1mmol) , DCC (42mg, 0.2mmol), NHS ester (25mg, 0.2mmol) were dissolved in DMF and refluxed at $50^0$C for 2 hours. The reaction progress was monitored using TLC. Upon the completion of the reaction, Peptide sequence (**C,** 30mg, 0.05mmol) was added and stirred at room temperature for overnight. After the reaction is complete, the solvent was evaporated and the crude was purified by employing silica gel column chromatography using chloroform: methanol as the solvent system. The peptide conjugate was obtained in satisfactory yield. ESI-Mass (measured 1594.78 $[M+Na]^+$; calculated 1571.88) confirms the successful synthesis of peptide conjugate. Scheme 3 depicts the synthetic scheme of peptide conjugate.

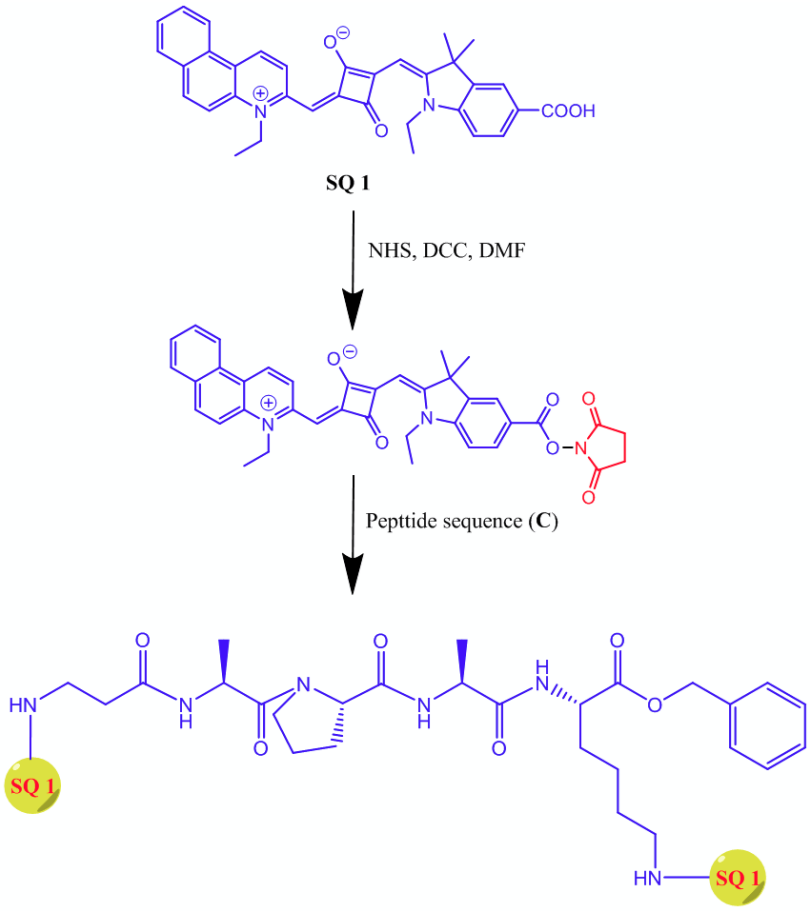


Scheme 3: Synthetic scheme of peptide conjugate

## 5.2. Results and Discussion

In this present work, efforts have been directed to design an internally quenched homo-labeled fluorescent-peptide substrate utilizing a far-red sensitive unsymmetrical squaraine dye coupled with a peptide sequence susceptible to the pancreatic elastase enzyme. Figure 1 exhibits the structure of the main building blocks like direct carboxy ring-functionalized unsymmetrical squaraine dye **SQ-1** (1a), Elastase enzyme specific peptide sequence β-Ala-Ala-Pro-Ala-Lys-(OBzl) (1b) along with fluorescent peptide substrate (1c). Figure 1(d) represents the MM2 energy minimized three-dimensional structure of (1b) and led to the proposal of a possible structure of peptide-dye conjugate as shown in the Fig. 1(c).

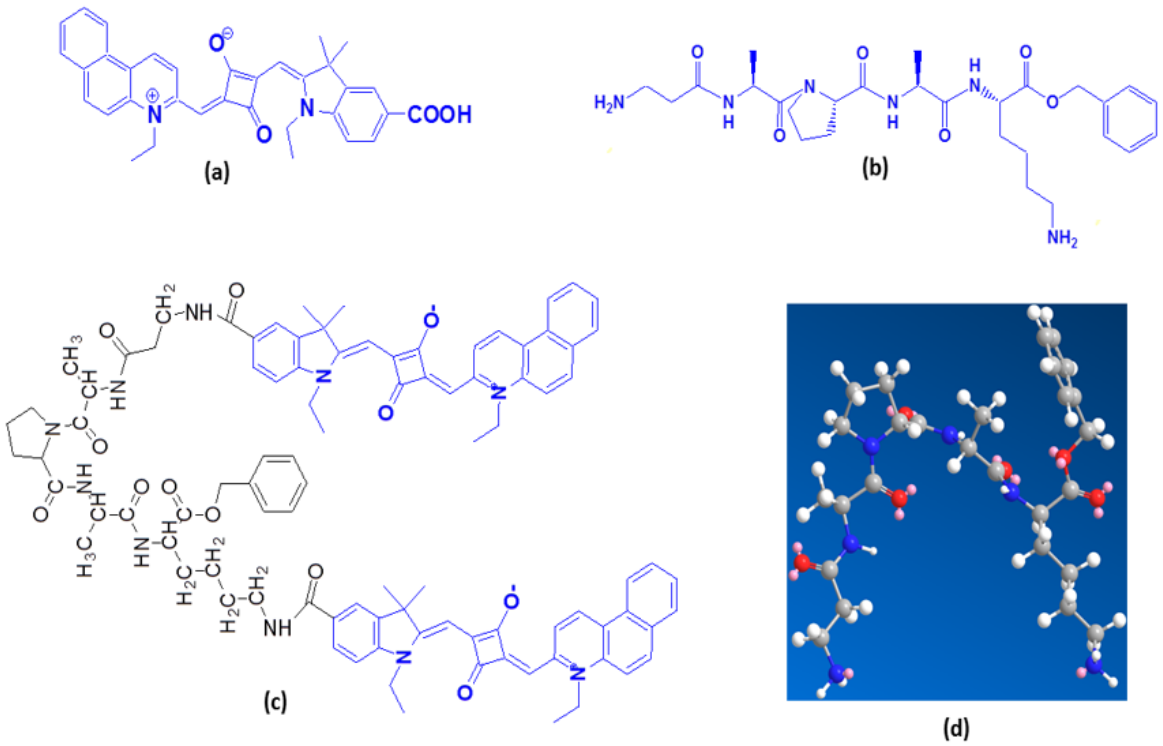


Figure 1. Chemical structure of unsymmetrical squaraine dye (a), elastase enzyme specific peptide (b), peptide-dye conjugate (c) and MM2 energy minimized 3D structure of the peptide (d).

It can be clearly seen from the structure of our newly proposed peptide-dye conjugate that two dye molecules are connected to one peptide at either end of the terminals. **SQ-1** was selected as model dye not only due to its NIR fluorescence capability but also an appreciably good interaction of squaraine dyes with most commonly used model proteins like bovine serum albumin and human serum albumin (45, 46). It has been reported that pancreatic serine protease elastase cleaves the substrate at peptide bonds on the carboxyl side of amino acid residues bearing small alkyl side chain which has led us to design Ala-Pro-Ala as target peptide for elastase enzyme (47). β-Ala and Lys-containing free amino groups have not only been used as a spacer but also for assisting the easy binding of the **SQ-1** dye with its free –COOH group in a single one pot reaction. A perusal of this newly designed substrate as shown in Fig. 1(c) reveals dense packing of the SQ-1, which is expected to bring the internal self-quenching of the fluorescence. At the same time, the flat molecular structure of squaraine dyes is also expected to promote the dye aggregation especially in the buffer solution and aggregated dye molecules have been reported to exhibit the quenched fluorescence (48). Internally

fluorescence quenched peptide-dye conjugate was synthesized by one-pot reaction of NHS-ester activated unsymmetrical squaraine SQ-1 and peptide H-β-Ala-A-P-A-K-OBzl as per the scheme-3.

Electronic absorption spectrum of SQ-1 in dimethylformamide (DMF) solution exhibits a strong electronic absorption with absorption maximum ($\lambda_{max}$) at 672 nm along with the feeble vibronic shoulder around 610 nm and molar extinction coefficient of 1.02 x $10^5$ $dm^3.mol^{-1}.cm^{-1}$ which is associated with π-π* electronic transition which is a typical characteristic of the squaraine dyes. The $\lambda_{max}$ absorption and emission, molar extinction coefficient and stoke shifts of SQ 1 dye and SQ 1 PC in both DMF and PBS solutions were shown in Table 1.

**Table 1**. Spectral properties of dye and dye-conjugate in DMF and 0.1 M PBS solution at pH 7.4.

| | **DMF Solution** | | | | **PBS Solution** | | | |
|---|---|---|---|---|---|---|---|---|
| | **$\lambda_{(max)}$ Absorption** | **$\lambda_{(max)}$ Emission** | **Stoke Shift** | **(ε) ($dm^3$ $M^{-1}$ $cm^{-1}$)** | **$\lambda_{(max)}$ Absorption** | **$\lambda_{(max)}$ Emission** | **Stoke Shift** | **(ε) ($dm^3$ $M^{-1}$ $cm^{-1}$)** |
| **SQ 1 Dye** | 672 nm | 754 nm | 82 nm | $1.02\times10^5$ | 644 nm | 700 nm | 56 nm | $0.66\times10^5$ |
| **SQ 1 PC** | 664 nm | 736 nm | 72 nm | $3.7\times10^5$ | 605 nm | 658 nm | 53 nm | $0.98\times10^5$ |

Merging of the vibronic shoulder with the main absorption for SQ-1 in DMF solution indicates the existence of dye aggregated species. It has been reported that in the case of H-aggregate formation by squaraine dye, sometimes shoulder becomes even more pronounced as compared to monomeric dye absorption peak. Prevention of this dye aggregation by using aggregation preventing species like chenodeoxycholic acid leads to decrease in the absorption corresponding to this shoulder verifying the suppression of dye aggregation (49). On the other hand, its emission spectrum shows fluorescence emission peak at 754 nm with relatively large Stokes shift of 82 nm. Typically, squaraine dyes exhibit a Stokes shift of 20-30 nm due to its rigid molecular structure and indicate the nearly similar molecular configuration of dyes in both of the ground as well as excited states (50). This large Stokes shift in the case of SQ-1 in DMF solution indicates rather diminished conformational stability of SQ-1 in an excited state as compared to typical squaraine dyes. On the other hand, the electronic absorption spectrum of a dye-peptide conjugate (SQ 1 PC) exhibits relatively broader optical absorption having a blue-shifted $\lambda_{max}$ at 664 nm and fluorescence emission maximum at 736 nm with a stoke shift

of 72 nm as shown in the Fig. 2(b). This blue-shift in the absorption and emission maximum could be attributed to the dye aggregate formation. It has been reported that squaraine dyes forms the blue-shifted H-aggregates and red-shifted J-aggregates depending on their structure and molecular environment owing to their relatively flat molecular structure (51).

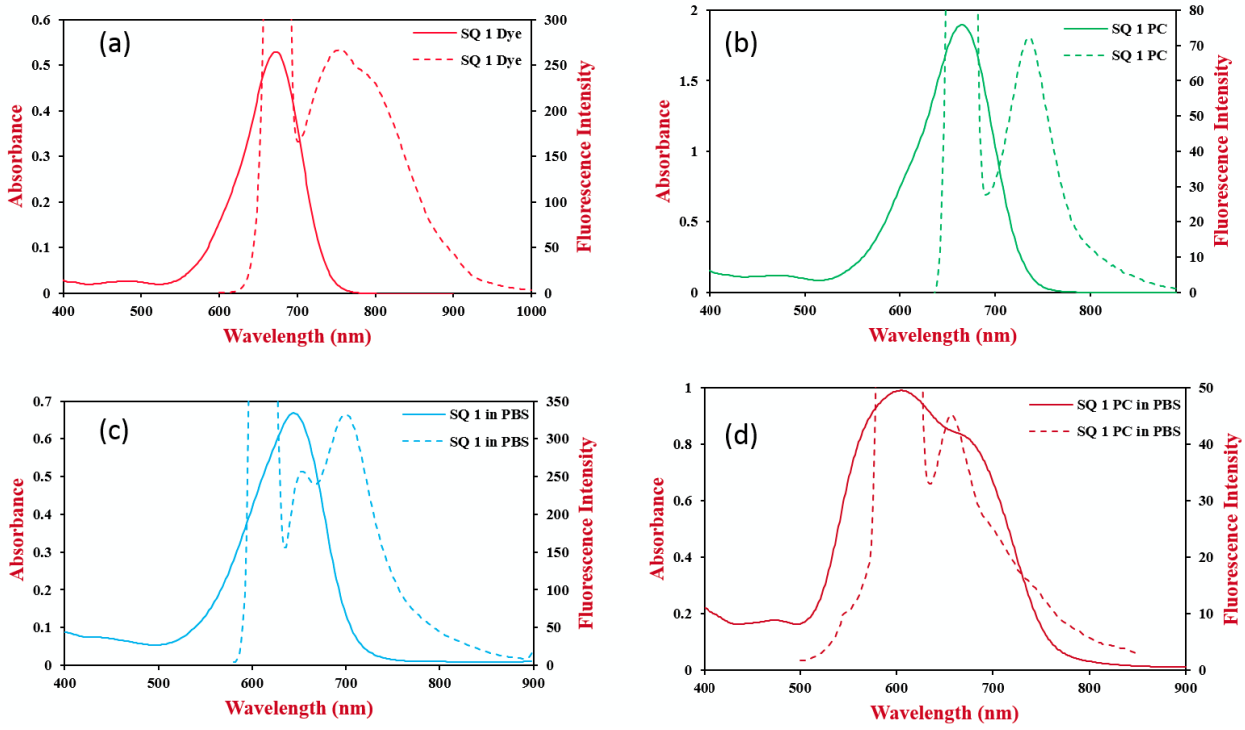


Figure 2. Electronic absorption and fluorescence emission spectra of (a) unsymmetrical squaraine dye SQ-1 and (b) peptide-dye conjugate (SQ 1 PC) in the DMF solution of concentration 5 µM. Figures (C) and (D) represents the same spectral profile for SQ-1 and SQ 1 (PC) in 0.1 M phosphate buffer at pH 7.4 and concentration of 10 µM, dotted line represents the emission spectra for corresponding solutions in all the case.

It is interesting to note here that there is a drastic decrease in the fluorescence intensity associated with SQ-1 for the dye-peptide conjugate as compared to the pure dye SQ-1 having a similar concentration (5 µM) and the same solvent (DMF). This indicates that SQ-1 undergoes the fluorescence quenching upon its conjugation with peptide under investigation (SQ 1 PC). In general two basic mechanisms have been proposed for the fluorescence quenching. First is related to quenching due to fluorescence resonance energy transfer (FRET) while the second one is related to the concentration dependent static internal quenching. In the

homo-dye labeled probes, FERT quenching generally occurs when stoke shift is very small allowing the sufficient overlapping between the absorption and emission spectra of the dye (52). On the other hand, in the case of static quenching, there is a change in the spectral shape generally blue-shift in the absorption maximum facilitated by H-aggregate formation (53). Although both of the mechanism seems to be applicable to explain the fluorescence quenching of SQ 1 PC, considering the large stoke shift and small spectral overlap contribution from FRET-based quenching seem to be small. At the same time, blue shifted absorption and emission maxima which are highly pronounced in the case of phosphate buffer solution (PBS) as shown in the Fig. 2 (c, d) clearly corroborates the dominance of the second mechanism based on static concentration dependent quenching. Thus considering the peak fluorescence intensities of dye alone (SQ-1) and dye-peptide conjugate (SQ 1 PC), fluorescence quenching efficiency was estimated to be 73 % and 86 % in the DMF and PBS, respectively.

Fairly good internal self-quenching fluorescence of dye SQ-1 after coupling with target peptide was observed. This property of conjugate enabled us to explore the application of dye-peptide conjugate as enzyme activity detection based on fluorescence ON bio-sensing. As discussed earlier, Elastase enzyme recognition probe Ala-Pro-Ala amino acid residue was chemically bound with the free –COOH group of SQ-1 by simple one pot reaction. It can be seen from the structure of SQ 1 PC that two terminal amino acids β-Alanine and Lysine have been introduced to solve the two purposes. Firstly, they function as a spacer to promote the access of Elastase enzyme towards the target tripeptide Ala-Pro-Ala. Secondly, availability of free amines allows dense incorporation of SQ-1 dye promoting the internal self-quenching. To demonstrate this, 10 μM solution of this target dye-peptide conjugate SQ 1 PC was subjected to enzymatic hydrolysis using Elastase enzyme in 0.1M phosphate buffer at pH 7.4 and fluorescence emission spectra were measured at different time intervals as shown in figure 3(a). A perusal of this figure clearly reveals that there was a pronounced recovery of quenched fluorescence of the dye within 30 seconds and reached to saturation after 30 min leading to about five-fold enhancement in the fluorescence signal compared to that in the absence of Elastase. This enhancement in the fluorescence after enzymatic hydrolysis could be attributed to the fact that dye-aggregate formation is promoted after conjugation of SQ-1 with peptide in phosphate buffer leading to the H-aggregate assisted efficient fluorescence quenching. After the enzymatic hydrolysis of the peptide bond, multiple copies of dyes are released and attain the special separation leading to the re-appearance of the dye fluorescence.

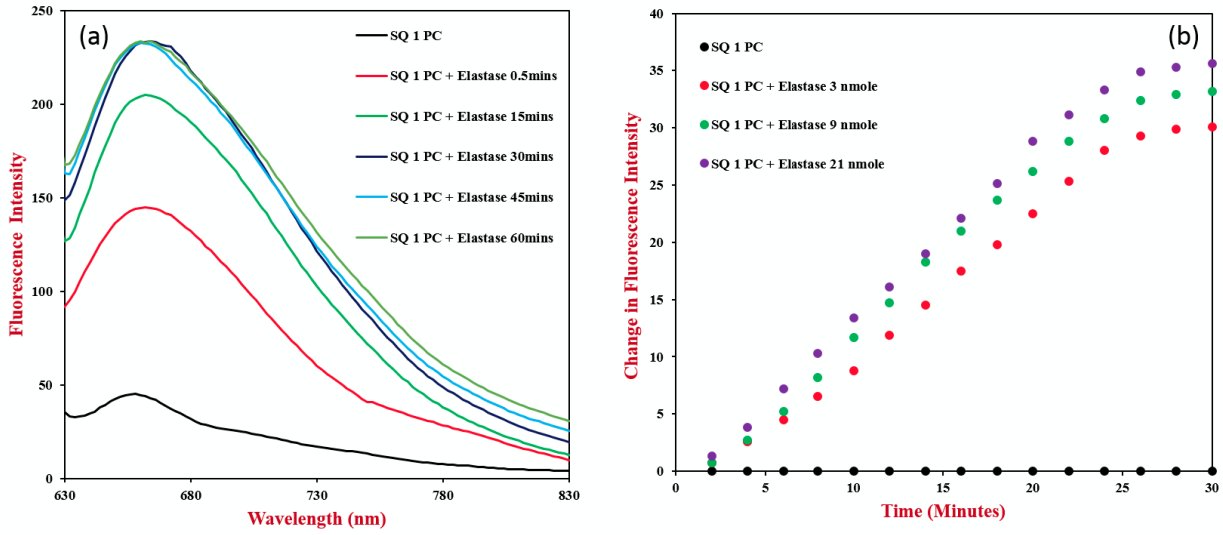


Figure 3. Fluorescence emission spectra of the 0.1M phosphate buffer solution of dye-peptide conjugate (10 μM) at pH 7.4 as a function of time after the addition of 21 nmol of elastase enzyme. Right hand side figure (b) represents the change in fluorescence intensity as a function of time with different concentrations of elastase for a fixed concentration of dye-peptide conjugate (10 μM).

Considering the fluorescence intensities before (control) and after enzymatic hydrolysis of SQ 1 PC, quenching efficiency was estimated to be 81 %. This indicates that such a simple and homo-labeled dye-peptide conjugate based on internal quenching is capable to efficiently detect the enzymatic activity based on fluorescence ON bio-sensing. Efforts were also directed to test this designed dye-peptide conjugate by changing the amount of Elastase enzyme (3 nmol to 21 nmol) for a fixed concentration of this dye-peptide conjugate (10 μM). Based on the change in the fluorescence intensity as a function of time, enzymatic hydrolysis was monitored for different enzyme concentration and has been shown in figure 3(b). A perusal of this figure also indicates that rate of change in fluorescence as a function of concentration is not much significant. On the other hand, saturation fluorescence intensity after complete hydrolysis exhibits clear and distinguishing change for different concentrations of the Elastase. Therefore, consideration of fluorescence intensity at saturation seems to be more plausible for the quantitative aspects of enzyme activity estimations using such dye-peptide conjugate by the fluorescence-ON biosensing. It can be seen that in all of the cases the fluorescence intensities

were reaching saturation after about 25 min. of the enzymatic hydrolysis, while there was completely no change in the case of control that is in the absence of enzyme.

Overall we have demonstrated the NIR fluorescence quenching promoted by enhanced dye aggregation of dye-peptide conjugate and disruption of this aggregation in the presence of enzyme led to the facile detection of proteases based on fluorescence-ON biosensing. Although detection of Elastase activity has been successfully demonstrated in this work, such design and concept can be easily implemented to any target protease by judicious selection of suitable central peptide sequence susceptible to the target enzyme under investigation. Use of single fluorophore and its one-pot coupling with target peptide sequence provide simplicity and rapid profiling of various proteases. Such a concept of fluorescence-ON biosensing based on aggregation-induced fluorescence quenching and re-appearance of fluorescence after enzyme hydrolysis bears good potential in medical diagnosis based on the qualitative and quantitative estimation of enzymes. Integration of such dye-peptide conjugates with microarray technology is expected to tremendously enhance the throughput of analysis. Utilization of such dye-peptide conjugate for microarray application has been schematically shown in figure 4. Amine functionalization of glass surface has been widely studied along with the report of very high-density amine functionalization using 3-amino propyltriethoxysilane (APTS) by Beyer et. al (54). It can be easily seen from the figure 4(b) that free –COOH group in our proposed dye-peptide conjugate can be easily obtained by hydrogenation of O-benzyl group using $H_2$, Pd/C, which is now ready to couple with the free amine group of amine functionalized glass surface (a) making glass surface-bound dye-peptide conjugate (c). Thus we can attach various kinds of such molecular probes on a single glass surface in the microarray format. At the same time, use of wavelength tunable squaraine dyes in such dye-peptide conjugate system not only imparts the widespread design of molecular probes but also provide the capability of efficient and simultaneous multi-target protease analysis facilitated by multi-wavelength fluorescence-ON biosensing.

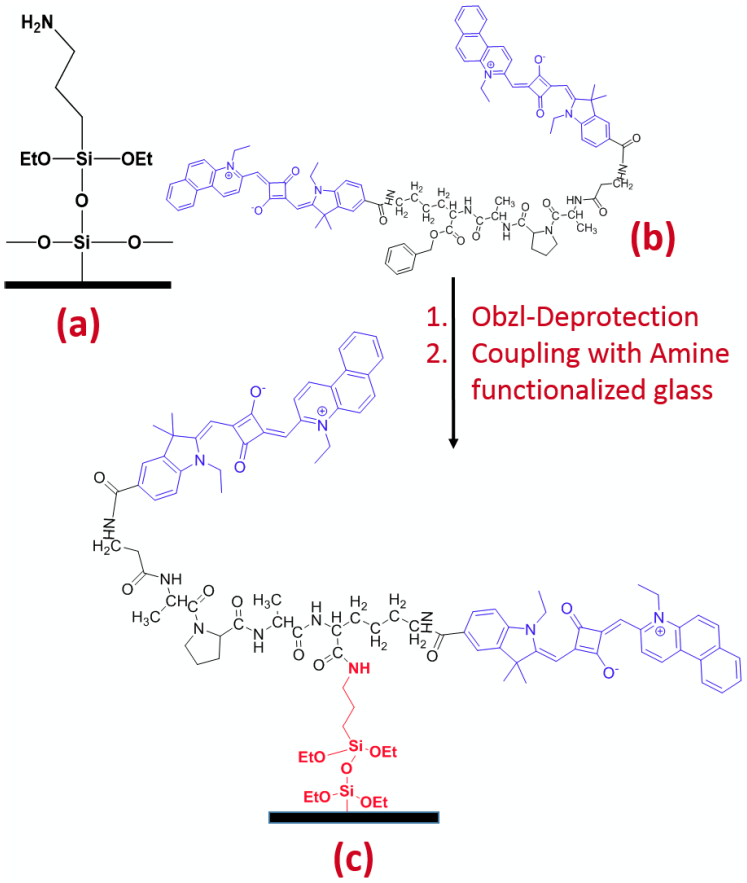


Figure 4. Schematic representation for application of proposed dye-peptide conjugate in peptide microarray for enzyme detection based on fluoresecence-ON biosensing. (a) Amine functionalized glass surface after treatment of glass with APTS (b) dye-peptide conjugate and (c) glass-surface modified with dye-peptide conjugate.

## 5.3. Conclusion

Carboxy functionalized unsymmetrical squaraine dye has been successfully synthesized from their quaternary indolium salts. The substrate specific to elastase were easily synthesized using liquid phase peptide technique. The NIR sensitive dye SQ 1 was conjugated on either end of the peptide substrate using NHS ester as the linker and was confirmed by ESI mass spectrum. The fluorescence of the peptide conjugate was self-quenched owing to the assembled fluorophores on the substrate. Fluorescence recovery was observed on hydrolysis of the peptide conjugate by elastase which enabled the release of fluorophores. Efficient quenched fluorescence of SQ 1 PC (> 50 % in 30 seconds) was observed on hydrolysis of the peptide-dye conjugate by elastase enzyme. Therefore, NIR sensitive self-quenching substrate under

investigation offers the potential application for the detection of diseases related to proteases by efficient and fast detection of their activities.

## 5.4. References


1) T.P. Mashamba-Thompson, B. Sartorius, P.K. Drain, Point-of-care diagnostics for improving maternal health in South Africa, Diagnostics, 6 (2016) 31.
2) P.R. Solanki, A. Kaushik, V.V. Agrawal, B.D. Malhotra, Nanostructured metal oxide-based biosensors, NPG Asia Materials, 3 (2011) 17-24.
3) Y. Zeng, L. Wang, S.-Y. Wu, J. He, J. Qu, X. Li, H.-P. Ho, D. Gu, B.Z. Gao, Y. Shao, High-throughput imaging surface plasmon resonance biosensing based on an adaptive spectral-dip tracking scheme, Optics Express, 24 (2016) 28303-28311.
4) M. Cretich, F. Damin, G. Pirri, M. Chiari, Protein and peptide arrays: recent trends and new directions, Biomolecular engineering, 23 (2006) 77-88.
5) Y.M. Foong, J. Fu, S.Q. Yao, M. Uttamchandani, Current advances in peptide and small molecule microarray technologies, Current opinion in chemical biology, 16 (2012) 234-242.
6) M.F. Templin, D. Stoll, M. Schrenk, P.C. Traub, C.F. Vöhringer, T.O. Joos, Protein microarray technology, Drug discovery today, 7 (2002) 815-822.
7) V. Trevino, F. Falciani, H.A. Barrera-Saldaña, DNA microarrays: a powerful genomic tool for biomedical and clinical research, MOLECULAR MEDICINE-CAMBRIDGE MA THEN NEW YORK-, 13 (2007) 527.
8) S.V. Chittur, DNA microarrays: tools for the 21st Century, Combinatorial chemistry & high throughput screening, 7 (2004) 531-537.
9) M. Bally, K. Bailey, K. Sugihara, D. Grieshaber, J. Vörös, B. Städler, Liposome and lipid bilayer arrays towards biosensing applications, Small, 6 (2010) 2481-2497.
10) J.B. Legutki, Z.-G. Zhao, M. Greving, N. Woodbury, S.A. Johnston, P. Stafford, Scalable high-density peptide arrays for comprehensive health monitoring, Nature communications, 5 (2014).
11) B. Turk, Targeting proteases: successes, failures and future prospects, Nature reviews Drug discovery, 5 (2006) 785-799.
12) S. Rakash, F. Rana, S. Rafiq, A. Masood, S. Amin, Role of proteases in cancer: A review, Biotechnology and Molecular Biology Reviews, 7 (2012) 90-101.

13) E. Kisin-Finfer, S. Ferber, R. Blau, R. Satchi-Fainaro, D. Shabat, Synthesis and evaluation of new NIR-fluorescent probes for cathepsin B: ICT versus FRET as a turn-ON mode-of-action, Bioorganic & medicinal chemistry letters, 24 (2014) 2453-2458.
14) R. Weissleder, C.-H. Tung, U. Mahmood, A. Bogdanov, In vivo imaging of tumors with protease-activated near-infrared fluorescent probes, Nature biotechnology, 17 (1999) 375-378.
15) M. Shamis, C.F. Barbas, D. Shabat, A new visual screening assay for catalytic antibodies with retro-aldol retro-Michael activity, Bioorganic & medicinal chemistry letters, 17 (2007) 1172-1175.
16) B. Korkmaz, T. Moreau, F. Gauthier, Neutrophil elastase, proteinase 3 and cathepsin G: physicochemical properties, activity and physiopathological functions, Biochimie, 90 (2008) 227-242.
17) N. Avlonitis, M. Debunne, T. Aslam, N. McDonald, C. Haslett, K. Dhaliwal, M. Bradley, Highly specific, multi-branched fluorescent reporters for analysis of human neutrophil elastase, Organic & biomolecular chemistry, 11 (2013) 4414-4418.
18) G. Doring, The role of neutrophil elastase in chronic inflammation, American journal of respiratory and critical care medicine, 150 (1994) S114.
19) S.D. Shapiro, Neutrophil Elastase: Path Clearer, Path ogen Killer, or Just Path ologic?, American journal of respiratory cell and molecular biology, 26 (2002) 266-268.
20) T. Abe, A. Usui, H. Oshima, T. Akita, Y. Ueda, A pilot randomized study of the neutrophil elastase inhibitor, Sivelestat, in patients undergoing cardiac surgery, Interactive cardiovascular and thoracic surgery, 9 (2009) 236-240.
21) S.J. Chung, Y.-M. Lee, Y.-J. Jeong, H.J. Kang, B.H. Chung, Cascade enzyme-linked immunosorbent assay, in, Google Patents, 2014.
22) A. Lesner, K. Brzozowski, G. Kupryszewski, K. Rolka, Design, chemical synthesis and kinetic studies of trypsin chromogenic substrates based on the proteinase binding loop of Cucurbita maxima trypsin inhibitor (CMTI-III), Biochemical and biophysical research communications, 269 (2000) 81-84.
23) J.L. Harris, B.J. Backes, F. Leonetti, S. Mahrus, J.A. Ellman, C.S. Craik, Rapid and general profiling of protease specificity by using combinatorial fluorogenic substrate libraries, Proceedings of the National Academy of Sciences, 97 (2000) 7754-7759.
24) H. Sun, R.C. Panicker, S.Q. Yao, Activity based fingerprinting of proteases using FRET peptides, Peptide Science, 88 (2007) 141-149.

25) K.y. Tomizaki, K. Usui, H. Mihara, Protein-Detecting Microarrays: Current Accomplishments and Requirements, ChemBioChem, 6 (2005) 782-799.
26) Y.-J. Gong, X.-B. Zhang, G.-J. Mao, L. Su, H.-M. Meng, W. Tan, S. Feng, G. Zhang, A unique approach toward near-infrared fluorescent probes for bioimaging with remarkably enhanced contrast, Chemical Science, 7 (2016) 2275-2285.
27) M. Fu, Y. Xiao, X. Qian, D. Zhao, Y. Xu, A design concept of long-wavelength fluorescent analogs of rhodamine dyes: replacement of oxygen with silicon atom, Chemical Communications, (2008) 1780-1782.
28) Y. Koide, Y. Urano, K. Hanaoka, T. Terai, T. Nagano, Evolution of group 14 rhodamines as platforms for near-infrared fluorescence probes utilizing photoinduced electron transfer, ACS chemical biology, 6 (2011) 600-608.
29) Y. Koide, Y. Urano, K. Hanaoka, W. Piao, M. Kusakabe, N. Saito, T. Terai, T. Okabe, T. Nagano, Development of NIR fluorescent dyes based on Si–rhodamine for in vivo imaging, Journal of the American Chemical Society, 134 (2012) 5029-5031.
30) J. Chen, W. Liu, B. Zhou, G. Niu, H. Zhang, J. Wu, Y. Wang, W. Ju, P. Wang, Coumarin-and rhodamine-fused deep red fluorescent dyes: synthesis, photophysical properties, and bioimaging in vitro, The Journal of organic chemistry, 78 (2013) 6121-6130.
31) A. Chevalier, P.Y. Renard, A. Romieu, Straightforward Access to Water-Soluble Unsymmetrical Sulfoxanthene Dyes: Application to the Preparation of Far-Red Fluorescent Dyes with Large Stokes' Shifts, Chemistry–A European Journal, 20 (2014) 8330-8337.
32) C.H. Tung, Y. Lin, W.K. Moon, R. Weissleder, A Receptor-Targeted Near-Infrared Fluorescence Probe for In Vivo Tumor Imaging, ChemBioChem, 3 (2002) 784-786.
33) A. Becker, C. Hessenius, K. Licha, B. Ebert, U. Sukowski, W. Semmler, B. Wiedenmann, C. Grötzinger, Receptor-targeted optical imaging of tumors with near-infrared fluorescent ligands, Nature biotechnology, 19 (2001) 327-331.
34) K. Marten, C. Bremer, K. Khazaie, M. Sameni, B. Sloane, C.H. Tung, R. Weissleder, Detection of dysplastic intestinal adenomas using enzyme-sensing molecular beacons in mice, Gastroenterology, 122 (2002) 406-414.
35) V. Ntziachristos, C.-H. Tung, C. Bremer, R. Weissleder, Fluorescence molecular tomography resolves protease activity in vivo, Nature medicine, 8 (2002) 757-761.

36) S. Sreejith, K.P. Divya, A. Ajayaghosh, A Near-Infrared Squaraine Dye as a Latent Ratiometric Fluorophore for the Detection of Aminothiol Content in Blood Plasma, Angewandte Chemie, 120 (2008) 8001-8005.
37) L. Yuan, W. Lin, S. Zhao, W. Gao, B. Chen, L. He, S. Zhu, A unique approach to development of near-infrared fluorescent sensors for in vivo imaging, Journal of the American Chemical Society, 134 (2012) 13510-13523.
38) Y. Zhang, F. Huo, C. Yin, Y. Yue, J. Hao, J. Chao, D. Liu, An off–on fluorescent probe based on maleimide for detecting thiols and its application for bioimaging, Sensors and Actuators B: Chemical, 207 (2015) 59-65.
39) D. Yao, Z. Lin, J. Wu, Near-Infrared Fluorogenic Probes with Polarity-Sensitive Emission for in Vivo Imaging of an Ovarian Cancer Biomarker, ACS applied materials & interfaces, 8 (2016) 5847-5856.
40) D. Sato, T. Kato, Novel fluorescent substrates for detection of trypsin activity and inhibitor screening by self-quenching, Bioorganic & Medicinal Chemistry Letters, 26 (2016) 5736-5740.
41) J.M. Ellard, T. Zollitsch, W.J. Cummins, A.L. Hamilton, M. Bradley, Fluorescence enhancement through enzymatic cleavage of internally quenched dendritic peptides: A sensitive assay for the AspN endoproteinase, Angewandte Chemie International Edition, 41 (2002) 3233-3236.
42) S.S. Pandey, R. Watanabe, N. Fujikawa, G.M. Shivashimpi, Y. Ogomi, Y. Yamaguchi, S. Hayase, Effect of extended π-conjugation on photovoltaic performance of dye sensitized solar cells based on unsymmetrical squaraine dyes, Tetrahedron, 69 (2013) 2633-2639.
43) S. Lee, E.J. Cha, K. Park, S.Y. Lee, J.K. Hong, I.C. Sun, S.Y. Kim, K. Choi, I.C. Kwon, K. Kim, A Near-Infrared-Fluorescence-Quenched Gold-Nanoparticle Imaging Probe for In Vivo Drug Screening and Protease Activity Determination, Angewandte Chemie, 120 (2008) 2846-2849.
44) S.S. Pandey, T. Inoue, N. Fujikawa, Y. Yamaguchi, S. Hayase, Substituent effect in direct ring functionalized squaraine dyes on near infra-red sensitization of nanocrystalline TiO 2 for molecular photovoltaics, Journal of Photochemistry and Photobiology A: Chemistry, 214 (2010) 269-275.

45) M. Sai kiran, Shyam. S. Pandey, S. Hayase, T. Kato, Photophysical characterization and BSA interaction of direct ring carboxy functionalized symmetrical squaraine dyes, *Journal of Physics: Conference Series. (In Press)*

46) V.S. Jisha, K.T. Arun, M. Hariharan, D. Ramaiah, Site-Selective Interactions: Squaraine Dye− Serum Albumin Complexes with Enhanced Fluorescence and Triplet Yields, The Journal of Physical Chemistry B, 114 (2010) 5912-5919.

47) R.B. Lefkowitz, G.W. Schmid-Schönb in, M.J. Heller, Whole blood assay for elastase, chymotrypsin, matrix metalloproteinase-2, and matrix metalloproteinase-9 activity, Analytical chemistry, 82 (2010) 8251-8258.

48) A.K. Galande, S.A. Hilderbrand, R. Weissleder, C.-H. Tung, Enzyme-targeted fluorescent imaging probes on a multiple antigenic peptide core, Journal of medicinal chemistry, 49 (2006) 4715-4720.

49) J. Yum, S. Moon, R. Humphry-Baker, P. Walter, T. Geiger, F. Nüesch, M. Grätzel, M. d K Nazeeruddin, Effect of coadsorbent on the photovoltaic performance of squaraine sensitized nanocrystalline solar cells, Nanotechnology, 19 (2008) 424005.

50) M.J. Marchena, G. de Miguel, B. Cohen, J.A. Organero, S. Pandey, S. Hayase, A. Douhal, Real-time photodynamics of squaraine-based dye-sensitized solar cells with iodide and cobalt electrolytes, The Journal of Physical Chemistry C, 117 (2013) 11906-11919.

51) L. Hu, Z. Yan, H. Xu, Advances in synthesis and application of near-infrared absorbing squaraine dyes, RSC Advances, 3 (2013) 7667-7676.

52) M. Ternon, J.J. Díaz-Mochón, A. Belsom, M. Bradley, Dendrimers and combinatorial chemistry—tools for fluorescent enhancement in protease assays, Tetrahedron, 60 (2004) 8721-8728.

53) B.Z. Packard, D.D. Toptygin, A. Komoriya, L. Brand, [2] Design of profluorescent protease substrates guided by exciton theory, Methods in enzymology, 278 (1997) 15-23.

54) M. Beyer, T. Felgenhauer, F.R. Bischoff, F. Breitling, V. Stadler, A novel glass slide-based peptide array support with high functionality resisting non-specific protein adsorption, Biomaterials, 27 (2006) 3505-3514.

## 5.5. Appendix

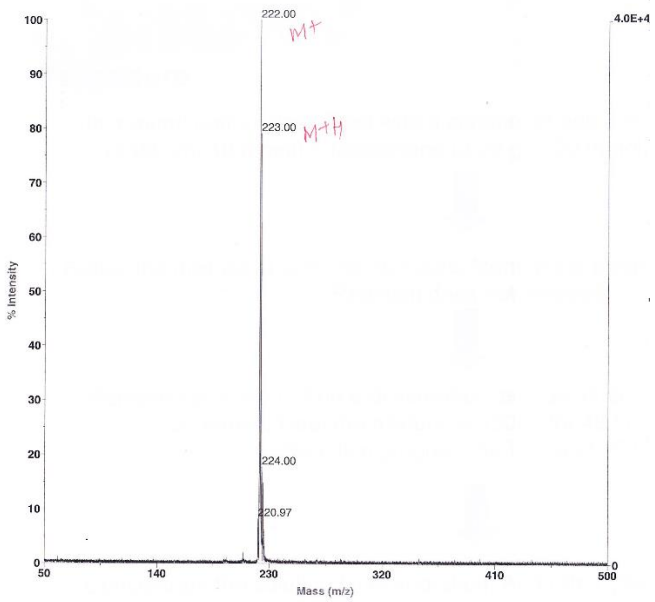


Figure 1. TOF Mass of *3-methyl-N-ethyl-5,6-benzoquinoline iodide.*

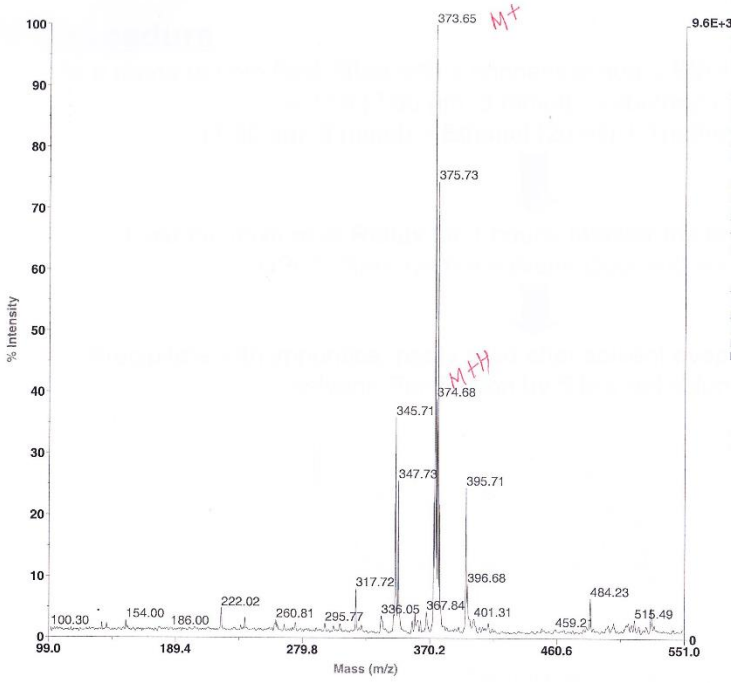


Figure 2. TOF Mass of Semi Squaraine.

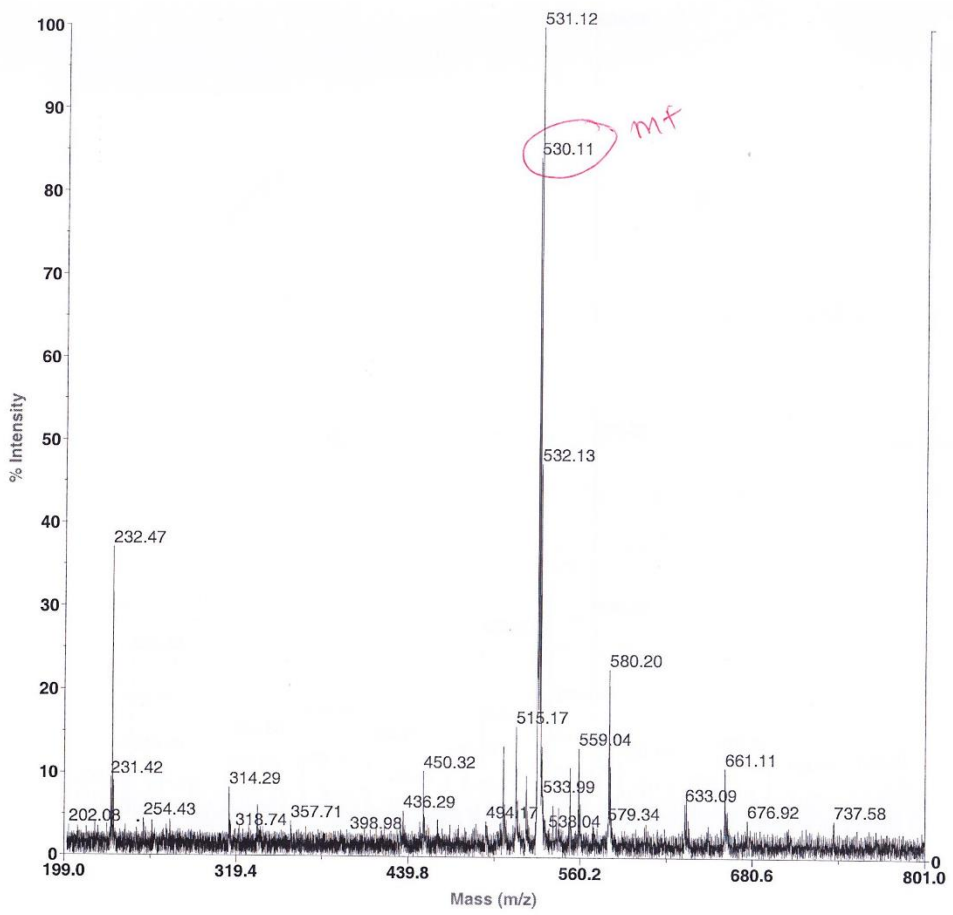


Figure 3. TOF Mass of SQ 1 Dye.

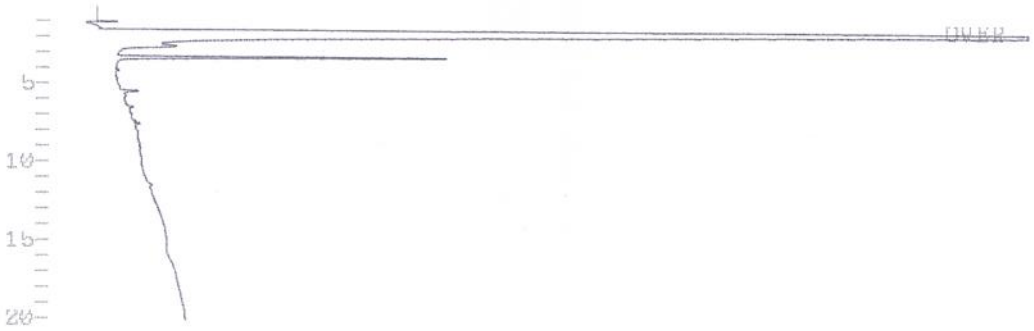


Figure 4. HPLC of BOC-Ala-OH.

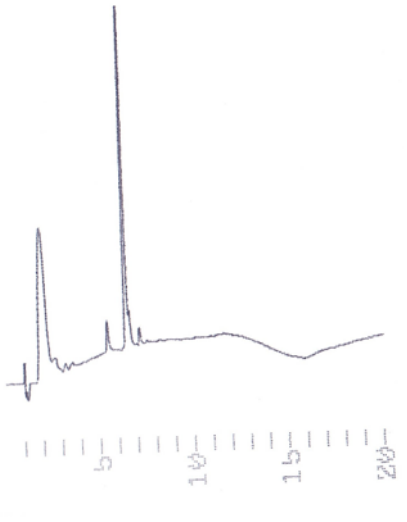


Figure 5. HPLC of BOC-Ala-OBzl.

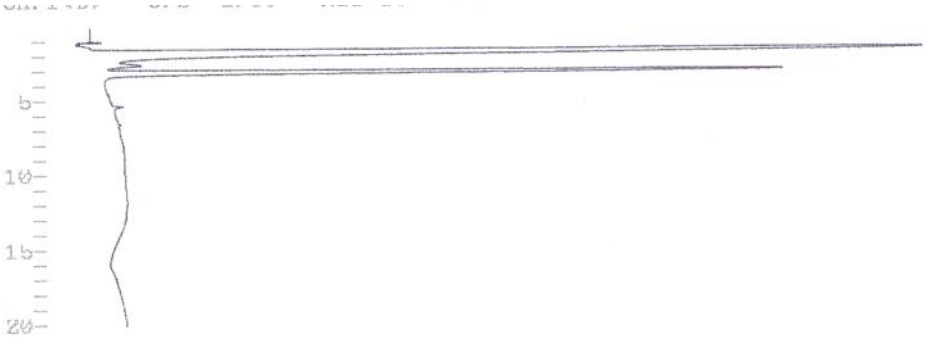


Figure 6. HPLC of HCl.H-Ala-OBzl.

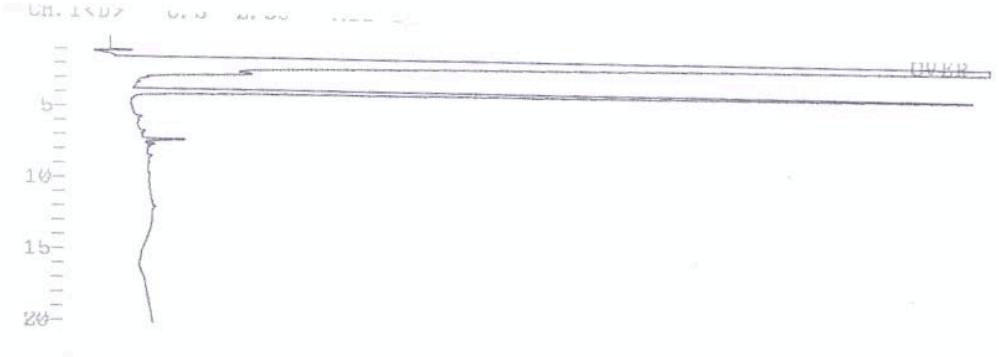


Figure 7. HPLC of BOC-Pro-OH.

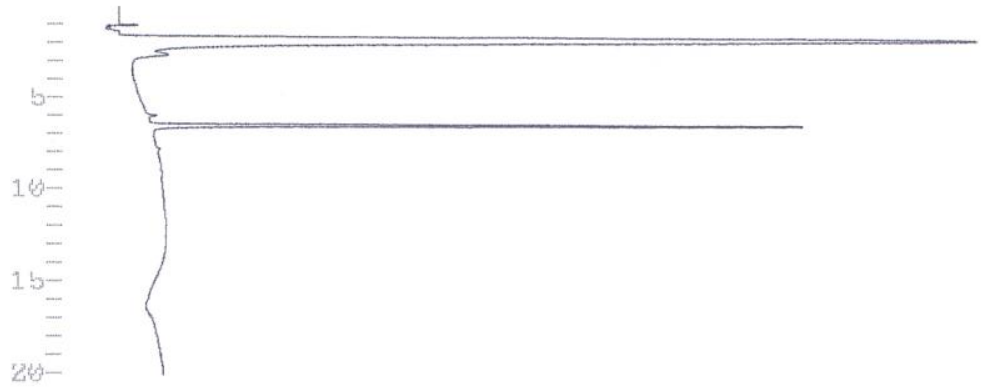


Figure 8. HPLC of BOC-Pro-Ala-OBzl.

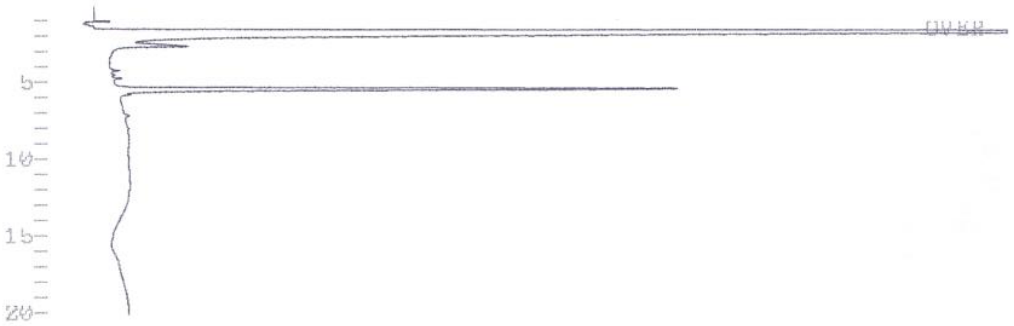


Figure 9. HPLC of BOC-β-Ala-Ala-Pro-Ala-OBzl.

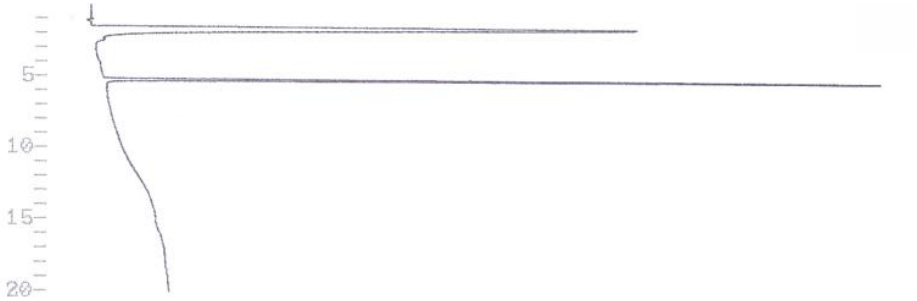


Figure 10. HPLC of Fmoc-Lys(Boc)-OH.

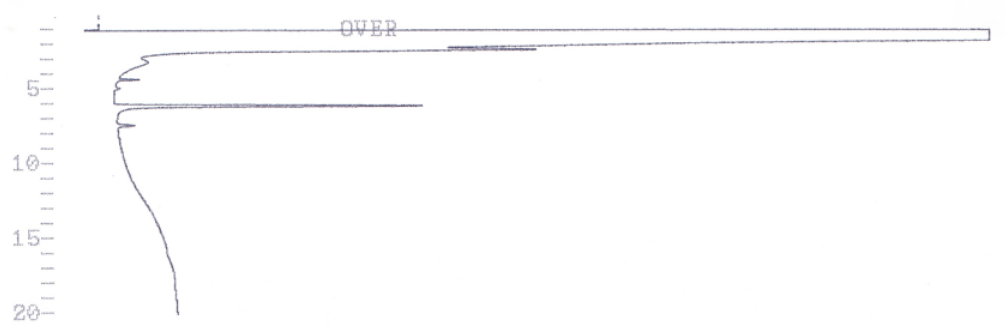


Figure 11. HPLC of Fmoc-Lys(Boc)-OBzl.

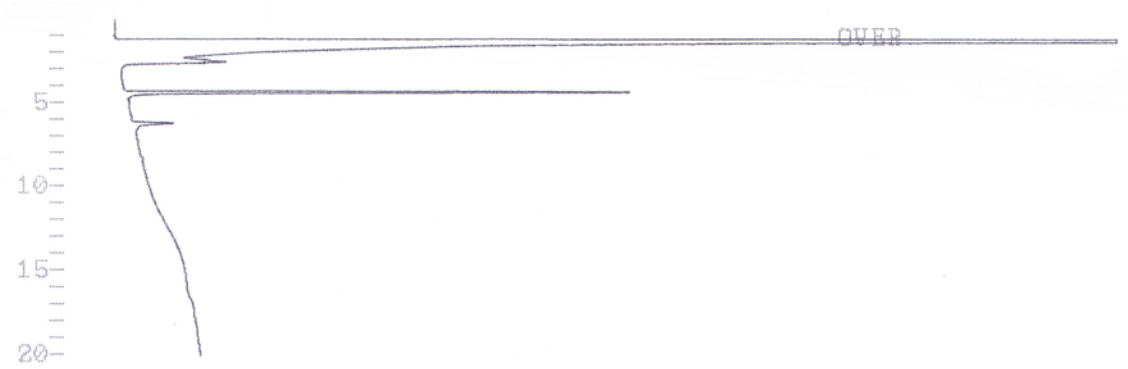


Figure 12. HPLC of H-Lys(Boc)-OBzl.

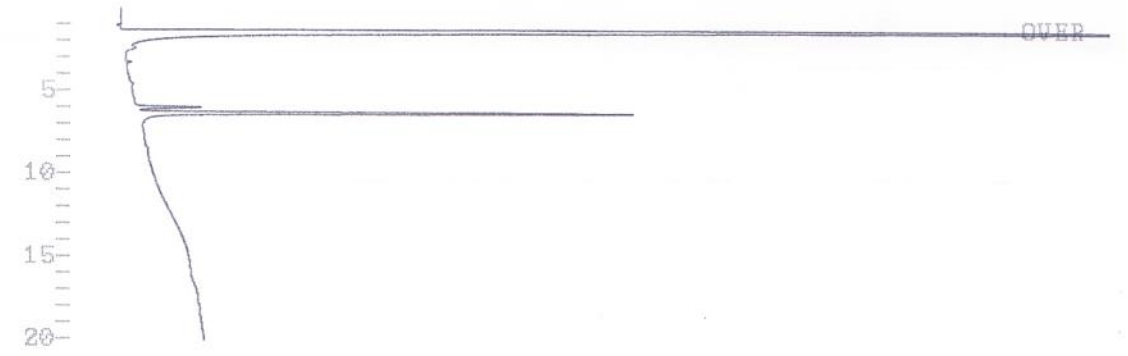


Figure 13. HPLC of BOC-β-Ala-Ala-Pro-Ala-Lys(Boc)-OBzl.

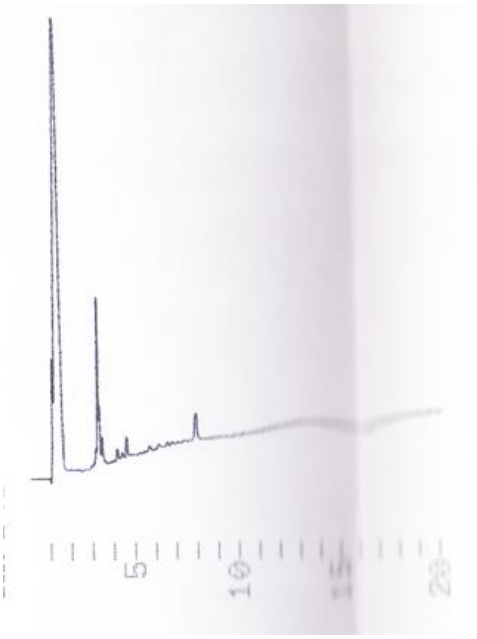

Figure 14. HPLC of H-β-Ala-Ala-Pro-Ala-Lys(Boc)-OBzl.

| Mass | Intensity | Calc. Mass | Mass Difference [mDa] | Mass Difference [ppm] | Possible Formula | Unsaturation Number |
|---|---|---|---|---|---|---|
| 569.30575 | 2166796.06 | 569.30635 | −0.60 | −1.05 | $^{12}C_{27}{}^{1}H_{42}{}^{14}N_{6}{}^{23}Na_{1}{}^{16}O_{6}$ | 9.5 |
| | | 569.31893 | −13.18 | −23.14 | $^{12}C_{28}{}^{1}H_{44}{}^{14}N_{5}{}^{23}Na_{1}{}^{16}O_{6}$ | 9.0 |

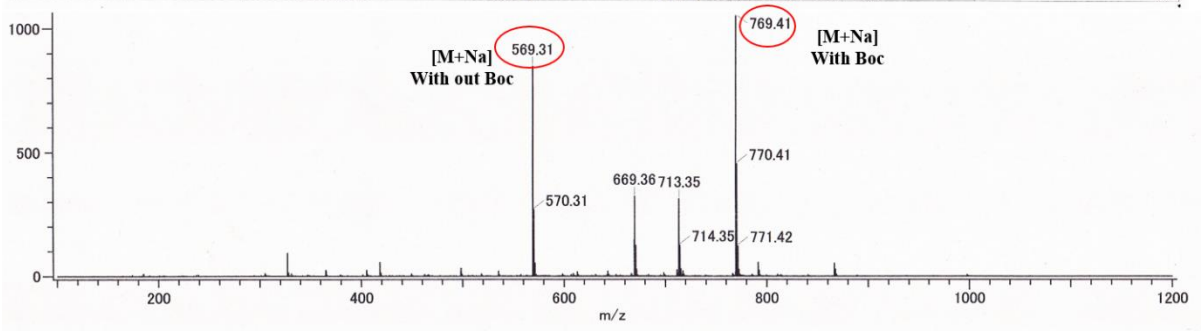


Figure 15. ESI Mass of Peptide chain.

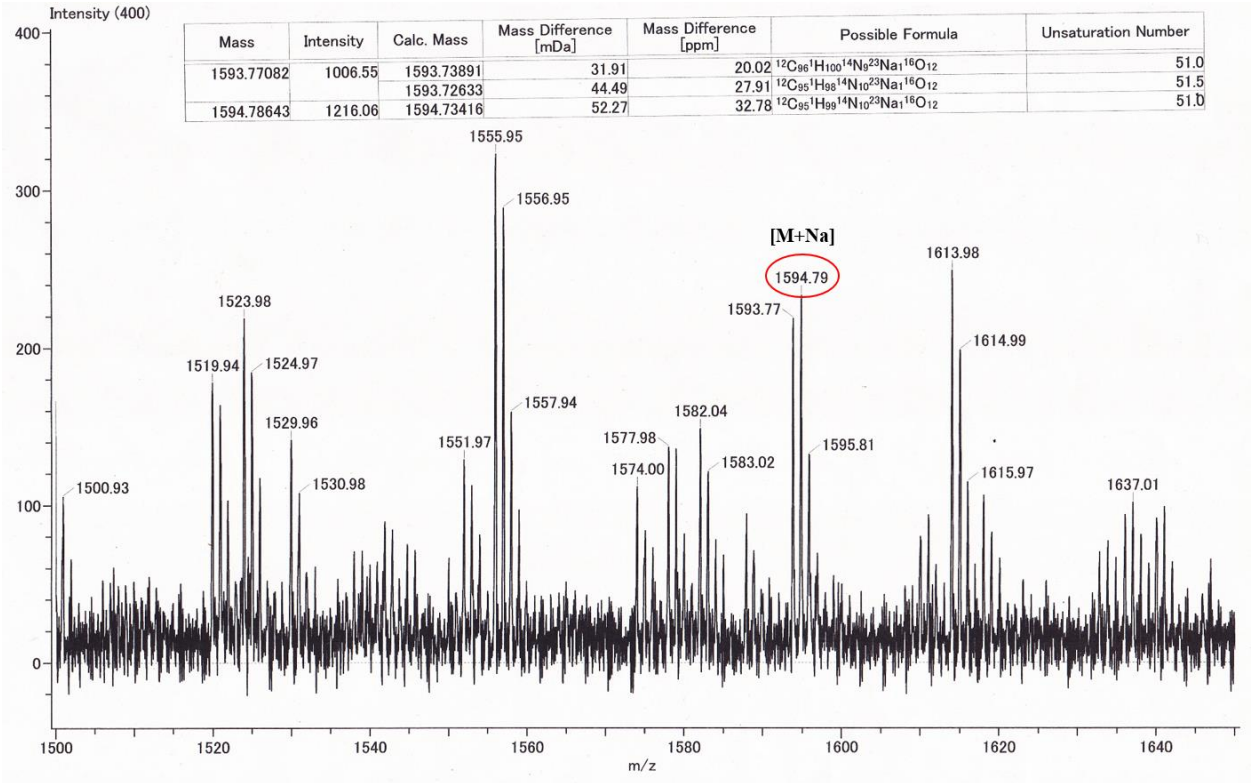


| Mass | Intensity | Calc. Mass | Mass Difference [mDa] | Mass Difference [ppm] | Possible Formula | Unsaturation Number |
|---|---|---|---|---|---|---|
| 1593.77082 | 1006.55 | 1593.73891 | 31.91 | 20.02 | $^{12}C_{96}{}^{1}H_{100}{}^{14}N_{9}{}^{23}Na_{1}{}^{16}O_{12}$ | 51.0 |
| | | 1593.72633 | 44.49 | 27.91 | $^{12}C_{95}{}^{1}H_{98}{}^{14}N_{10}{}^{23}Na_{1}{}^{16}O_{12}$ | 51.5 |
| 1594.78643 | 1216.06 | 1594.73416 | 52.27 | 32.78 | $^{12}C_{95}{}^{1}H_{99}{}^{14}N_{10}{}^{23}Na_{1}{}^{16}O_{12}$ | 51.0 |

Figure 16. ESI mass of Peptide conjugate.

# Future Prospect

In the future prospect, I would like to continue on the similar lines to develop NIR region FRET system for the protein based chip to detect diseases associated with proteases activity. Though methods based on immunoassay comprised of specific binding of proteases with antibody were commercialized and able to estimate quantitatively. They are not appropriate for the detection of diseases associated with proteases. Therefore much attention has been drawn towards the optical based fluorescence detection with suitable peptide substrates. There is much attention and scope to overcome the challenges such as detection of multiple analytes, high throughput sensing and to reduce signal to noise ratio by employing NIR fluorophores where they lack auto-fluorescence from biological samples should be considered for developing an efficient and flexible point of care testing devices by utilizing fluorescent peptide substrates labelled with NIR fluorophores due to their enhanced sensitivity and biocompatibility with high throughput mapping. Thinking on above prospects to overcome the challenges, utilization of fluorophores which emit in NIR wavelength region are in demand to attain greater sensitivity, owing to their reduced auto-fluorescence and deep tissue penetration ability.

In present thesis work was focused on design and synthesis of peptide substrates labeled with fluorescent moieties which are capable of self-quenching and re-appearance of fluorescence after enzyme hydrolysis. This was successfully demonstrated by developing peptide substrate marked with similar fluorophores on either end of the peptide at a foster radius which leads to self-quenching. My future prospect is to design NIR region FRET based system for protein chip as mentioned above. In order to achieve this at first, evaluation of amino acid sequences which are selective to specific target enzyme should be modelled. Secondly, to design a wavelength tunable NIR dyes with selective aromatic or heterocyclic system to encompass from visible to IR region. Finally to incorporate the evaluated amino acid sequence along with fluorochromes to develop a model for the NIR-FRET system to detect NIR fluorescence due to enzyme specificity and diseases associated with protease activity through imaging technique.

# Achievements

## (A) Publications

1. **Maryala Sai kiran**, Daisuke Sato, Shyam S Pandey and Tamaki Kato, "Photophysical investigations of squaraine and cyanine dyes and their interaction with bovine serum albumin", ***Journal of physics IOP conference series Vol. 704. No. 1. IOP Publishing, 2016.***

2. **Maryala Sai kiran,** Daisuke Sato, Shyam S. Pandey, Takeshi Ohta, Shuzi Hayase and Tamaki Kato, "Photophysical characterization and BSA interaction of the direct ring Carboxy functionalized unsymmetrical NIR cyanine dyes", ***Dyes and Pigments,* 140 (2017): 6-13.**

3. **Maryala Sai Kiran**, Shyam S. Pandey, Shuzi Hayase and Tamaki Kato, "Photophysical Characterization and BSA Interaction of Direct Ring Carboxy Functionalized Symmetrical Squaraine Dyes", ***Journal of physics IOP conference series IOP Publishing, 2017.***

4. **Maryala Sai kiran**, Daisuke Sato, Shyam S Pandey, Shuzi Hayase and Tamaki Kato, "Efficient near infrared fluorescence detection of elastase enzyme using peptide-bound unsymmetrical squaraine dye", ***Journal of Bioorganic and medicinal chemistry letters* 27.17 (2017): 4024-4029.**

5. Anusha Pradhan, **Maryala Sai kiran**, Gaurav Kapil, Shyam S. Pandey, Shuzi Hayase, "Parametric Optimization of Dye-Sensitized Solar Cells Using Far red Sensitizing Dye with Cobalt Electrolyte", ***Journal of physics IOP conference series IOP Publishing, 2017.***

## (B) National and International Conferences

1. **Maryala Sai Kiran**, Shyam S. Pandey, Shuzi Hayase and Tamaki Kato, "Photophysical Characterization and BSA Interaction of Direct Ring Carboxy Functionalized Symmetrical Squaraine Dyes", 12$^{th}$ International Conference on Nano-Molecular Electronics (ICNME), December 14-16 (2016), Kobe International Conference Center, Kobe, Japan.
2. **Maryala Sai Kiran**, Shyam S. Pandey, Shuzi Hayase and Tamaki Kato, "Protein Interactions of Far-red Sensitive Symmetrical Squaraine dyes", 4$^{th}$ International

Symposium on Applied Engineering and Sciences (SAES), December 17-18, (2016), Kyushu Institute of Technology, Tobata, Japan.

3. **Maryala Sai Kiran**, Daisuke Sato, Shyam S. Pandey, Shuzi Hayase and Tamaki Kato, "Synthesis and Characterization of Symmetrical Squaraine Dyes along with their Interaction with BSA", Chemical Society Japan (CSJ) 96th Annual meeting, March 24-27 (2016), Kyotanabe Campus, Doshisha University, Kyoto, Japan.
4. **Maryala Sai Kiran**, Daisuke Sato, Shyam S. Pandey, and Tamaki Kato, "Photophysical investigations of squaraine/cyanine dyes and their interaction with protein towards NIR FRET applications", India-Japan Expert Group Meeting on Biomolecular Electronics & Organic Nanotechnology for Environment Preservation (IJEGMBE), December 22-25 (2015), Nakamura Centenary Memorial Hall, Kyushu Institute of Technology, Fukuoka, Japan.
5. **Maryala Sai Kiran**, Daisuke Sato, Shyam S. Pandey, and Tamaki Kato, "Synthesis and photophysical characterization of the direct ring functionalized unsymmetrical NIR cyanine dyes", Chemical Society Japan (CSJ) 95th Annual meeting, March 26-29 (2015), Funabashi Campus, College of Science and Technology, Nihon University/ School of Pharmacy, Nihon University, Chiba, Japan.
6. Anusha Pradhan, **Maryala Sai kiran**, Gaurav Kapil, Shyam S. Pandey and Shuzi Hayase, "Effect of Compact Okide Layer Surface Passivation for Dye-Sensitized Solar Cells utilizing Cobalt Complex Based Redox Electrolyte", 9th International Conference on Materials for Advanced Technologies (ICMAT 2017), Suntec Singapore Convention & Exhibition Centre, 1 Raffles Boulevard, Suntec City, Singapore, 039593, June 18-23 (2017), Singapore.
7. Anusha Pradhan, **Maryala Sai kiran**, Gaurav Kapil, Shuzi Hayase and Shyam S. Pandey, "Novel NIR dyes in Combination with Cobalt Redox shuttles for high Efficiency Dye Sensitized Solar Cells", 54th chemical-related branch Joint Kyushu tournament, Kitakyushu International Conference Hall, 1 JULY 2017, Kokura, 3-9-30 Asano, Kitakyushu-shi.
8. Shyam S Pandey, Takuya Morimoto, Anusha Pradhan, **Maryala Sai Kiran**, Shuzi Hayase, "Molecular Design of far-red Sensitive Squaraine Dyes in-order to Probe the Minimum Energy Barrier for Dye-Regeneration", 26th Annual Meeting of Materials Research Society Japan, December 19-22 (2016), Yokohama Port Opening Plaza, Yokohama, Japan.

9. Shyam S. Pandey, Anusha Pradhan, Takuya Morimoto, **Maryala Sai kiran** and Shuzi Hayase, "Theoretical Molecular Design of Novel Near Infra-red Sensitizers for Dye-Sensitized Solar Cells using Gaussian Program Package", 3rd International Conference on Computational Methods in Engineering and Health Sciences (ICCMEH2016), December 17-18 (2016), Kyushu Institute of Technology, Tobata, Kitakyushu, Japan.
10. Anusha Pradhan, **Maryala Sai kiran**, Gaurav Kapil, Shyam S. Pandey and Shuzi Hayase, "Parametric Optimization for Dye-Sensitized Solar Cells using Far-Red Sensitizing Dyes with Cobalt Electrolyte", 4th International Symposium on Applied Engineering and Sciences (SAES 2016) Kyushu Institute of Technology, 17-18 Dec (2016), Tobata, Kitakyushu, Japan.
11. Shyam S. Pandey, Takuya Morimoto, Anusha Pradhan, **Maryala Sai kiran** and Shuzi Hayase, "Mapping of Minimum Energy Barrier for Electron Injection and Dye Regeneration Utilizing Model Squaraine Dyes", 4th International Symposium on Applied Engineering and Sciences (SAES 2016) Kyushu Institute of Technology, 17-18 Dec (2016), Tobata, Kitakyushu, Japan.
12. Anusha Pradhan, **Maryala Sai kiran**, Gaurav Kapil, Shyam S. Pandey, Shuzi Hayase, "Dye-Sensitized Solar Cells utilizing Far-red Sensitive Dyes in Combination with Cobalt Complex based Redox Electrolyte", 12th International Conference on Nano-Molecular Electronics (ICNME), December 14-16 (2016), Kobe International Conference Center, Kobe, Japan.
13. Shyam S. Pandey, Takuya Morimoto, **Maryala Sai kiran** and Shuzi Hayase, "Molecular Design and Photophysical Characterization of Squaraine Dyes with Small Energy Barrier for Electron Injection and Dye Regeneration", International Union of Materials Research Societies: International Conference on Electronic Materials (IUMRS-ICEM 2016), July 4-8 (2016), Suntec Singapore.
14. Shyam S. Pandey, Takuya Morimoto, **Maryala Sai kiran** and Shuzi Hayase, "Constraints of NIR Dyes for Dye-Sensitized Solar Cells and Its Amicable Solution by Theoretical Molecular Design", International Conference on Science and Technology of Synthetic Metals (ICSM-2016), June 26-July 1 (2016), Guanzhou, China.
15. Shyam S. Pandey, Takuya Morimoto, **Maryala Sai kiran** and Shuzi Hayase, "Design and Photophysical Characterizations of Far-red Sensitive Squaraine Dyes with Small Energy Barrier for Dye Regeneration", Chemical Society Japan (CSJ) 96th Annual meeting, March 24-27 (2016), Kyotanabe Campus, Doshisha University, Kyoto, Japan.

# Acknowledgement

I would like to thank **Prof. Tamaki Kato** for providing me this opportunity to join his group and acquire knowledge, experience and expertise which was offered selflessly. I am very thankful to have been part of your extended student family, and for the supervision that was provided to me when needed.

I would like to express my sincere gratitude to **Prof. Shyam S Pandey** who played a key role in recommending me under **Prof. Tamaki Kato** and also in accepting me to work under him. His vast experience and technical knowledge have given me an excellent support and background to pursue research without whose support this work can never be possible. His zeal and enthusiasm to work with students in the lab have always inspired me. I hope to be guided by you even in future.

I take this opportunity to thank **Prof. Shuzi Hayase** for allowing me to use the lab facilities throughout my study in Japan.

My sincere thanks to **prof. Takenaka**, for his constant support in using TOF mass for improving the quality of thesis work and his valuable ideas.

I would also like to thank **Dr. Takeshi Ohta** for his helping hand in teaching me in how to handle, record and analyze NMR spectroscopy and also for his constant help in the lab as and when it`s required which are of great help in my project and career.

I would also like to thank **Dr. Tarun chand and Dr. Suvratha Krishnamurthy** for introducing me to Kyushu Institute of Technology and for their cooperation and encouragement which was a constant source of inspiration for me.

I would like to express my deep sense of appreciation to **Mr. Daisuke Sato** who helped me personally and academically out of his way and made my stay in Japan a memorable one.

I take this opportunity to thank the **present and past members of the laboratory** for their kind co-operation and also for maintaining the decorum of the lab without which the work can never be potential.

I would also like to take this opportunity in thanking my friend **Dr. J. Venkat Prasad** for his help in recording NMR for the samples as and when it was required.

I would like to acknowledge **Kyushu Institute of Technology** for its support, excellent facilities, and aid for conferences and lectures, which helped me a lot both scientifically and socially. Am also grateful to the International student office section, Kyushu Institute of Technology for their constant help throughout my period of stay in Japan.

I also thank the **Indian community in KIT** for making my stay a delightful one, by organizing get together more frequently which was a kind of family environment at home away from home.

I am deeply thankful to all those who helped me either directly or indirectly in the completion of this work.

Moreover, I indebted to my mother **(Mrs. Uma rani)**, my sister **(Mrs. Swathi)** brother **(Mr. Ashwanth Kumar)**, my uncles (**Mr. Srinivasulu** and **Mr. Sudhakar)** who are of constant inspiration and driving force to complete my doctoral studies successfully.

Above all, this remains incomplete if I fail to express my heartfelt gratitude to **Bhagawan Sri Sathya Sai Baba**, for guiding me at every step in this wonderful journey of 3 years. With all my humility and reverence, I offer this endeavor of mine at thy Lotus feet.